A NEW METHOD FOR THE CALCULATION OF STATIC FLIGHT LOADS OF RIGID FUSELAGE OF ROTORCRAFT

A THESIS SUBMITTED TO
THE GRADUATE SCHOOL OF NATURAL AND APPLIED SCIENCES
OF
MIDDLE EAST TECHNICAL UNIVERSITY

BY

SEYHAN GÜL

IN PARTIAL FULFILLMENT OF THE REQUIREMENTS
FOR
THE DEGREE OF MASTER OF SCIENCE
IN
AEROSPACE ENGINEERING

DECEMBER 2016

Approval of the thesis:

A NEW METHOD FOR THE CALCULATION OF STATIC FLIGHT LOADS OF RIGID FUSELAGE OF ROTORCRAFT

submitted by **SEYHAN GÜL** in partial fulfillment of the requirements for the degree of **Master of Science in Aerospace Engineering Department, Middle East Technical University** by,

Prof. Dr. Gülbin Dural Ünver
Director, Graduate School of **Natural and Applied Sciences** _______________

Prof. Dr. Ozan Tekinalp
Head of the Department, **Aerospace Engineering** _______________

Prof. Dr. Yavuz Yaman
Supervisor, **Aerospace Engineering Dept., METU** _______________

Examining Committee Members:

Assoc. Prof. Dr. Melin Şahin
Aerospace Engineering Dept., METU _______________

Prof. Dr. Yavuz Yaman
Aerospace Engineering Dept., METU _______________

Asst. Prof. Dr. Tuncay Yalçınkaya
Aerospace Engineering Dept., METU _______________

Asst. Prof. Dr. Ercan Gürses
Aerospace Engineering Dept., METU _______________

Prof. Dr. Metin Uymaz Salamcı
Mechanical Engineering Dept., Gazi University _______________

Date: 28.12.2016

I hereby declare that all information in this document has been obtained and presented in accordance with academic rules and ethical conduct. I also declare that, as required by these rules and conduct, I have fully cited and referenced all material and results that are not original to this work.

Name, Last name **:**

Signature **:**

ABSTRACT

A NEW METHOD FOR THE CALCULATION OF STATIC FLIGHT LOADS OF RIGID FUSELAGE OF ROTORCRAFT

Gül, Seyhan
M.S., Department of Aerospace Engineering
Supervisor: Prof. Dr. Yavuz Yaman

December 2016, 134 pages

The loads acting on a rotorcraft fuselage in pull-up, push-over, and yaw maneuvers and gust conditions are required to be calculated by civil and military standards. For each maneuver and the gust condition, different flight and rotor speeds, mass states, altitudes, and temperatures are required to be analyzed. This may add up to thousands of conditions. Calculation of fuselage loads for all these conditions with transient analysis is not only computationally expensive but it also requires a lot of engineering effort. Moreover, a stability augmentation system model is required for the transient analysis. In order to reduce the computation time and engineering effort and to eliminate the need for a stability augmentation system model, an approach named as ROFLOT (ROtorcraft Fuselage LOads with Trim) has been developed which represents the transient analysis by trim point(s).

Fuselage sectional axial force, shear force, torsional moment, and bending moment diagrams have been generated by using both transient analysis and ROFLOT approach and the results have been compared. It has been observed that the results are generally in good agreement except from M_x and M_z obtained from high-g forward flight trim method which is one of the two methods developed to represent the high vertical load factor in a pull-up maneuver. Furthermore, the loads are slightly underestimated with ROFLOT approach when the overall comparison of the gust conditions is considered.

Keywords: Rotorcraft Loads Analysis, Pull-up Maneuver, Push-over Maneuver, Yaw Maneuver, Rotorcraft Gust Loads

ÖZ

HELİKOPTERİN RİJİT GÖVDESİNE ETKİYEN STATİK UÇUŞ YÜKLERİNİN HESAPLANMASI İÇİN YENİ BİR YÖNTEM

Gül, Seyhan
Yüksek Lisans, Havacılık ve Uzay Mühendisliği Bölümü
Tez Yöneticisi: Prof. Dr. Yavuz Yaman

Aralık 2016, 134 sayfa

Sivil ve askeri standartlara göre, çekme, itme, sapma manevraları ve ani rüzgar koşullarında helikopter gövdesi üzerinde oluşan yüklerin hesaplanması gerekmektedir. Her bir manevra ve ani rüzgar koşulu için, farklı uçuş ve rotor hızları, kütle durumları, irtifa ve sıcaklık değerleri için analizler yapılmalıdır. Toplam koşul sayısı binlerce olabilir. Bütün bu koşullardaki yükleri zamana bağlı analizlerle hesaplamak sadece hesaplama yükü olarak pahalı değil, aynı zamanda yüksek miktarda mühendislik çabası gerektirmektedir. Ayrıca, uygun bir kararlılık artırma sistemi modeli gerekmektedir. Hesaplama zamanı ve mühendislik çabasını azaltmak ve kararlılık artırma modeli ihtiyacını ortadan kaldırmak amacıyla ROFLOT adı verilen ve zamana bağlı analizleri trim noktalarıyla temsil eden bir yaklaşım geliştirilmiştir.

Hem zamana bağlı analizler hem de ROFLOT yaklaşımıyla gövde kesit çekme kuvveti, kesme kuvveti, burulma momenti ve bükme momenti grafikleri oluşturulmuş ve sonuçlar karşılaştırılmıştır. Çekme manevrasındaki yüksek dikey yük faktörünü temsil etmek için geliştirilen iki yöntemden biri olan yüksek-g ileri uçuş trim yöntemi

ile elde edilen M_x ve M_z haricindeki sonuçların genellikle birbirine yakın olduğu gözlenmiştir. Ayrıca, ani rüzgar koşullarının tamamının genel karşılaştırılması göz önünde bulundurulduğunda ROFLOT yaklaşımıyla yükler zamana bağlı analizlere göre kısmen daha az olarak tahmin edilmiştir.

Anahtar Kelimeler: Helikopter Yük Analizi, Çekme Manevrası, İtme Manevrası, Sapma Manevrası, Helikopter Ani Rüzgar Yükleri

To My Mother, Father, and Brother...

ACKNOWLEDGMENTS

The author wishes to express his deepest gratitude to his supervisor Prof. Dr. Yavuz Yaman for his guidance and advice throughout the research.

The author is also grateful to his supervisor Derya Gürak at Turkish Aerospace Industries for her technical assistance and encouragements.

Finally, the author would also like to thank his colleagues Fatih Karadal, Pınar Arslan, Harun Tıraş, and Uğur Kalkan for all the technical discussions and help.

TABLE OF CONTENTS

LIST OF TABLES

TABLES

LIST OF FIGURES

FIGURES

LIST OF SYMBOLS

SYMBOLS

a	:	Acceleration on the beam
$a_{x,y}$	:	Acceleration in x or y direction
$\begin{Bmatrix} a_{x_{body}} \\ a_{y_{body}} \\ a_{z_{body}} \end{Bmatrix}^{j}$	:	Acceleration vector of point 'j' in body axis system
$\begin{Bmatrix} a_{x_{body}} \\ a_{y_{body}} \\ a_{z_{body}} \end{Bmatrix}^{i/j}$	:	Acceleration vector of point 'i' with respect to point 'j' in body axis system
A_{mesh}	:	Area of mesh
c_{ref}	:	Reference length
$\begin{Bmatrix} C_{F_{x_{body}}} \\ C_{F_{y_{body}}} \\ C_{F_{z_{body}}} \end{Bmatrix}_{i}^{j}$	:	Aerodynamic force coefficient vector in body axis system due to source 'i' acting at location 'j'
$\begin{Bmatrix} C_{M_{x_{body}}} \\ C_{M_{y_{body}}} \\ C_{M_{z_{body}}} \end{Bmatrix}_{i}^{j}$	:	Aerodynamic moment coefficient vector in body axis system due to source 'i' acting at location 'j'
C_T	:	Thrust coefficient
dy	:	Infinitesimal segment length of the beam
$dF_{Inertia}$	:	Inertial force acting on the infinitesimal segment of the beam
$f(x_n)$	:	Value of the function for the variable at n_{th} iteration in Newton-Raphson Method
F	:	Force acting on the beam
F_{shear}	:	Sectional shear force
$F_{x,y}$	:	Force in x or y direction

$\begin{Bmatrix} F_{x_k} \\ F_{y_k} \\ F_{z_k} \end{Bmatrix}_i^j$	:	Force vector in 'k' axis system due to source 'i' acting at location 'j'
g	:	Gravitational acceleration
$\begin{Bmatrix} g_{x_{body}} \\ g_{y_{body}} \\ g_{z_{body}} \end{Bmatrix}$	:	Gravitational acceleration vector in body axis system
$I^{cg,airf}$	:	Moment of inertia matrix of the airframe at the airframe center of gravity location with respect to body axis system
$I_{ab}^{cg,airf}$	:	Moment of inertia of the airframe at the airframe center of gravity location with respect to 'a' and 'b' axes of body axis system
I_c	:	Moment of inertia at point c
L	:	Length of the beam
L_T	:	Lift acting on tailplane
m	:	Mass
m_{airf}	:	Mass of the airframe
$m_{mp,n}$	:	Mass of mass point 'n'
m_{mr}	:	Mass of the main rotor
$m_{r/c}$	:	Mass of the rotorcraft
m_{tr}	:	Mass of the tail rotor
$M_{bending}$	:	Sectional bending moment
M_c	:	Moment acting at point c
$\begin{Bmatrix} M_{x_k} \\ M_{y_k} \\ M_{z_k} \end{Bmatrix}_i^j$	:	Moment vector in 'k' axis system due to source 'i' acting at location 'j'
n	:	Load factor
$\begin{Bmatrix} n_{x_{body}} \\ n_{y_{body}} \\ n_{z_{body}} \end{Bmatrix}$	:	Load factor vector in body axis system

$\begin{Bmatrix} N_{x_{LAS}} \\ N_{y_{LAS}} \\ N_{z_{LAS}} \end{Bmatrix}$	:	Mesh normal vector in LAS
p	:	Rotorcraft roll rate
P_i	:	Pressure at node 'i'
P_{mesh}	:	Pressure on mesh
$\dot{p}$	:	Rotorcraft roll acceleration
q	:	Rotorcraft pitch rate
Q	:	Dynamic pressure
$\dot{q}$	:	Rotorcraft pitch acceleration
r	:	Rotorcraft yaw rate
$\dot{r}$	:	Rotorcraft yaw acceleration
$\dot{r}_1$	:	Value of the yaw acceleration due to the pedal input for the yaw maneuver
$\dot{r}_2$	:	Value of the yaw acceleration corresponding to the maximum transient sideslip angle
$\begin{Bmatrix} r_{x_k} \\ r_{y_k} \\ r_{z_k} \end{Bmatrix}^{i/j}$	:	Position of point 'i' with respect to point 'j' in 'k' axis system
S_a	:	Lateral cyclic stick position
S_b		Longitudinal cyclic stick position
S_c	:	Collective stick position
S_p	:	Pedal position
S_{ref}	:	Reference area
$\begin{Bmatrix} t_{x_{LAS}} \\ t_{y_{LAS}} \\ t_{z_{LAS}} \end{Bmatrix}$	:	Mesh unit normal vector in LAS
t_1	:	Rise time of pedal input and yaw acceleration for yaw maneuver
t_2	:	Time when maximum transient sideslip angle is achieved at yaw maneuver
u	:	Component of rotorcraft velocity in x_{body} direction
$\dot{u}$	:	Time derivative of the velocity in x_{body} direction

v	:	Component of rotorcraft velocity in y_{body} direction
$\dot{v}$	:	Time derivative of the velocity in y_{body} direction
V	:	Velocity
V_H	:	Maximum speed in level flight with maximum continuous power
V_∞	:	Free-stream velocity
V_{NE}	:	Never-exceed speed
w	:	Component of rotorcraft velocity in z_{body} direction
w_I	:	Inertial force per length acting on the beam
$\dot{w}$	:	Time derivative of the velocity in z_{body} direction
W_F	:	Weight of vertical fin
W_{RF}	:	Weight of rear fuselage
W_T	:	Weight of tailplane
W_{TC}	:	Weight of tailcone
x_c	:	Geometrical center of mesh x_{LAS} location
$x_{cg,mp,n}$	:	Mass point 'n' center of gravity x_{LAS} location
$\begin{Bmatrix} x_{cg,airf} \\ y_{cg,airf} \\ z_{cg,airf} \end{Bmatrix}$	:	Airframe center of gravity location vector in body axis system
$\begin{Bmatrix} x_{cg,r/c} \\ y_{cg,r/c} \\ z_{cg,r/c} \end{Bmatrix}$	:	Rotorcraft center of gravity location vector in body axis system
$\begin{Bmatrix} x_{hub,mr} \\ y_{hub,mr} \\ z_{hub,mr} \end{Bmatrix}$	:	Main rotor hub location vector in body axis system
$\begin{Bmatrix} x_{hub,tr} \\ y_{hub,tr} \\ z_{hub,tr} \end{Bmatrix}$	:	Tail rotor hub location vector in body axis system
x_i	:	Node 'i' location in x_{LAS} direction
x_n	:	Value of the variable at n_{th} iteration in Newton-Raphson method
y	:	Distance from the center of rotation on the beam
y_c	:	Geometrical center of mesh location in y_{LAS} direction
$y_{cg,mp,n}$	:	Mass point 'n' center of gravity location in y_{LAS} direction
y_i	:	Node 'i' location in y_{LAS} direction
z_c	:	Geometrical center of mesh location in z_{LAS} direction

$z_{cg,mp,n}$	:	Mass point ‘n’ center of gravity location in z_{LAS} direction
z_i	:	Node ‘i’ location in z_{LAS} direction
α	:	Angle of attack
$\ddot{\alpha}$	:	Angular acceleration
β	:	Sideslip angle
η	:	Non-dimensional spanwise station
μ	:	Mass per length of the beam
ϕ	:	Rotorcraft roll angle
ϕ_{mr}	:	Main rotor axis system roll orientation with respect to body axis system
ϕ_{tr}	:	Tail rotor axis system roll orientation with respect to body axis system
ψ	:	Rotorcraft yaw angle
ψ_{mr}	:	Main rotor axis system yaw orientation with respect to body axis system
ψ_{tr}	:	Tail rotor axis system yaw orientation with respect to body axis system
ρ	:	Density
σ	:	Rotor solidity ratio
θ		Rotorcraft pitch angle
θ_{mr}	:	Main rotor axis system pitch orientation with respect to body axis system
θ_{tr}	:	Tail rotor axis system pitch orientation with respect to body axis system

CHAPTER 1

INTRODUCTION

Fuselage loads analysis plays an important role in the design of a rotorcraft. External loads on the rotorcraft should be known for various conditions, comprised of different maneuver types, rotorcraft configurations, and flight conditions, so that the internal loads, which are axial forces, shear forces, torsional moments, and bending moments, can be calculated. After calculation of the internal loads, critical conditions should be chosen based on some pre-defined criteria. The relevant structural analysis should then be performed on these critical conditions.

1.1. Motivation

A rotorcraft may fly in many different configurations and flight conditions and may perform different maneuvers. External and internal forces and moments on the fuselage should be calculated for combinations of each critical mass state, flight and rotor speed, density, and maneuver type. The mass state mentioned here is the combination of center of gravity location and weight and density is a function of ambient temperature and altitude. The maneuver types that should be analyzed are specified in related civil and military standards. For example, for small rotorcraft (maximum weight of 3175 [kg] or less and nine or less passenger seats), CS-27 is an applicable civil standard [1] while for large rotorcraft, CS-29 applies [2] as the civil standard.

Combination of all these conditions creates thousands of load conditions to be analyzed. Moreover, considering the fact that the loads on the rotorcraft should be calculated many times during different phases of the design, simulating these maneuvers by using a transient analysis requires a lot of computation time and engineering effort. Furthermore, a stability augmentation system is often required for the transient analysis of the maneuvers because of high coupling between roll, pitch, and yaw motions of a rotorcraft. Therefore, a faster yet accurate method that requires no stability augmentation system model needs to be established. In this work, it is sought to develop such a method for different maneuver types and gust conditions for the limit loads calculation of the rotorcraft fuselage.

1.2. Extend of the Developed Method

Rotorcraft fuselage loads calculation is performed in two steps. The first step is to perform flight dynamics analysis (trim or transient analysis). A mathematical model of the full rotorcraft is established by using integrated (total) inertial and aerodynamic parameters to perform flight dynamics analysis to be able to obtain the hub loads acting on the fuselage and the states of the rotorcraft for each maneuver type, rotorcraft configuration, and flight condition. The states include angle of attack and sideslip angle, orientation of the rotorcraft, which are denoted by Euler angles, linear and angular velocities, and linear and angular accelerations. These parameters and hub loads are used as inputs for the second step.

The second step is the calculation of the distributed fuselage loads and integrating them to the monitor stations. Distributed inertial and aerodynamic parameters are used to build the loads model of the fuselage in order to perform these calculations. The inertial loads are due to inertia of each mass item and aerodynamic loads are due to the pressure distribution around the fuselage. The monitor stations are used to monitor the integrated loads and choose the critical conditions. The locations of these monitor stations are chosen based on the locations of the mass items, frames and critical cross-sections on the fuselage. After choosing the critical conditions, the distributed loads are reported for structural analysis purposes as load cards in the format depending on the finite element analysis tool.

This thesis aims to develop an original approach, named as ROFLOT (ROtorcraft Fuselage LOads with Trim), to reduce the computation time and engineering effort required for the rotorcraft fuselage loads calculation and to eliminate the need for a stability augmentation system model. This can be possible by analyzing the loads on the rotorcraft fuselage during maneuvering by using transient analysis, determining critical instants of the maneuvers and estimating the rotorcraft states and main rotor and tail rotor hub loads at these phases by using trim analysis. In ROFLOT approach, the transient analysis normally employed in fuselage loads calculations is represented by trim point(s) in an efficient manner.

This thesis intends to calculate the external and internal loads only, hence it does not cover stress calculation aspects. Therefore, it is intended to state forces and moments with the term 'loads', not stress. In addition, the loads on only the fuselage is covered in this thesis. In other words, the internal loads on the horizontal tail and vertical fin are not analyzed. Throughout the thesis, the term 'airframe' is used to state the structure comprised of fuselage, horizontal tail, and vertical fin.

1.3. Layout of the Thesis

The first chapter is the introduction chapter. It includes information about the motivation and the extend of the developed method.

The second chapter is devoted for the literature review. In this chapter, the information in the literature about the maneuvers analyzed in this thesis is summarized. Moreover, information available in the literature about the methodology employed for the rotorcraft fuselage loads calculation is presented. Finally, the comprehensive analysis tools developed and used in the industry for rotorcraft flight dynamics analysis are explained. Their development history and their capabilities are summarized.

The third chapter includes information about the axis systems used and the fictitious rotorcraft modeled for this thesis. The rotorcraft model is divided into three sub-sections as main rotor model, tail rotor model, and airframe model.

The fourth chapter explains the theory behind flight dynamics analysis and fuselage loads calculation and the relationship between them. This chapter elaborates the point loads used for the flight dynamics analysis and distributed loads used for the fuselage loads calculation.

The fifth chapter gives information about the software and the scripts used. It also gives information about the methodology employed for both transient solution and ROFLOT approach for pull-up, push-over, and yaw maneuvers and gust conditions.

The sixth chapter presents the fuselage load results of pull-up, push-over, and yaw maneuvers and gust conditions obtained by using both transient solution and ROFLOT approach. The axial force, shear force, torsional moment, and bending moment diagrams for each condition (maneuver type and flight condition) are presented as well as the same diagrams showing the maximum and minimum loads for many conditions and comparisons are performed.

The seventh chapter provides a conclusion for the study. A summary for the discussion of the results obtained is presented in this chapter as well as the benefits of the approach developed in this thesis.

CHAPTER 2

LITERATURE REVIEW

This chapter gives an extensive literature review. Rigid fuselage loads calculation method, the flight conditions to be performed and various important tools that can be used for fuselage loads calculation in the literature are detailed.

2.1. Maneuvers

This thesis investigates pull-up, push-over, and yaw maneuvers and also studies the gust condition that the rotorcraft may face. The loads to be encountered during these maneuvers and the gust condition should be calculated and structural analysis should be conducted in order to make sure that the rotorcraft can operate safely. This is required by EASA (European Aviation Safety Agency) [1, 2], which is the civil certification authority for Europe.

2.1.1. Pull-up and Push-over Maneuvers

According to EASA [1, 2], the rotorcraft should be designed for a positive limit load factor of 3.5 and for a negative limit load factor of -1. However, load factors of 2 and -0.5 can also be used if,

a. The probability of exceeding these values, in absolute sense, is shown to be low by analysis and flight tests and
b. These values are appropriate for each weight condition between the design maximum and design minimum weights

These high-g and low-g requirements are met with pull-up and push-over maneuvers when transient analysis is employed. Although some standards such as MIL-S-8698 [3] and AMCP 706-201 [4] mention pull-up and push-over maneuvers, where the cyclic stick is pulled aft (pull-up) and pushed forward (push-over) in order to generate pitch rate as shown in Figure 1, EASA [1, 2] does not state that pull-up and push-over maneuvers should be performed. These conditions are rather bookcases [6], which means ‘a relatively artificial state of the aircraft, in which applied and inertia loads are in equilibrium’ [6]. Therefore, instead of performing transient pull-up and push-over analyses, a flight case with the application of the load factor where the rotorcraft is in equilibrium by taking advantage of D’Alembert’s principle can be considered [6].

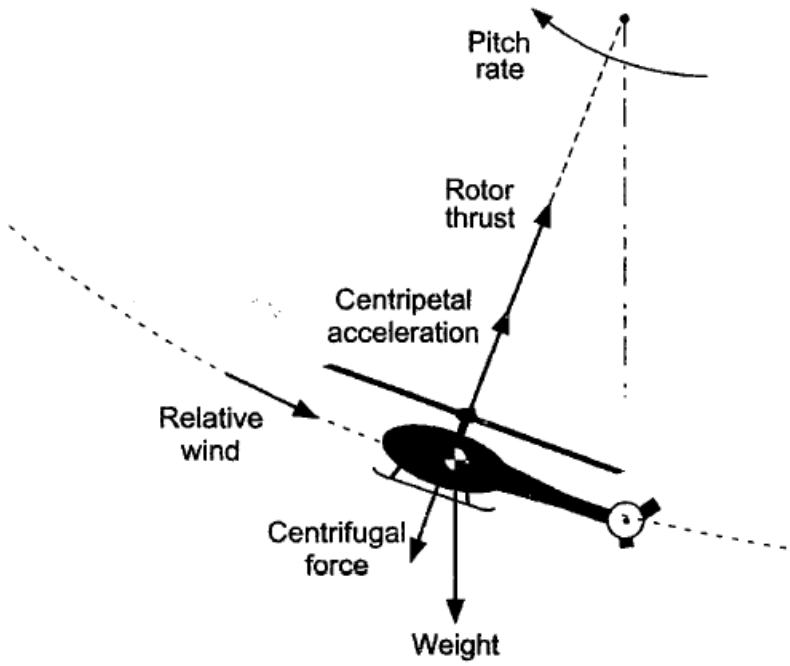

Figure 1. Schematic Representation of the Pull-up Maneuver [5]

2.1.2. Yaw Maneuver

EASA [1, 2] and AC 29-2C [7] require the loads to be calculated in the yaw maneuver by performing the following steps;

From an initial unaccelerated trim condition with zero yaw, the cockpit directional control is suddenly displaced to the maximum deflection limited by the control stops or by the maximum pilot force. This is intended to generate high tail rotor thrust.

1. The rotorcraft is allowed to yaw to the maximum transient sideslip angle or to the value defined in Figure 2, whichever is less (entry phase).

2. The rotorcraft is allowed to stabilize at the maximum steady-state sideslip angle. If the maximum steady-state sideslip angle is greater than the value defined in Figure 2, cockpit directional control deflection less than the maximum should be used.
3. The directional control is suddenly returned to its initial trim position (return phase).

AC 29-2C [7] states that the loads should be evaluated within the limits of Figure 2 or the maximum capability of the rotorcraft, whichever is less. It is also stated in AC 29-2C that no flight demonstration is required.

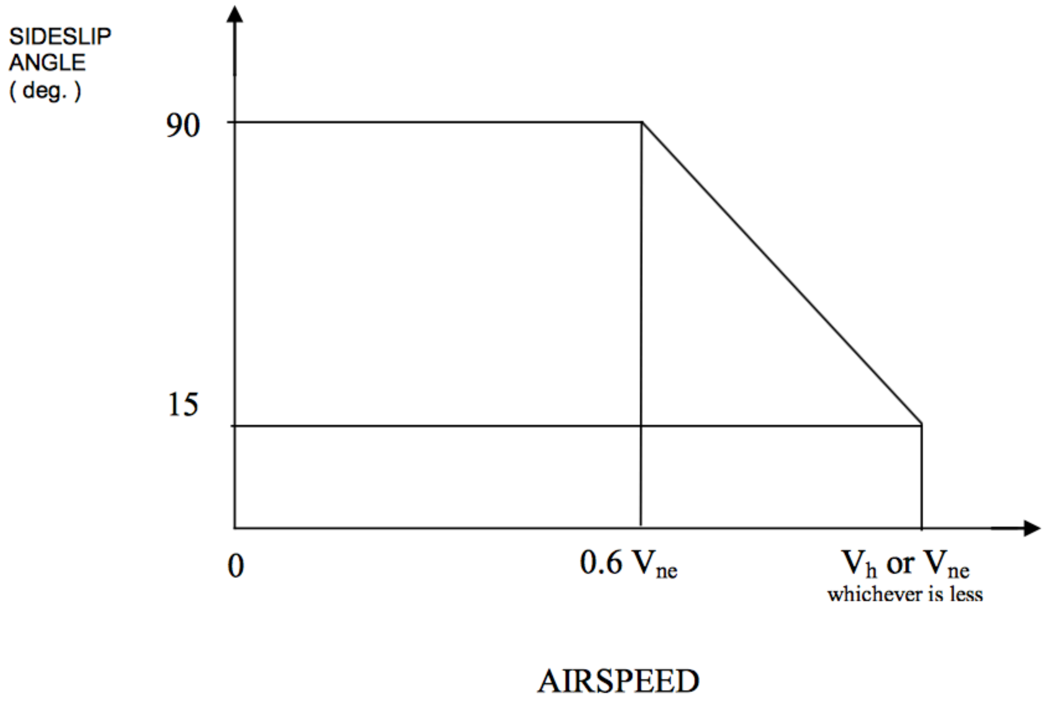

Figure 2. Resulting Sideslip Angle vs. Flight Speed for Yaw Maneuver [7]

MIL-S-8698 [3] states that a sudden pedal input limited by the stops or by a control force of 300 [lbf], whichever is less, should be applied. The pedal displacement should be maintained until the maximum sideslip angle is developed, and then returned to its original position at the same rate of displacement. It is also stated in MIL-S-8698 that this maneuver is performed in order to generate high side loads on the fuselage.

Quantification of the term ‘sudden input’ according to MIL-S-8698 depending on the class of the rotorcraft is given in Table 1. These values are to be used as the so-called ‘rise time’ of the control input. AC 29-2C [7] defines the rise time of a ‘sudden input’ as 0.2 [s], as well.

Table 1. Quantification of ‘Sudden Input’ Stated in MIL-S-8698 [3]

Class I	Rise time of 0.2 [s]
Class II	Rise time of 0.3 [s]
Class III	Rise time of 0.4 [s]

The classes of the rotorcraft are described in MIL-S-8698 as in Table 2.

Table 2. Rotorcraft Class Description of MIL-S-8698 [3]

Class I	Rotorcrafts with primary mission of rescue, evacuation, assault, liaison, reconnaissance, artillery spotting, utility, training, or antisubmarine warfare.
Class II	Rotorcrafts with primary mission of cargo with cargo loading of 5000 [lbf] or less.
Class II	Rotorcrafts with primary mission of cargo with cargo loading of more than 5000 [lbf].

AMCP 706-201 [4] mentions that yaw maneuver provides the highest lateral load factor, which is important for the sizing of the tail boom.

2.1.3. Gust Conditions

Gust is an abrupt change in the free-stream velocity amplitude and direction. Gusts result in change in angle of attack and sideslip angles on both main rotor and tail rotor blades and the airframe [8]. As a result, gust loads occur on the rotorcraft fuselage.

EASA [1, 2] requires that the gust conditions with a gust velocity of 30 [ft/s] while the rotorcraft is in hover or in forward flight with different flight speeds should be considered. Although CS-27 [1] mentions only horizontal gusts, CS-29 [2] states that both horizontal and vertical gust analyses should be performed.

MIL-S-8698 [3], however, states that the gust speed should be 50 [ft/s]. An alleviation factor to be used with respect to the disk loading is given in MIL-S-8698 as in Figure 3. Gust alleviation factor is a factor to be multiplied with the gust velocity [9]. Disk loading is the ratio of the thrust to the rotor disk area [10].

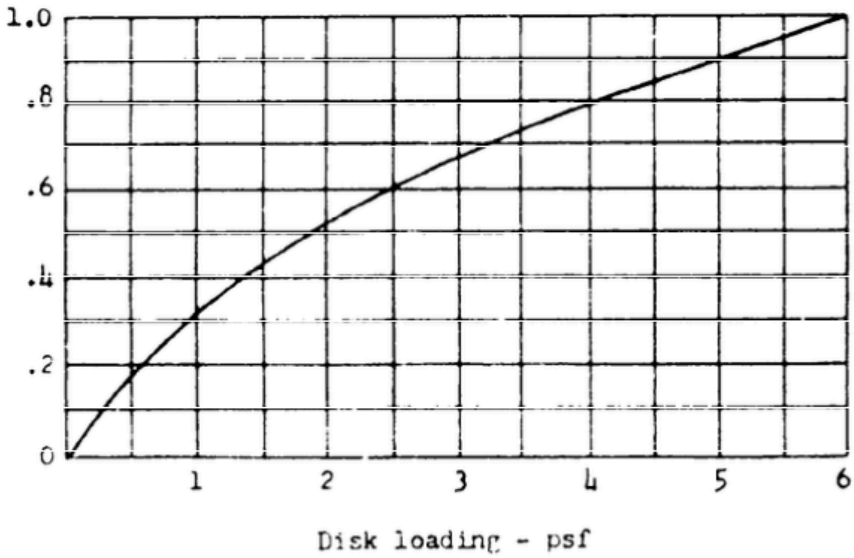

Figure 3. Change of Gust Alleviation Factor with Disk Loading [3]

AMCP 706-201 [4] explains that the gust loads for the rotorcraft become more significant as the rotorcrafts fly with higher speeds. However, it is stated in AMCP 706-201 [4] and in a paper about rotorcraft gust response [11] that the gust velocity values given in MIL-S-8698 are too conservative. It is stated in AMCP 706-201 that between the altitudes of 2000 [ft] and 10000 [ft], one occurrence of 50 [fps] or higher gust speed is encountered in 1.3 million flight miles as shown in Figure 4. Furthermore, the probability for a gust velocity of 30 [fps], which is the gust velocity required by EASA [1, 2], or higher is between one occurrence per 40000 [miles] and one occurrence per 65000 [miles], depending on the altitude.

AC 29-2C [7] states that sharp-edged gust analysis should be performed. Sharp-edged gust means that the rotorcraft enters and exits the gust field suddenly. Sharp-edged gust is reported to generate slightly higher loads than a 1-cosine shaped and a ramp gust profile [11]. The major effect of the gust profile type is on the time required for the load to build up [11].

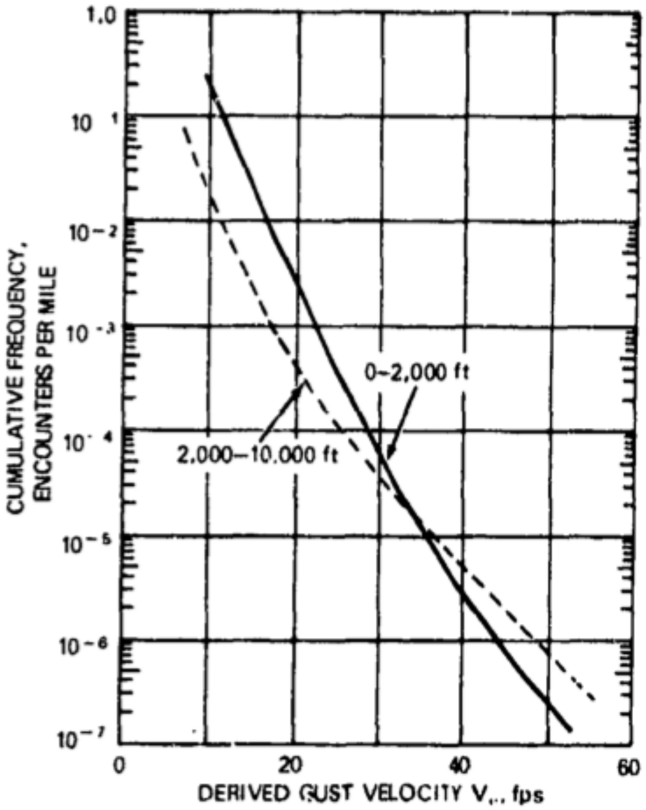

Figure 4. Gust Velocity Probability Curve [4]

2.2. Rotorcraft Fuselage Loads Calculation

The distributed loads along the fuselage should be calculated and integration of these loads along the fuselage needs to be performed after calculating the aircraft behavior in maneuver and gust conditions [6]. The distributed loads are comprised of inertial and aerodynamic loads. In order to calculate the distributed inertial loads, D'Alembert's Principle can be employed which reduces a dynamic problem to an equivalent static problem [6]. D'Alembert's Principle defines the product of a particle's mass with its acceleration as an inertial force and this is used to have a dynamic system in equivalent static equilibrium. The comparison of Newton's Law and D'Alembert's principle is given in Figure 5 [6].

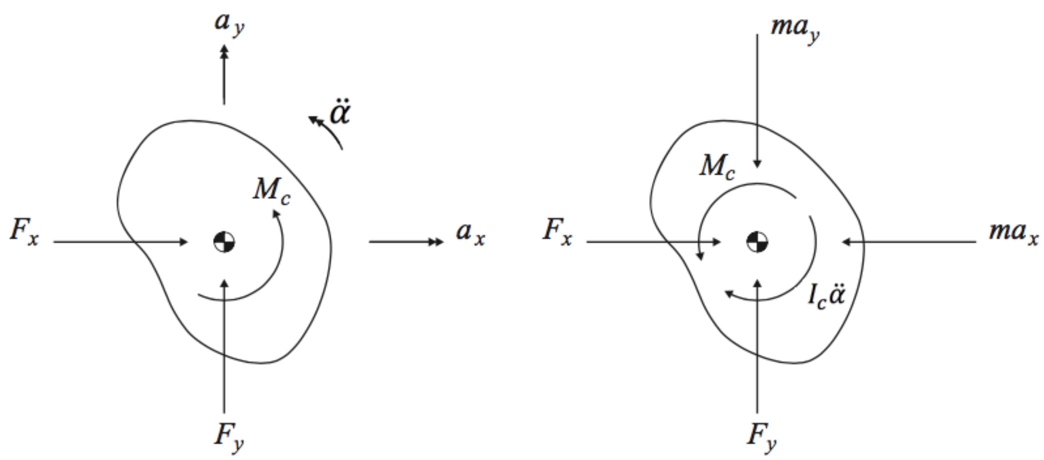

a. Newton's Law **b.** D'Alembert's Principle

Figure 5. Comparison of Newton's Law and D'Alembert's Principle [6]

A very simple application of D'Alembert's Principle on distributed inertial loads is presented for a translating and rotating body in Figure 6.

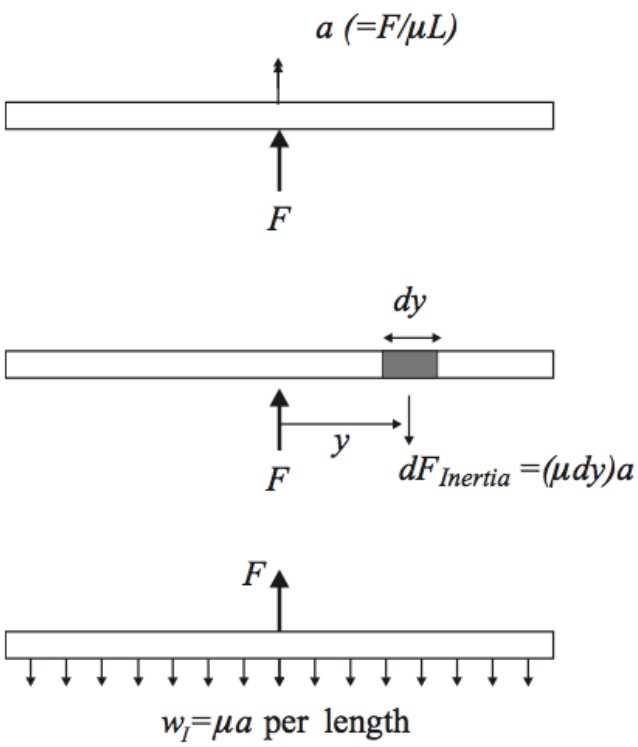

a. Translating Body

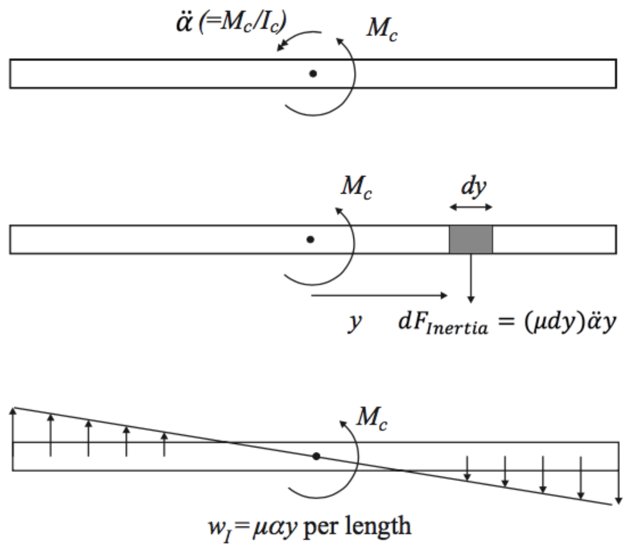

b. Rotating Body

Figure 6. Application of D'Alembert's Principle on Distributed Inertial Loads for a Translating and Rotating Body [6]

In order to calculate the distributed inertial loads by using D'Alembert's Principle, detailed distribution of the weight of the rotorcraft is required [12]. Moreover, for the calculation of the distributed aerodynamic loads, surface pressure data is required for complete range of angle of attack and sideslip angles [12], definition and sign convention of which are given in Figure 36.

After calculating the distributed loads and determining the 'discrete' loads, the internal loads can be calculated by taking 'cuts' along the fuselage. The loads on either side of the cut are equal and opposite in direction by Newton's Third Law **[**6**]**. A cut on the rear fuselage of an aircraft and the distributed inertial loads together with a discrete aerodynamic load in maneuvering is presented in Figure 7.

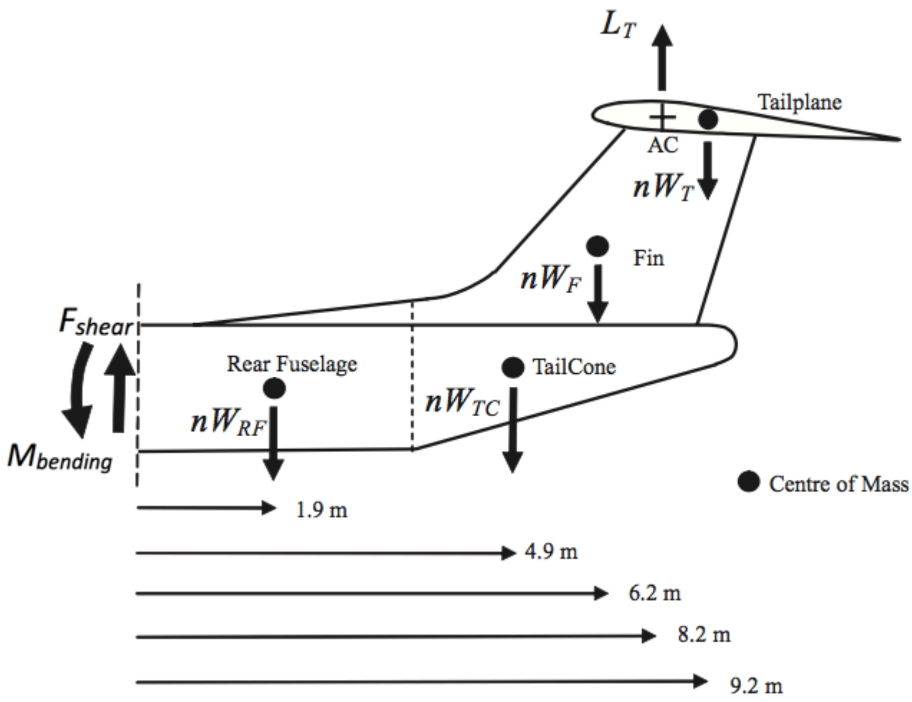

Figure 7. Cut on the Rear Fuselage and Distributed Inertial Loads together with a Discrete Aerodynamic Load in Maneuvering [6]

2.3. Comprehensive Analysis Tools

There are many different software for rotorcraft trim and transient analysis in the literature that can be used for the first step of the rotorcraft fuselage loads calculation, flight dynamics analysis. These programs use different mathematical models for aerodynamics and structure of both rotors and airframe including rigid and elastic equations of motion. Fuselage loads can be calculated by using some of the outputs that these software can provide, as described in detail in Chapter 4.2. Some of these software are called as 'comprehensive analysis tools' which means that they use the most advanced models for the geometry, structure, dynamics and aerodynamics available [13]. Comprehensive analysis tools can perform different kinds of computations such as rotorcraft performance and trim, structural loads, vibration, aeroelastic stability and flight dynamics at all stages of the design [13]. Some important tools developed in the history are given in Figure 8.

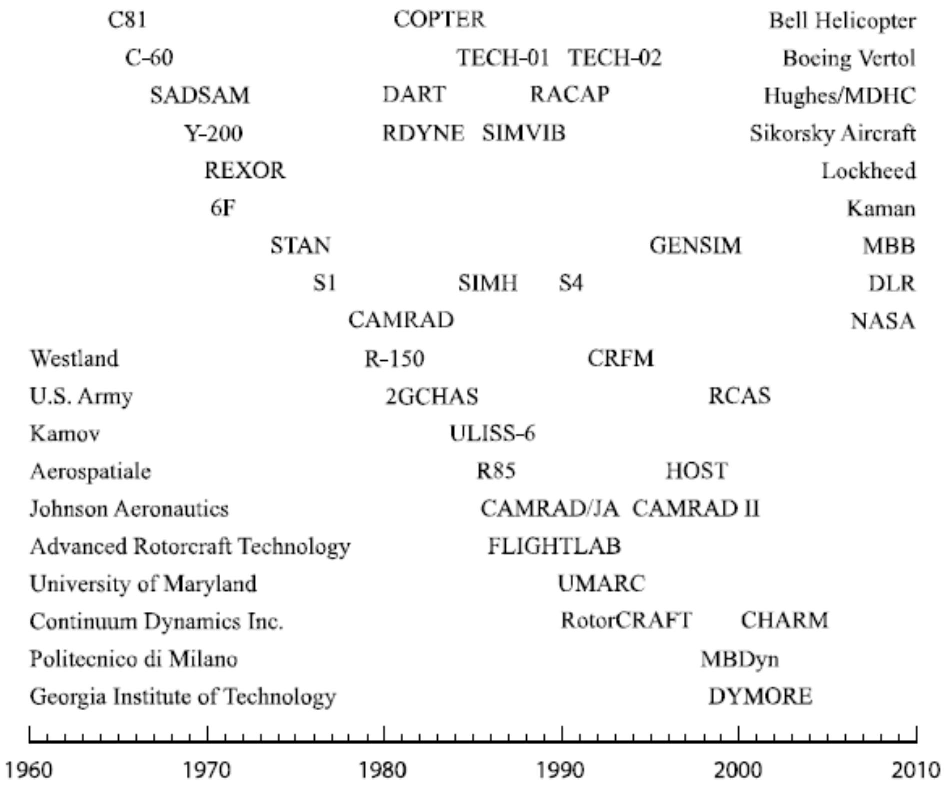

Figure 8. Summary of the Most Important Comprehensive Tools [13]

2.3.1. C81

The first and the oldest tool shown in Figure 8 is the helicopter flight simulation computer program C81. It was developed by Bell Helicopter with major support from the U.S. Army [13]. It is a multidisciplinary mathematical model that can analyze different rotorcraft configurations (such as conventional, tandem, side-by-side, etc.). This tool can estimate performance, stability, control, maneuvering characteristics and rotor blade loads [14]. The development history of C81 as of 1973 is given in Figure 9 which shows that it took many years to develop and correlate C81. Furthermore, the inputs required and the outputs of C81 are given in Figure 10.

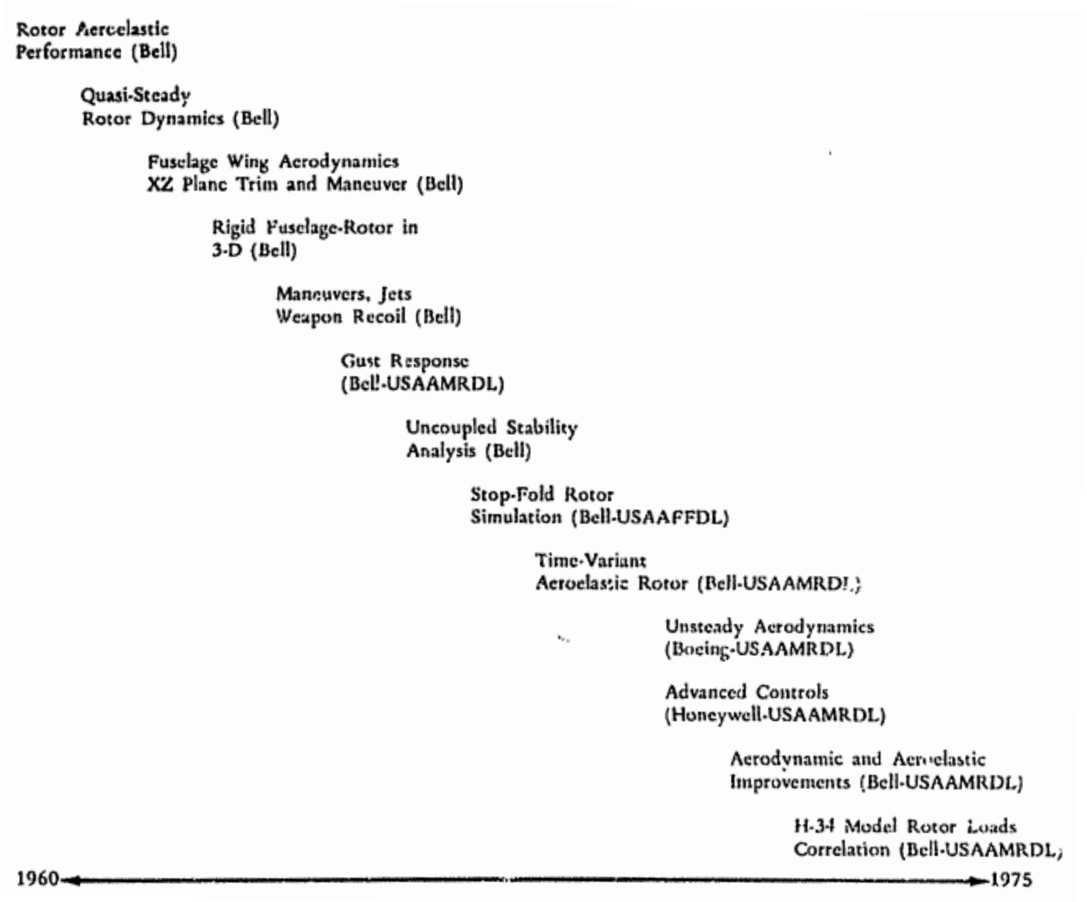

Figure 9. C81 Development History [14]

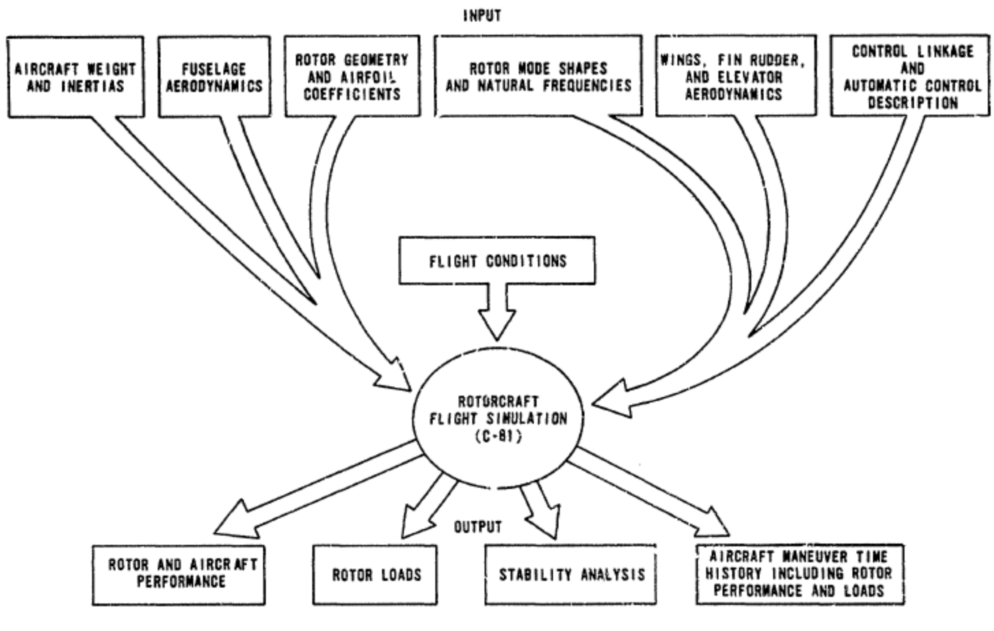

Figure 10. Inputs and Outputs of C81 [14]

C81 calculates the forces and moments on the fuselage due to [14]:

1. Fuselage aerodynamics
2. Main rotor and tail rotor aerodynamics
3. Wing aerodynamics
4. Elevator aerodynamics
5. Fin/rudder aerodynamics
6. Auxiliary thrust
7. Weapon recoil force

C81 can calculate these loads for both trim and non-linear response (transient) analysis [14]. Trim includes level or climbing flight, steady turn or steady pull-ups [14]. For both trim and non-linear response analysis, the components above act at their points of application and fuselage loads can be calculated using these outputs and rotorcraft states after extensive post-processing explained in detail in Chapter 4.2.

2.3.2. Second Generation Comprehensive Helicopter Analysis System, 2GCHAS

2GCHAS (Second Generation Comprehensive Helicopter Analysis System) was developed being sponsored by U.S. Army [13]. Several companies involved in the development of 2GCHAS. The development team included representatives from Kaman Aerospace Corporation, Advanced Rotorcraft Technology Inc., McDonnell Douglas Helicopter Corporation, Sterling Federal Systems, Boeing Helicopter Company, United Technologies Research Center, Sikorsky Aircraft Company, Computer Sciences Corporation, University of Maryland, Georgia Tech Research Institute, and Rensselaer Polytechnic Institute [15]. The first version was released in December 1990 [15].

2GCHAS is a multi-disciplinary, comprehensive software that can perform analysis for performance, stability and control, aeroelastic stability, loads and vibration, and acoustic characteristics of a rotorcraft [15]. The decision to develop this new code was made in 1976 because it was believed that existing codes were not sufficient for rotorcraft comprehensive analysis [13]. Some of the insufficiencies were such that the level of detail and validity in the mathematical models were not consistent, the codes were difficult to use, the structure of the codes was poor and the documentation was poor [13].

In order to perform an analysis using 2GCHAS, the user must supply structural and aerodynamic model and analysis data. The structural model is made of subsystems, primitives, and elements. Subsystems are fuselage, rotor(s), and control system(s) [15]. For each subsystem, there are arbitrary number of primitives. Each subsystem contains elements that are the fundamental building block of the structural model. The element library includes elements such as linear and geometrically non-linear beam, which can be used for the blades and fuselage respectively, rigid body mass, non-linear spring and damper, rigid blade, and transfer function, in order for the user to model the structure accurately [15].

The aerodynamic model is composed of supercomponents, components, and segments. Aerodynamic supercomponents are wing, rotor, and aerobody (not a lifting surface such as fuselage). Supercomponents are composed of components that are created by segments which are the basic elements that create aerodynamic forces [15]. This building block approach mentioned above is summarized in Figure 11.

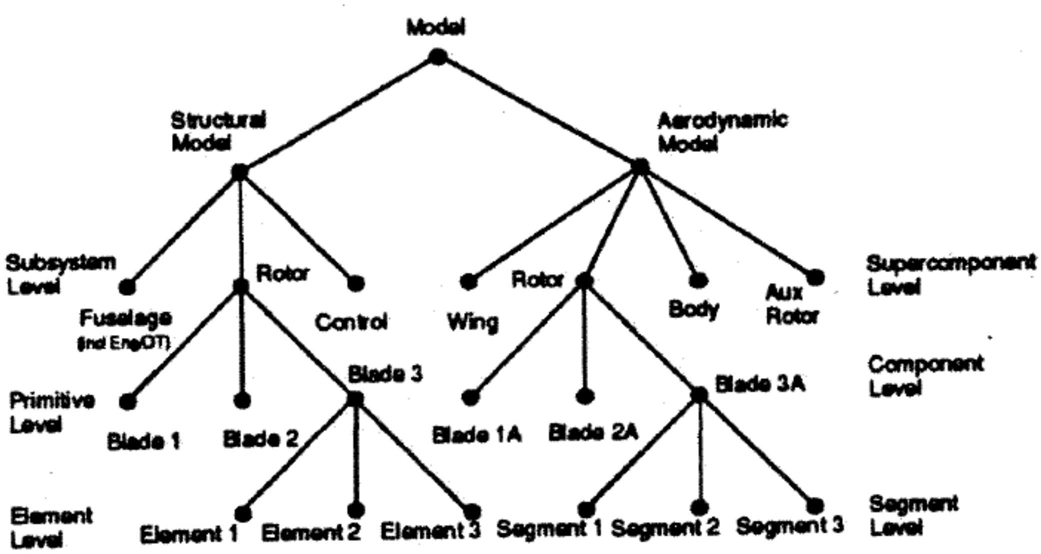

Figure 11. 2GCHAS Hierarchical System Model [15]

2GCHAS can model a conventional rotorcraft with a main rotor and a tail rotor to counteract the torque generated by the main rotor and a tandem helicopter model with two counter rotating rotors (one is at the front and the other one is at the back) are illustrated in Figure 12.

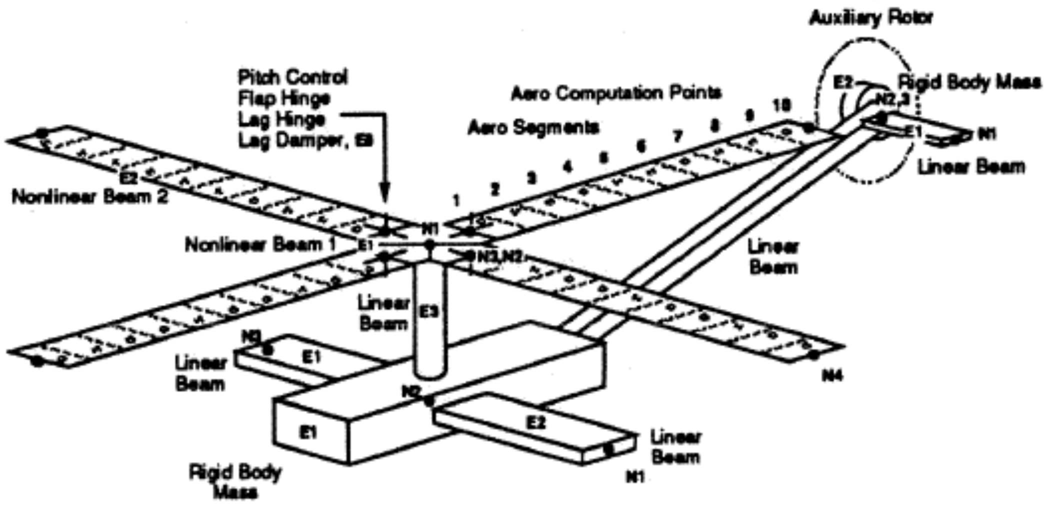

a. Conventional Rotorcraft Model

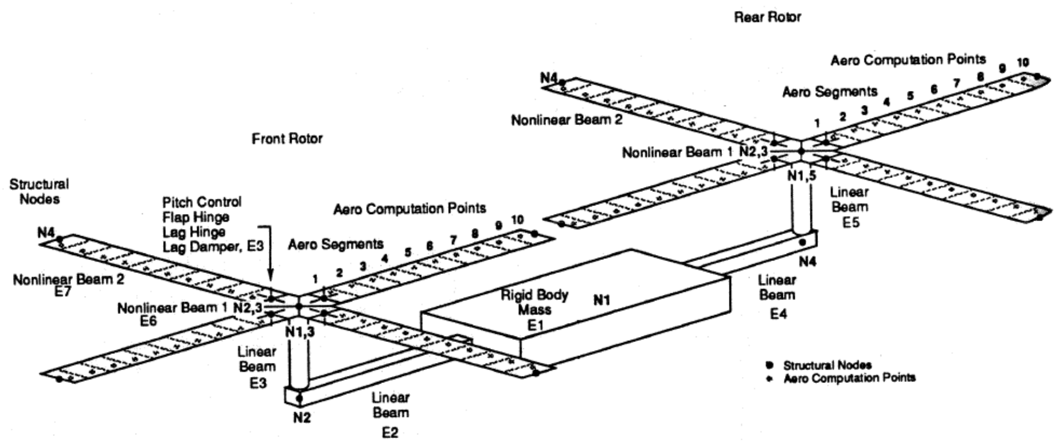

b. Tandem Rotorcraft Model

Figure 12. 2GCHAS Rotorcraft Models [15]

2GCHAS can perform trim, stability, non-linear response, and linearized response analyses [15]. Trim analysis includes free flight and wind tunnel trim [15]. Free flight can be hover, forward flight, sideward flight and rearward flight [15]. For the maneuvers, non-linear response analysis should be used. Using both trim and transient analysis, performance results that includes point loads and rotorcraft states can be obtained as shown in Figure 13. These parameters can later be used for the calculation of the fuselage loads. Moreover, although not fully clear, it may be possible to obtain fuselage sectional loads since the fuselage can be modeled by several aerobodies and mass items [15]. This, of course, requires a detailed fuselage model. In the example models shown in Figure 12, the fuselage is represented by a single mass.

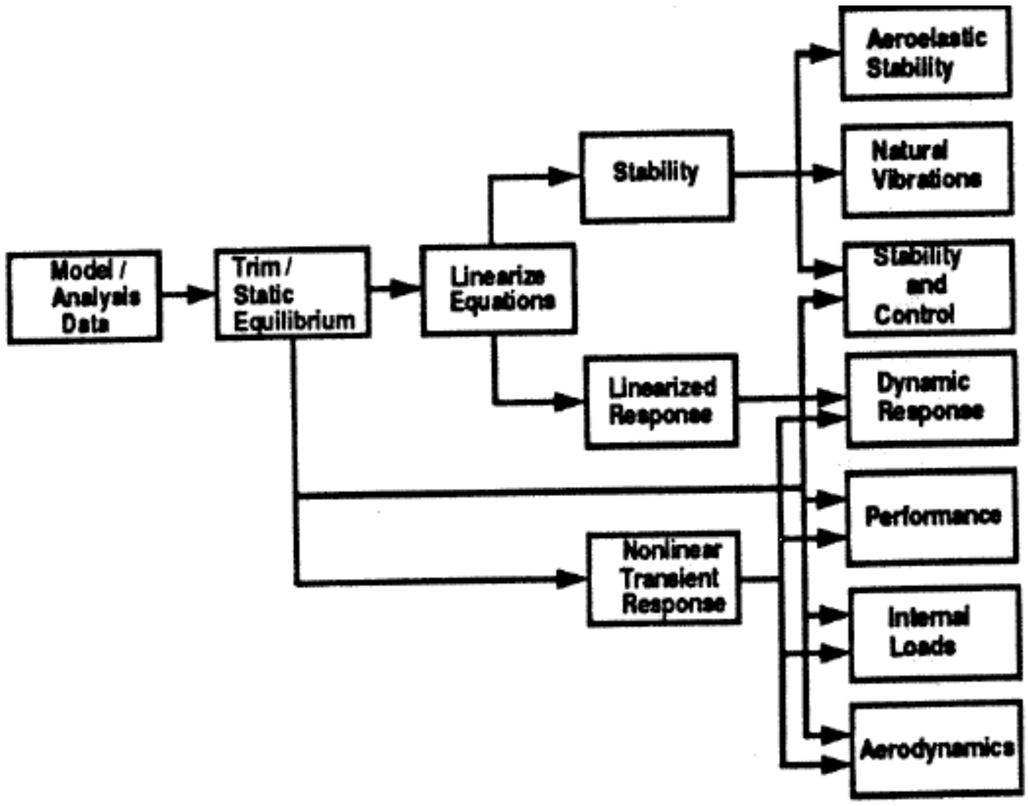

Figure 13. 2GCHAS Analysis Options [15]

2.3.3. Rotorcraft Comprehensive Analysis System, RCAS

RCAS (Rotorcraft Comprehensive Analysis System) was developed by Advanced Rotorcraft Technology, Inc. for U.S. Army because of the limitations observed in 2GCHAS particularly on maneuver analysis (RCAS could not handle large rigid motion or elastic structural deformation) and poor computational efficiency [13]. There has been some modifications made on the element library, finite element assembly and solution procedures of 2GCHAS [13]. Therefore, it can be said that RCAS is an improved version of 2GCHAS. It took four years to build RCAS on top of 2GCHAS which took an additional fourteen years to develop [16]. Since RCAS offers aeroelastic modeling and it has general purpose features, it is not only used for rotorcrafts but also for the wind turbines [16].

The engineering analyses that RCAS can perform is very similar to 2GCHAS and can be classified into three categories [16]:

1. Trim analysis
2. Non-linear response analysis
3. Stability analysis

Trim analysis includes static equilibrium, periodic steady-state, and trim [16]. Static equilibrium analysis provides the static response under steady conditions that could be steady external loading and/or steady motion. An example could be the bending response of the blade under steady lift force. On the other hand, periodic steady-state analysis can calculate the periodic response of the blade under steady external loading and/or steady motion [16]. For example, periodic blade loads and deflections under steady cyclic input can be calculated. Finally, trim is used to determine the values of number of trim variables that would satisfy the same number of trim targets. For example, RCAS can calculate the required pilot stick controls and roll and pitch angles in order for the rotorcraft to fly in a forward flight condition.

Non-linear response analysis is used to obtain the response of the rotorcraft under external controls or applied loads as mentioned before. These controls and loads can be time varying.

Stability analysis includes linearization, model reduction, multi-blade coordinate transformation, Floquet transformation matrix, modal analysis, and aeroelastic stability analysis.

Similar to 2GCHAS, it may be possible to obtain fuselage sectional loads by modelling the fuselage with several aerobodies and mass items. However, whether this option is available or not is not fully clear in the literature. Another option to calculate the fuselage loads is by using the hub load and rotorcraft state outputs of 2GCHAS.

2.3.4. Comprehensive Analytical Model of Rotorcraft Aerodynamics and Dynamics, CAMRAD

CAMRAD (Comprehensive Analytical Model of Rotorcraft Aerodynamics and Dynamics) was originally developed at Ames Research Center for NASA and the U.S. Army in 1980 [13]. The codes present at the time could only solve a particular technical problem for a particular type of rotorcraft. Therefore, in the development of CAMRAD, it was aimed to use the recently developed technology to perform various types of analysis on various types of rotorcrafts [13]. CAMRAD can be used for the design and testing of rotors and rotorcraft for rotor performance, loads, noise, rotorcraft gust response, flight dynamics, and handling qualities [17,18,19]. It can model rotorcrafts with two rotors whether it is single main rotor and tail rotor, tandem, side-by-side or tilting proprotor with articulated, hingeless, gimballed, and teetering rotors having any number of blades [17]. The rotorcraft or rotor can be in wind tunnel or free flight [17]. The rotorcraft configurations that CAMRAD can model is given in Figure 14. The rotorcraft shown at bottom right corner of Figure 14 is a wind tunnel model while the other four are free flight models.

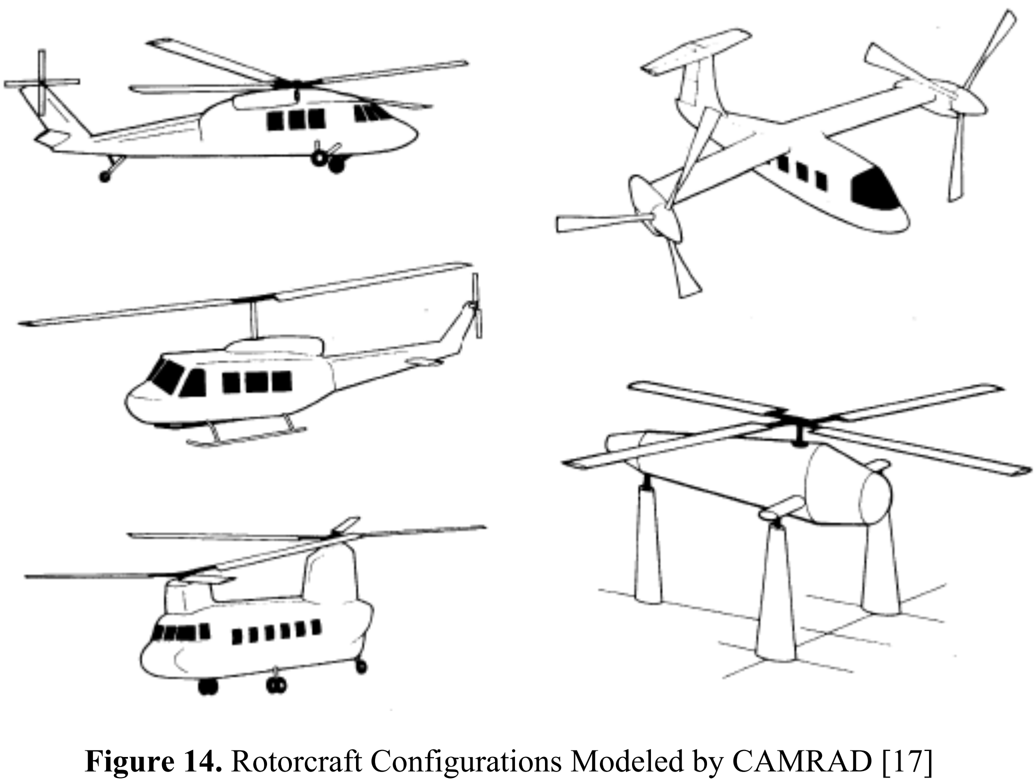

Figure 14. Rotorcraft Configurations Modeled by CAMRAD [17]

CAMRAD/JA was developed by Johnson Aeronautics during 1986-1988 [13]. It is an improved version of CAMRAD. Again, the rotorcraft configurations given in Figure 14 can be analyzed [20]. Similar to CAMRAD, CAMRAD/JA can be used for predicting rotor performance, loads, noise, rotorcraft vibration and gust response, flight dynamics, handling qualities and aeroelastic stability for design (both conceptual and detailed) and testing of rotors and rotorcraft [20,21].

Structural dynamic model of CAMRAD has not been changed but CAMRAD/JA has major new capabilities over CAMRAD [13]. The wake model was improved, the aerodynamic model was extended to be able to model swept tips and wing/body interactions. Loose computational fluid dynamics (CFD) coupling capability has been added [13].

After development of CAMRAD/JA, Johnson Aeronautics developed CAMRAD II [13]. It can be used for the same purposes as it is the case for CAMRAD and CAMRAD/JA. Development started in 1989 because of the limitations observed in CAMRAD/JA. One of the limitations was such that 'it was not possible to change one part of the analysis without considering the entire code' [13]. Furthermore, the blade model was a single load path model and control system load path was not modeled well. The first release was in 1993 [13]. CAMRAD II splits the system into environmental, physical, and logical pieces. Environmental pieces define the environment in which the rotorcraft operates. Physical pieces are mainly components and interfaces and logical pieces are the solution procedures [22]. These system pieces are summarized in Table 3.

Table 3. CAMRAD II System Pieces [22]

Environmental	**Physical**	**Logical**
case	component	loop
wind	frame	part
operating condition	interface	transform
period	output	modes
	input	response

CAMRAD II uses building block approach to model the true geometry of an arbitrary rotorcraft. Building block approach results in flexibility in the modeling. Even the vibration control devices can be modeled thanks to this approach [22].

The rotor model can use uniform inflow, non-uniform inflow with a rigid wake geometry or non-uniform inflow with a free wake geometry [23]. Uniform inflow does not cover the blade-vortex interaction [23]. Rigid wake is the ‘undisturbed helical wake geometry’ while free wake computes the distortion from the helix [10]. The helix mentioned above is generated by the combination of rotor speed and flight speed. The correlation of CAMRAD II sectional lift results with SA349/2 helicopter, which is an experimental variant of Aérospatiale Gazelle, test data with these different inflow and wake models is given in Figure 15.

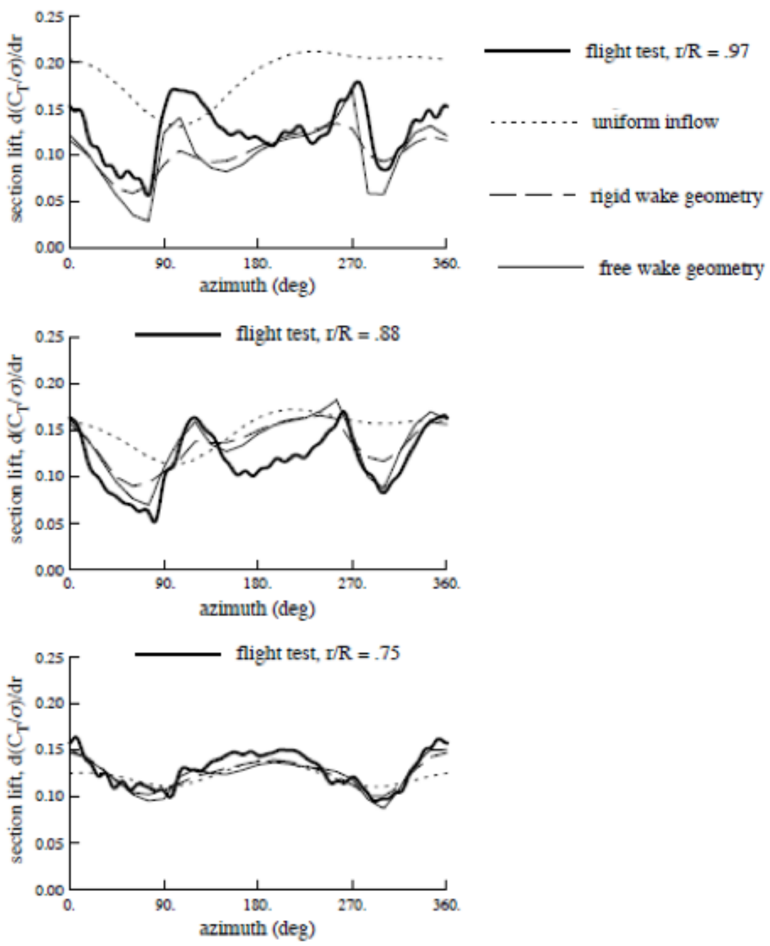

Figure 15. CAMRAD II Section Lift Correlation with SA349/2 Helicopter Flight Test Data at CT/σ = 0.065 and μ = 0.14 [23]

CAMRAD, CAMRAD/JA and CAMRAD II can all perform trim and non-linear response analysis. Figure 16 shows that for both of the analyses, results regarding performance, loads, vibration and noise can be obtained. Trim analysis includes level flight, steady climb and descent, and steady turns [17,20,22]. Transient analysis is performed after the trim analysis to perform maneuvers similar to 2GCHAS and RCAS.

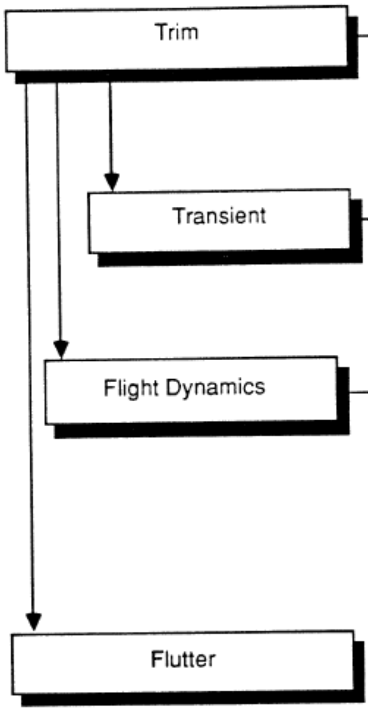

Figure 16. CAMRAD, CAMRAD/JA, and CAMRAD II Tasks [20]

CAMRAD, CAMRAD/JA and CAMRAD II are all able to provide the necessary inputs for fuselage loads calculations for both trim and transient analysis. Again, extensive post-processing after both trim and transient analysis is required in order to calculate the fuselage loads.

2.3.5. FLIGHTLAB

Advanced Rotorcraft Technology, Inc. (ART) started working on GENHEL blade-element model [24, 25] in 1985 and restructured it to show the potential of real-time simulation by using parallel processing on affordable computers [13]. Using the experience gained from this work, ART started developing a ‘generic, modular, reconfigurable' tool for real-time simulation in 1986 [13]. The software, FLIGHTLAB, became commercially available in 1990 [13]. ART has also been involved in the development of 2GCHAS as mentioned before. FLIGHTLAB and 2GCHAS has been developed in parallel. FLIGHTLAB focused more on handling quality analysis and real-time simulation at the time [13]. Although it was originally developed as a handling qualities and real time simulation tool, an important number of components and capabilities have been added in time to cover increasing areas of rotorcraft analysis [26]. For example, vortex wake aerodynamic, finite element structural dynamics, and a non-linear beam model [26] was integrated into FLIGHTLAB in 1995 [13].

FLIGHTLAB utilizes an object oriented environment with modular components [27]. The components include linear/non-linear control blocks, engine/drive train components, finite state dynamic inflow, prescribed and free vortex wake, unsteady airloads with ONERA dynamic stall model, aerodynamic interference, rigid masses, non-linear springs and dampers, and modal blade component for elastic blades [26]. This object oriented multi-body modeling technique makes it possible to model any rotorcraft and rotorcraft configuration. For example, for slung load analyses, different slung load configurations can be modeled by using different components and connecting them in different ways as shown in Figure 17.

In the model assemble process, the elements of the components are connected at nodes and motion and loads are transferred through these nodes. For example, the motion of the rotorcraft is transferred to the elements of rotor component, such as mass points and aerodynamic panels on the blades, through connection nodes. Given the motion and the flight condition, the aerodynamic and inertial loads on the blades are calculated and transferred to the center of gravity of the rotorcraft again through the connection nodes in order to solve the equations of motion of the rotorcraft [27].

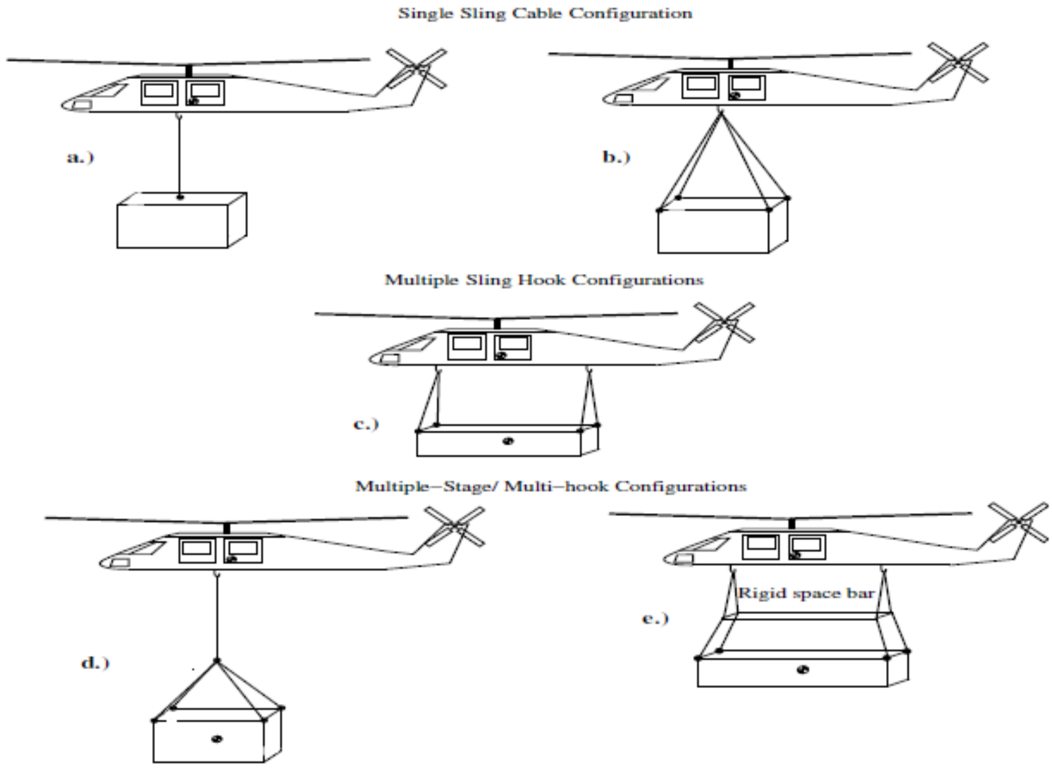

Figure 17. Various Sling Configurations Supported by FLIGHTLAB [28]

For the rotor component, FLIGHTLAB can model a rigid blade by using the blade element method and an elastic blade by supplying the mode shapes as input to the program. The time required for an elastic blade solution is around six times of the time required for a blade element solution [27].

FLIGHTLAB can perform trim and transient analyses like the other codes described in this chapter. The trim analysis includes both accelerated and unaccelerated flight conditions. For unaccelerated flight conditions, forward flight, climb and descent conditions can be given as examples. For the accelerated flight conditions, trim algorithm allows the user to set the linear and angular accelerations as floating or to some value and required control inputs and rotorcraft behavior can be obtained. Accelerated condition can be a time instant of a transient analysis that the engineer is particularly interested in because of the loads generated. The parameters required for rotorcraft fuselage loads calculation can be obtained by using FLIGHTLAB's trim or transient analysis.

CHAPTER 3

AXIS SYSTEMS AND MATHEMATICAL MODEL

3.1. Axis Systems

In this section, all the axis systems used in this thesis are explained. Some of these axis systems are illustrated on a schematic of a rotorcraft in Figure 18.

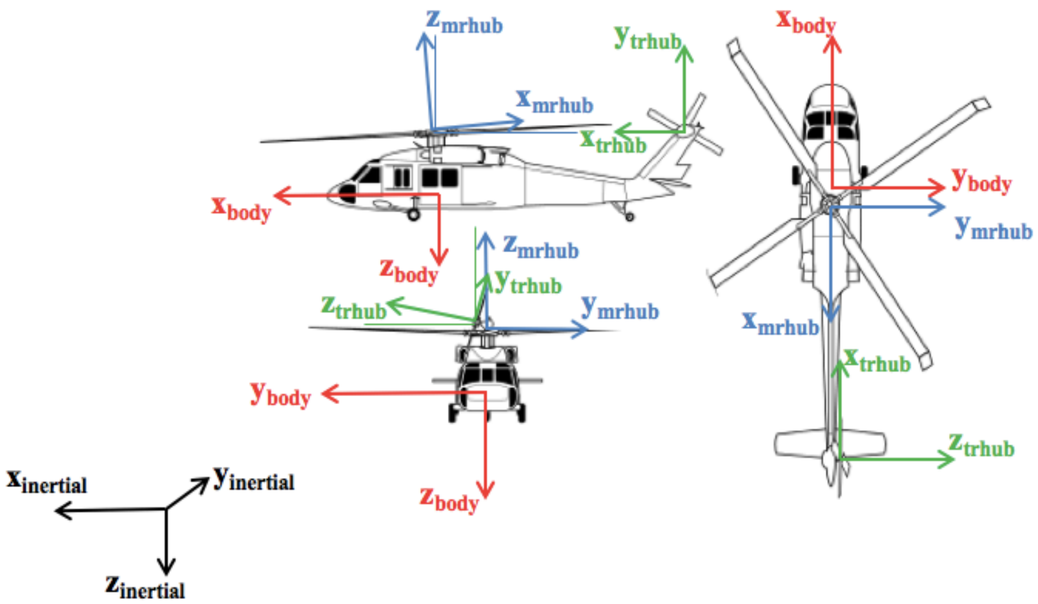

Figure 18. Body Axis System, Inertial Axis System, and Main Rotor and Tail Rotor Hub Axis Systems

3.1.1. Body Axis System

Body axis system rotates and translates with the rotorcraft and its origin is at the airframe (fuselage, horizontal tail, and vertical fin) center of gravity. This axis system is explained below and illustrated in Figure 18. Furthermore, Equations 1 and 2 explain airframe mass and center of gravity location calculation.

- ✓ x is towards the nose of the rotorcraft
- ✓ y is towards starboard
- ✓ z is down

$$m_{airf} = m_{r/c} - m_{mr} - m_{tr} \tag{1}$$

$$\begin{Bmatrix} x_{cg,airf} \\ y_{cg,airf} \\ z_{cg,airf} \end{Bmatrix} = \frac{m_{r/c}\begin{Bmatrix} x_{cg,r/c} \\ y_{cg,r/c} \\ z_{cg,r/c} \end{Bmatrix} - m_{mr}\begin{Bmatrix} x_{hub,mr} \\ y_{hub,mr} \\ z_{hub,mr} \end{Bmatrix} - m_{tr}\begin{Bmatrix} x_{hub,tr} \\ y_{hub,tr} \\ z_{hub,tr} \end{Bmatrix}}{m_{airf}} \tag{2}$$

This axis system is used for flight dynamics analysis and all the states of the rotorcraft are with respect to the body axis system.

3.1.2. Main Rotor Hub Axis System

The origin of main rotor hub axis system is at the main rotor hub where hub forces and moments act. The main rotor hub point is defined as the intersection of the pitch change axes of all the blades, also called as reference line, of the rotor blades assuming there is no torque offset as shown in Figure 19. This axis system is explained below and illustrated in Figure 18.

- ✓ x is towards the tail of the rotorcraft, affected by the shaft tilt angle
- ✓ y is towards starboard
- ✓ z is towards up, affected by the shaft tilt angle

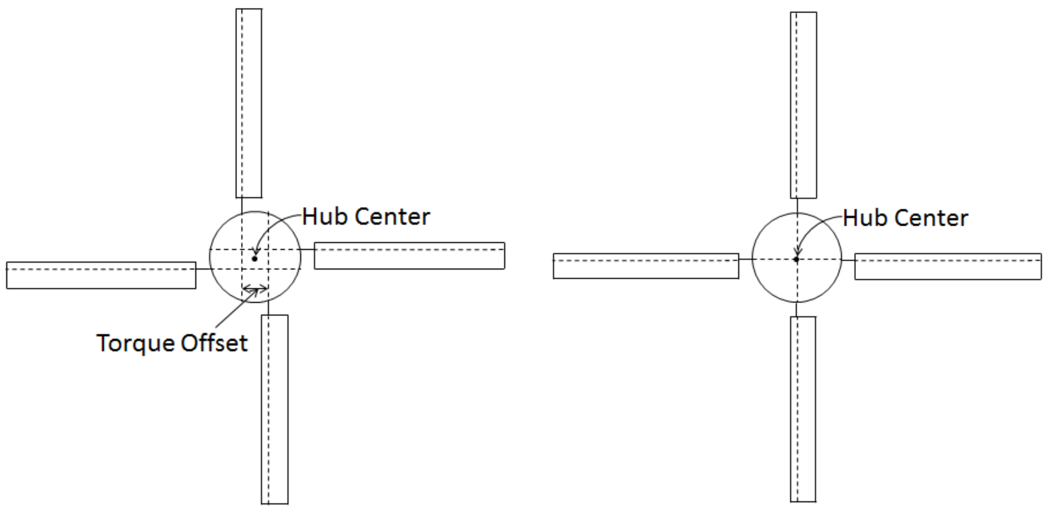

Figure 19. Hub Center Location with and without Torque Offset

3.1.3. Tail Rotor Hub Axis System

The origin of tail rotor hub axis system is at the tail rotor hub where hub forces and moments act. The tail rotor hub point is defined similar to the main rotor hub point. This axis system is explained below and illustrated in Figure 18.

- ✓ x is towards the nose of the rotorcraft
- ✓ y is determined by right hand rule, affected by the cant angle
- ✓ z is in the thrust direction, affected by the cant angle

3.1.4. Inertial Axis System

The origin of the inertial axis system is fixed to the earth. It is assumed that this axis system is not translating and rotating. Inertial axis system is explained below and illustrated in Figure 18.

- ✓ x is towards north
- ✓ y is towards east
- ✓ z is towards down

3.1.5. Blade Axis System

The blade axis system is used to define cross-sectional parameters of the blades. The origin is at the quarter chord location for each cross-section. Reference line (pitch change axis) is obtained by connecting the origins of each cross-section along the span. This axis system is explained below and illustrated in Figure 20.

- ✓ x is radially outwards
- ✓ y is towards leading edge
- ✓ z is towards up

Figure 20. Blade Axis System

3.1.6. Loads Axis System

The loads axis system (LAS) is used to define positions on the rotorcraft and calculate and interpret the fuselage loads. The origin is arbitrary since it does not change the positions of the rotorcraft with respect to each other. This axis system is explained below and illustrated in Figure 21. The sign convention of the sectional loads are also given in Figure 21.

- ✓ x is towards the rear of the rotorcraft
- ✓ y is towards starboard
- ✓ z is up

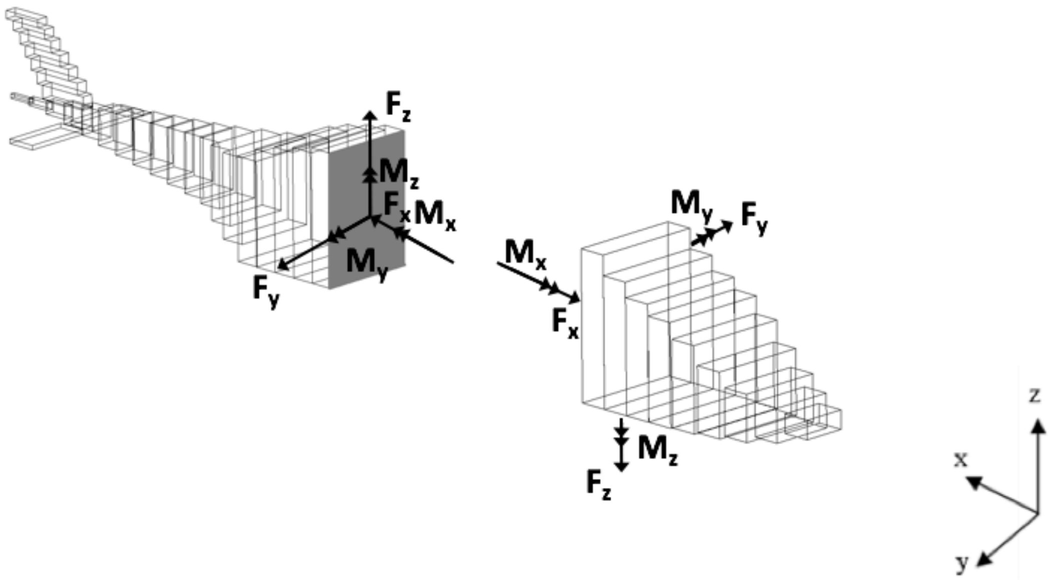

Figure 21. Fuselage Loads Axis System

3.2. Mathematical Model

In this chapter, the fictitious rotorcraft that has been modeled and used in this thesis is detailed. The mathematical model is used to calculate the loads using transient solution normally employed for fuselage loads calculation, explained in Chapters 5.2.1.1, 5.2.2.1, 5.2.3.1, and 5.2.4.1; and ROFLOT approach, explained in Chapters 5.2.1.2, 5.2.2.2, 5.2.3.2, and 5.2.4.2.

Schematic representation of the rotorcraft modeled is given in Figure 22 to Figure 25.

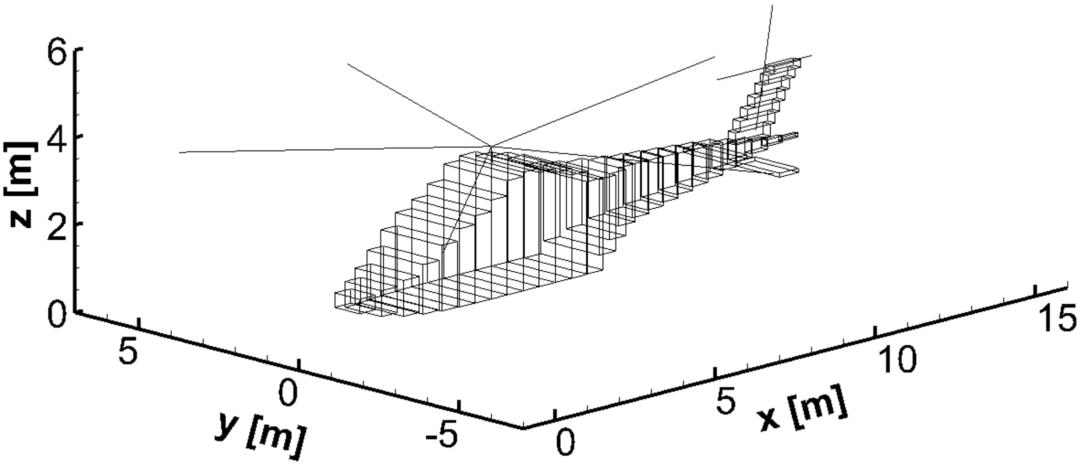

Figure 22. Schematic Representation of the Rotorcraft, Isometric View

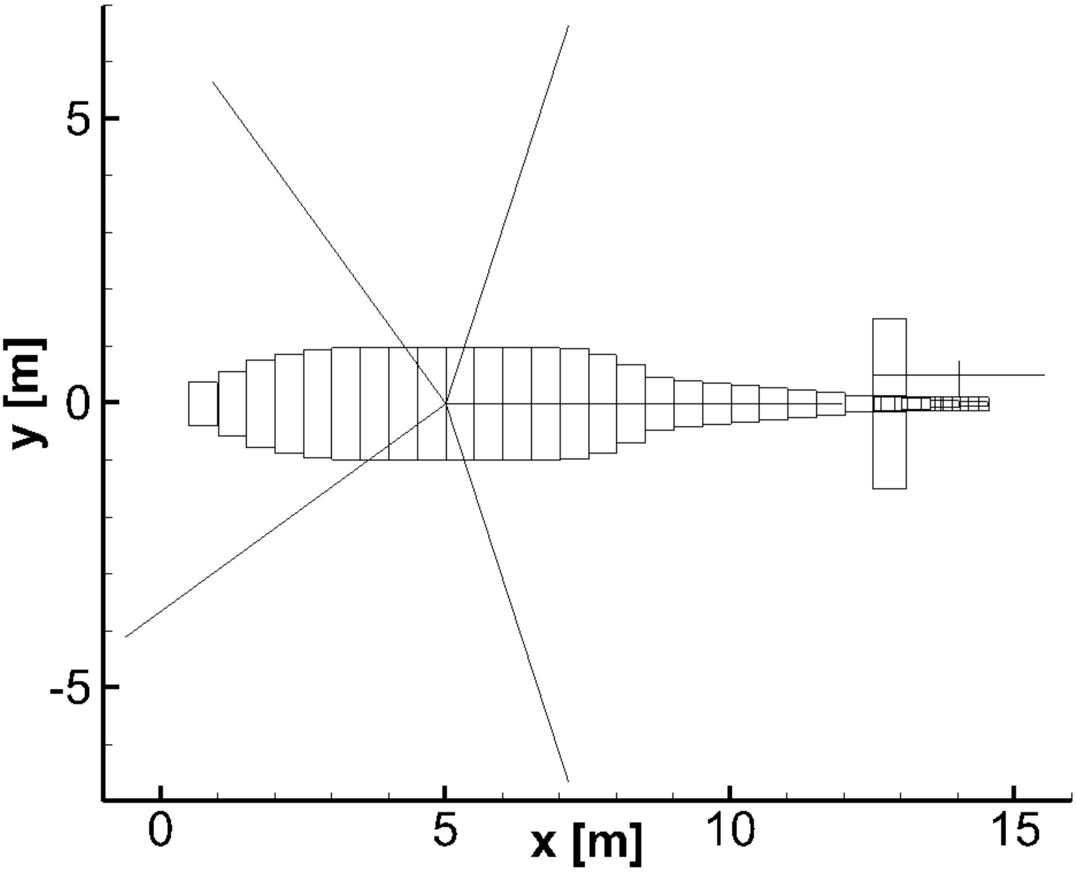

Figure 23. Schematic Representation of the Rotorcraft, Top View

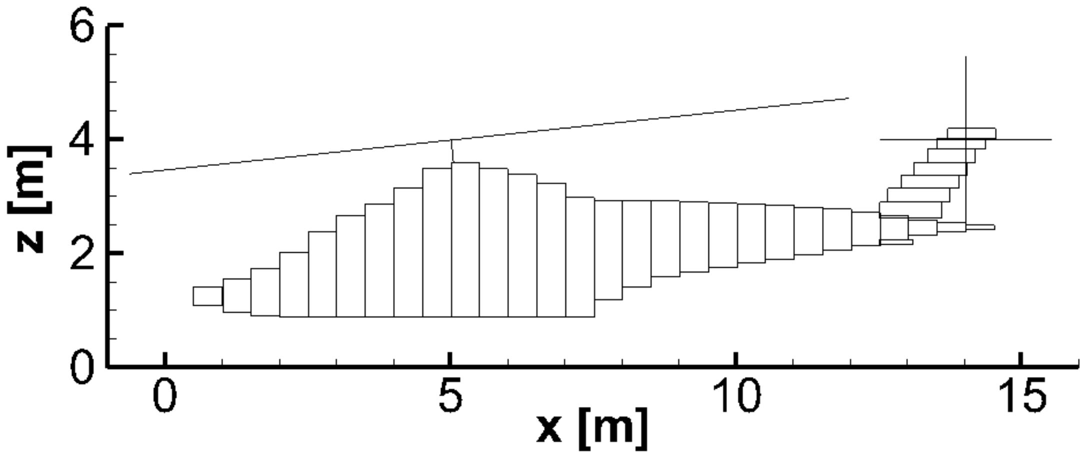

Figure 24. Schematic Representation of the Rotorcraft, Side View

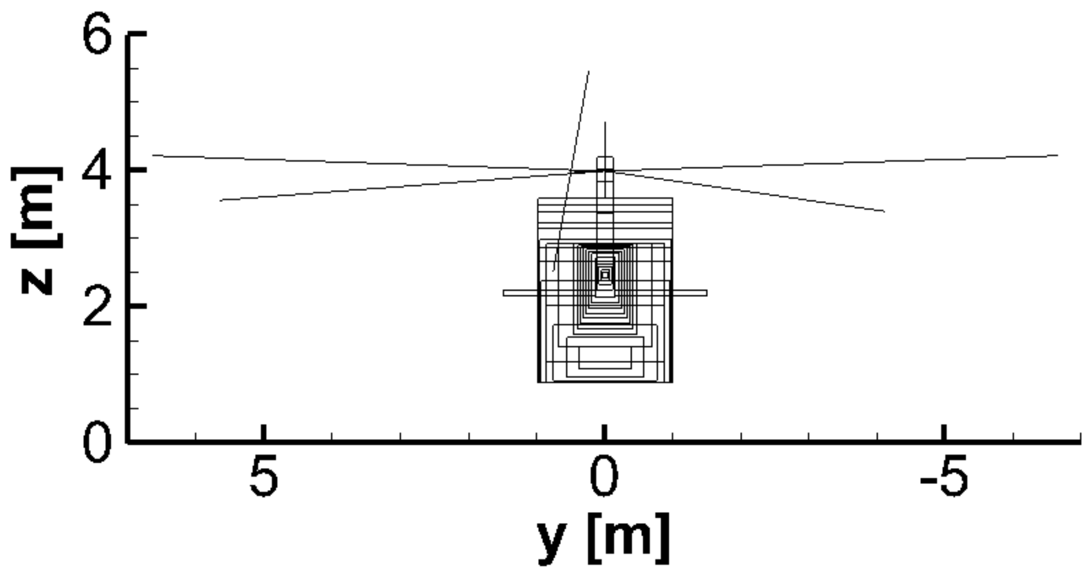

Figure 25. Schematic Representation of the Rotorcraft, Front View

3.2.1. Main Rotor Model

Some fundamental parameters of the main rotor are given in Table 4.

Table 4. Main Rotor Fundamental Parameters

Name	Value/Information	Unit	Explanation
Hub Location	5, 0, 4	m	In loads axis system
Rotation Direction	Counter-Clockwise	n/a	When viewed from top
Number of Blades	5	n/a	n/a

Table 4 continued

Name	Value/Information	Unit	Explanation
Rotor Orientation	0, 174, 0	deg	Ψ_{mr}, Θ_{mr}, Φ_{mr}, respectively With respect to body axis system 6^0 tilt forward
Rotor Speed	290	rpm	n/a
Radius	7	m	From rotor hub center to blade tip

3.2.1.1. Structural Model

Main rotor blades are modeled as rigid since blade elasticity does not have an important effect on the fuselage static limit loads. Structural model of the main rotor is detailed in Table 5 and schematic representation of the blade geometry is presented in Figure 26. Note that η in Table 5 is the fraction of the blade radius and it is measured from the hub point.

Table 5. Main Rotor Structural Model

Name	Value/Information	Unit	Explanation
Rotor Type	Fully Articulated	n/a	Flap, lead-lag hinges and pitch bearings exist on the rotor
Precone Angle	0	deg	The preset cone angle [10]
Hinge Offset	0.05	η	Flap, lead-lag hinges and pitch bearing are at the same spanwise location Measured from rotor hub center
Blade Mass	60	kg	Mass of a blade

Table 5 continued

Name	Value/Information	Unit	Explanation
Torque Offset	0	m	Offset of pitch change axis from rotor hub center in blade axis system y direction (see Figure 19)
Blade Center of Gravity Chordwise Location	quarter chord	m	n/a
Blade Center of Gravity Spanwise Location	0.531	η	Measured from the rotor hub center

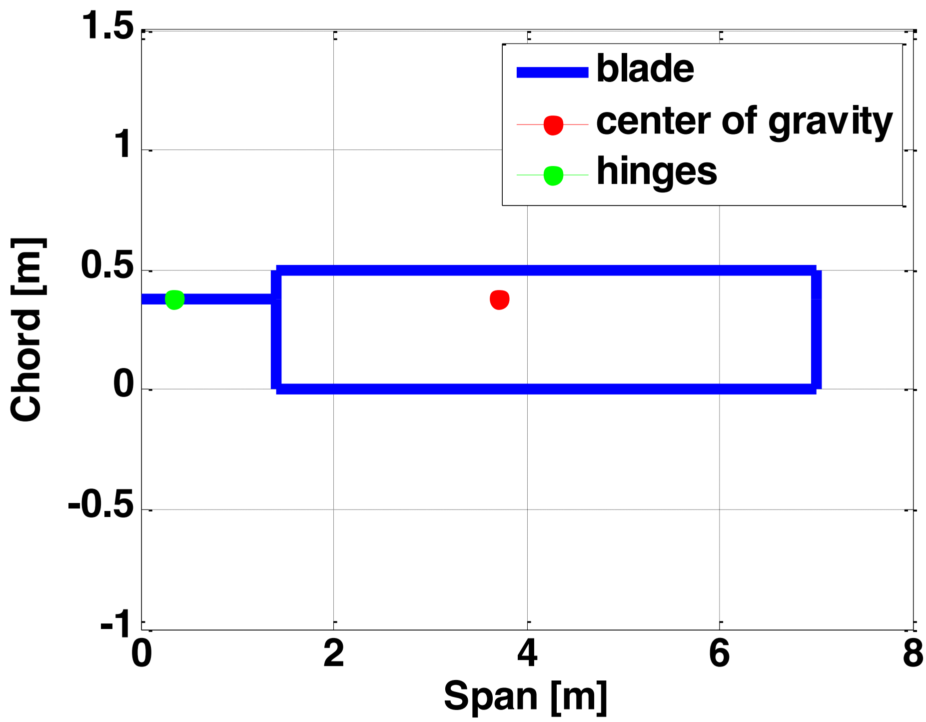

Figure 26. Schematic Representation of Main Rotor Blade Geometry

3.2.1.2. Aerodynamic Model

Aerodynamic model of the main rotor is detailed in Table 6. Note that η in Table 6 is the fraction of the blade radius and it is measured from the hub point.

Table 6. Main Rotor Aerodynamic Model

Name	Value/Information	Unit	Explanation
Root Cutout	0.2	η	The length of the root portion at which no aerodynamic load is generated since chord length is zero
Airfoil	NACA 0012	n/a	Same for every cross-section along the span
Blade Chord Length	0.5	m	Uniform along the span
Blade Sweep Angle	0	deg	Uniform along the span
Blade Twist Angle	0	deg	Uniform along the span
Blade Droop Angle	0	deg	Uniform along the span

3.2.2. Tail Rotor Model

Some fundamental parameters of the tail rotor are given in Table 7.

Table 7. Tail Rotor Fundamental Parameters

Name	Value/Information	Unit	Explanation
Hub Location	14, -0.5, 4	m	In loads axis system
Rotation Direction	Counter-Clockwise	n/a	When viewed from right
Number of Blades	4	n/a	n/a

Table 7 continued

Name	Value/Information	Unit	Explanation
Rotor Orientation	0, 0, -100	deg	Ψ_{tr}, Θ_{tr}, Φ_{tr}, respectively With respect to body axis system 10^0 cant up
Rotor Speed	1300	rpm	n/a
Radius	1.5	m	From rotor hub center to blade tip

3.2.2.1. Structural Model

Tail rotor blades are modeled as rigid since blade elasticity does not have an important effect on the fuselage static limit loads. Structural model of the tail rotor is detailed in Table 8 and schematic representation of the blade geometry is presented in Figure 27. Note that η in Table 8 is the fraction of the blade radius and it is measured from the hub point.

Table 8. Tail Rotor Structural Model

Name	Value/Information	Unit	Explanation
Rotor Type	Fully Articulated	n/a	Flap, lead-lag hinges and pitch bearings exist on the rotor
Precone Angle	0	deg	The preset cone angle [10]
Hinge Offset	0.1	η	Flap, lead-lag hinges and pitch bearing are at the same spanwise location Measured from rotor hub center
Blade Mass	4	kg	Mass of a blade

Table 8 continued

Name	Value/Information	Unit	Explanation
Torque Offset	0	m	Offset of pitch change axis from rotor hub center in blade axis system y direction (see Figure 19)
Blade Center of Gravity Chordwise Location	quarter chord	m	n/a
Blade Center of Gravity Spanwise Location	0.557	η	Measured from the rotor hub center

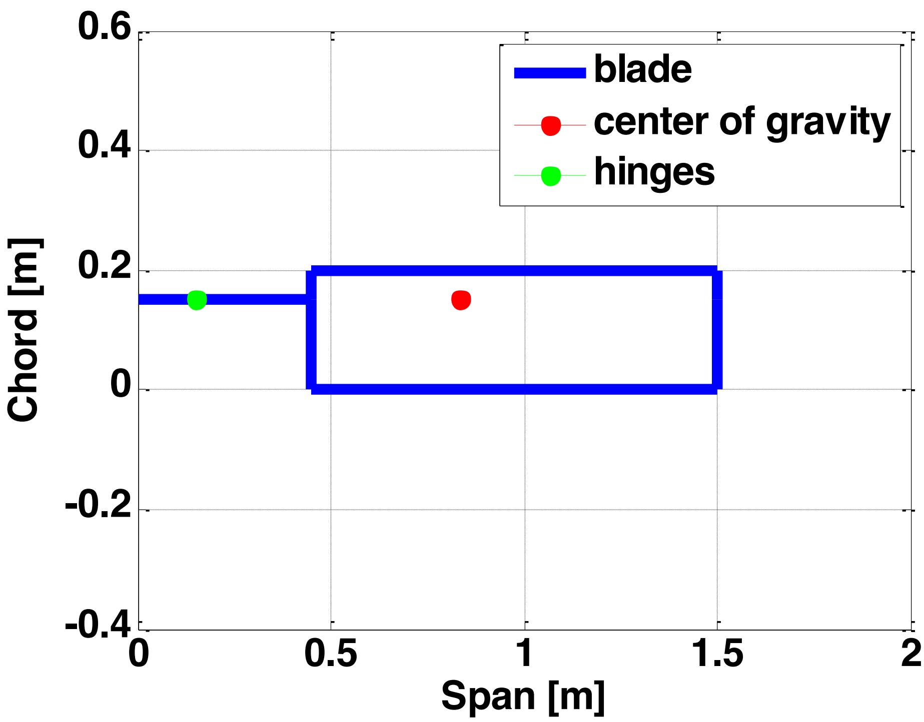

Figure 27. Schematic Representation of Tail Rotor Blade Geometry

3.2.2.2. Aerodynamic Model

Aerodynamic model of the tail rotor is detailed in Table 9. Note that η in Table 9 is the fraction of the blade radius and it is measured from the hub point.

Table 9. Tail Rotor Aerodynamic Model

Name	Value/Information	Unit	Explanation
Root Cutout	0.3	η	The length of the root portion at which no aerodynamic load is generated since chord length is zero
Airfoil	NACA 0012	n/a	Same for every cross-section along the span
Blade Chord Length	0.2	m	Uniform along the span
Blade Sweep Angle	0	deg	Uniform along the span
Blade Twist Angle	0	deg	Uniform along the span
Blade Droop Angle	0	deg	Uniform along the span

3.2.3. Airframe Model

Some fundamental dimensions of the airframe are given in Table 10.

Table 10. Airframe Fundamental Parameters

Name	Value/Information	Unit
Length	14	m
Max Width	3	m
Max Height	2.7	m

3.2.3.1. Structural Model

Airframe is modeled as rigid since this thesis aims to calculate the static limit loads on the fuselage. Therefore, structural model is comprised of inertia model only. However, the monitor stations used to monitor the loads on the fuselage and generate axial force, shear force, torsional moment, and bending moment diagrams are also explained in this chapter.

3.2.3.1.1. Inertia Model

Mass states can be defined as mass conditions that the rotorcraft can fly. Its effect on flight dynamics analysis is through mass, center of gravity location, and moment of inertia matrix about the center of gravity location. However, for the fuselage loads, the airframe cannot be modeled as a single rigid body. Instead, an inertia model with higher resolution is necessary. The accuracy of the loads increase as the resolution increases.

A mass state, named as M01, representing maximum take-off weight with nominal center of gravity location is used in this thesis. The mass and center of gravity locations in loads axis system of the mass items constituting this mass state can be found in Table 11. Furthermore, schematic representation of mass state M01 is presented in Figure 28 to Figure 31. Note that the green dots in these figures represent the mass items. Finally, airframe mass and the center of gravity location of mass state M01 in LAS can be found in Table 12.

Table 11. Mass Items Constituting Mass State M01

Fuselage Structural Mass				
Mass Item	**Mass [kg]**	**cg_x [m]**	**cg_y [m]**	**cg_z [m]**
x = 0.00 [m] - 0.50 [m]	0.000	0.250	0.000	1.200
x = 0.50 [m] - 1.00 [m]	18.000	0.750	0.000	1.200
x = 1.00 [m] - 1.50 [m]	28.000	1.250	0.000	1.260
x = 1.50 [m] - 2.00 [m]	37.500	1.750	0.000	1.320
x = 2.00 [m] - 2.50 [m]	42.500	2.250	0.000	1.440
x = 2.50 [m] - 3.00 [m]	55.000	2.750	0.000	1.550

Table 11 continued

Mass Item	Mass [kg]	cg_x [m]	cg_y [m]	cg_z [m]
x = 3.00 [m] - 3.50 [m]	65.000	3.250	0.000	1.720
x = 3.50 [m] - 4.00 [m]	75.000	3.750	0.000	1.920
x = 4.00 [m] - 4.50 [m]	85.000	4.250	0.000	1.920
x = 4.50 [m] - 4.75 [m]	90.000	4.625	0.000	1.920
x = 4.75 [m] - 5.25 [m]	110.000	5.000	0.000	1.920
x = 5.25 [m] - 5.50 [m]	90.000	5.375	0.000	1.920
x = 5.50 [m] - 6.00 [m]	85.000	5.750	0.000	1.920
x = 6.00 [m] - 6.50 [m]	80.000	6.250	0.000	1.920
x = 6.50 [m] - 7.00 [m]	70.000	6.750	0.000	1.920
x = 7.00 [m] - 7.50 [m]	65.000	7.250	0.000	2.000
x = 7.50 [m] - 8.00 [m]	50.000	7.750	0.000	2.100
x = 8.00 [m] - 8.50 [m]	35.000	8.250	0.000	2.200
x = 8.50 [m] - 9.00 [m]	27.000	8.750	0.000	2.290
x = 9.00 [m] - 9.50 [m]	22.000	9.250	0.000	2.330
x = 9.50 [m] - 10.00 [m]	18.000	9.750	0.000	2.360
x = 10.00 [m] - 10.50 [m]	15.000	10.250	0.000	2.390
x = 10.50 [m] - 11.00 [m]	12.000	10.750	0.000	2.415
x = 11.00 [m] - 11.50 [m]	10.000	11.250	0.000	2.440
x = 11.50 [m] - 12.00 [m]	8.000	11.750	0.000	2.445
x = 12.00 [m] - 12.50 [m]	7.000	12.250	0.000	2.450
x = 12.50 [m] - 13.00 [m]	6.000	12.750	0.000	2.470
x = 13.00 [m] - 13.50 [m]	5.000	13.250	0.000	2.480
x = 13.50 [m] - 14.00 [m]	4.000	13.750	0.000	2.480
x = 14.00 [m] - 14.50 [m]	2.000	14.250	0.000	2.480
Horizontal Tail Structural Mass				
Mass Item	**Mass [kg]**	**cg_x [m]**	**cg_y [m]**	**cg_z [m]**
x = 12.75 [m] y = 1.00 [m] - 1.50 [m]	2.500	12.750	1.250	2.220
x = 12.75 [m] y = 0.50 [m] - 1.00 [m]	2.500	12.750	0.750	2.220

Table 11 continued

Mass Item	Mass [kg]	cg_x [m]	cg_y [m]	cg_z [m]
x = 12.75 [m] y = 0.00 [m] - 0.50 [m]	2.500	12.750	0.250	2.220
x = 12.75 [m] y = 0.00 [m] - (-0.50) [m]	2.500	12.750	-0.250	2.220
x = 12.75 [m] y = (-0.50) [m] - (-1.00) [m]	2.500	12.750	-0.750	2.220
x = 12.75 [m] y = (-1.00) [m] - (-1.50) [m]	2.500	12.750	-1.250	2.220
Vertical Fin Structural Mass				
Mass Item	**Mass [kg]**	**cg_x [m]**	**cg_y [m]**	**cg_z [m]**
Section 1	6.000	13.150	0.000	3.000
Section 2	6.000	13.500	0.000	3.450
Section 3	6.000	13.850	0.000	3.870
Landing Gear				
Mass Item	**Mass [kg]**	**cg_x [m]**	**cg_y [m]**	**cg_z [m]**
Left Main Landing Gear (Retracted)	50.000	6.100	-0.650	1.000
Right Main Landing Gear (Retracted)	50.000	6.100	0.650	1.000
Nose Landing Gear (Retracted)	30.000	1.400	0.000	1.000
Fuel				
Mass Item	**Mass [kg]**	**cg_x [m]**	**cg_y [m]**	**cg_z [m]**
Left Fuel Tank	150.000	5.400	-0.600	1.500
Right Fuel Tank	150.000	5.400	0.600	1.500
Engines				
Mass Item	**Mass [kg]**	**cg_x [m]**	**cg_y [m]**	**cg_z [m]**
Left Engine	150.000	6.000	-0.500	3.000

Table 11 continued

Mass Item	**Mass [kg]**	**cg_x [m]**	**cg_y [m]**	**cg_z [m]**
Right Engine	150.000	6.000	0.500	3.000
Transmission				
Mass Item	**Mass [kg]**	**cg_x [m]**	**cg_y [m]**	**cg_z [m]**
Main Gearbox	250.000	5.200	0.000	3.000
Tail Gearbox	20.000	14.000	0.120	3.930
Intermediate Gearbox	10.000	12.750	0.000	2.600
Main Rotor				
Mass Item	**Mass [kg]**	**cg_x [m]**	**cg_y [m]**	**cg_z [m]**
Main Rotor Hub	100.000	5.000	0.000	4.000
Main Rotor Swashplate	40.000	5.025	0.000	3.750
Tail Rotor				
Mass Item	**Mass [kg]**	**cg_x [m]**	**cg_y [m]**	**cg_z [m]**
Tail Rotor Hub	20.000	14.000	0.500	4.000
ECS and FLIR				
Mass Item	**Mass [kg]**	**cg_x [m]**	**cg_y [m]**	**cg_z [m]**
ECS (Cooling System)	30.000	4.200	0.000	3.000
FLIR	100.000	1.000	0.000	0.900
Cargo				
Mass Item	**Mass [kg]**	**cg_x [m]**	**cg_y [m]**	**cg_z [m]**
Internal Cargo	100.000	4.700	0.000	1.500
Pilots and Seats				
Mass Item	**Mass [kg]**	**cg_x [m]**	**cg_y [m]**	**cg_z [m]**
Pilot with Seat	110.000	2.500	-0.500	1.500
Co-pilot with Seat	110.000	2.500	0.500	1.500

Table 11 continued

Passengers and Seats				
Mass Item	**Mass [kg]**	**cg_x [m]**	**cg_y [m]**	**cg_z [m]**
Passenger 1 with Seat	100.000	3.400	-0.750	1.500
Passenger 2 with Seat	100.000	3.400	-0.250	1.500
Passenger 3 with Seat	100.000	3.400	0.250	1.500
Passenger 4 with Seat	100.000	3.400	0.750	1.500
Passenger 5 with Seat	100.000	4.000	-0.750	1.500
Passenger 6 with Seat	100.000	4.000	-0.250	1.500
Passenger 7 with Seat	100.000	4.000	0.250	1.500
Passenger 8 with Seat	100.000	4.000	0.750	1.500

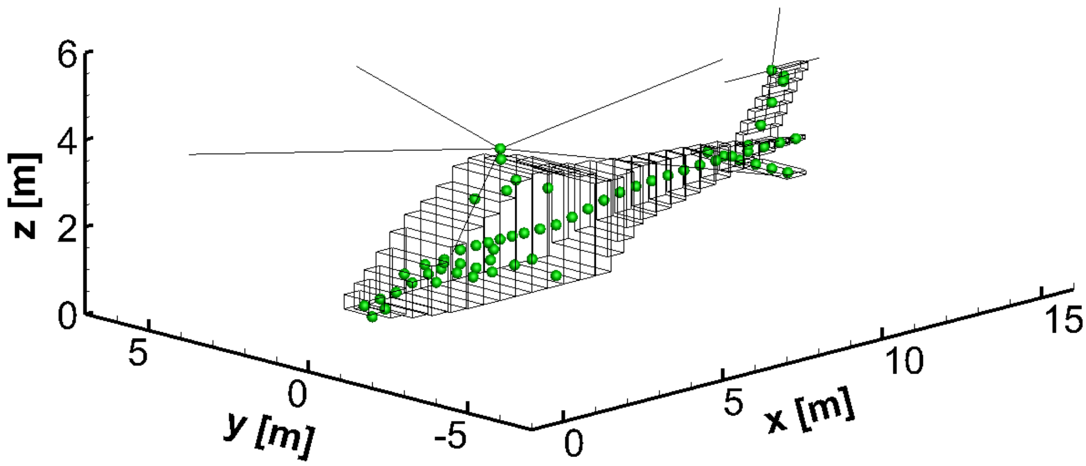

Figure 28. Schematic Representation of Mass State M01, Isometric View

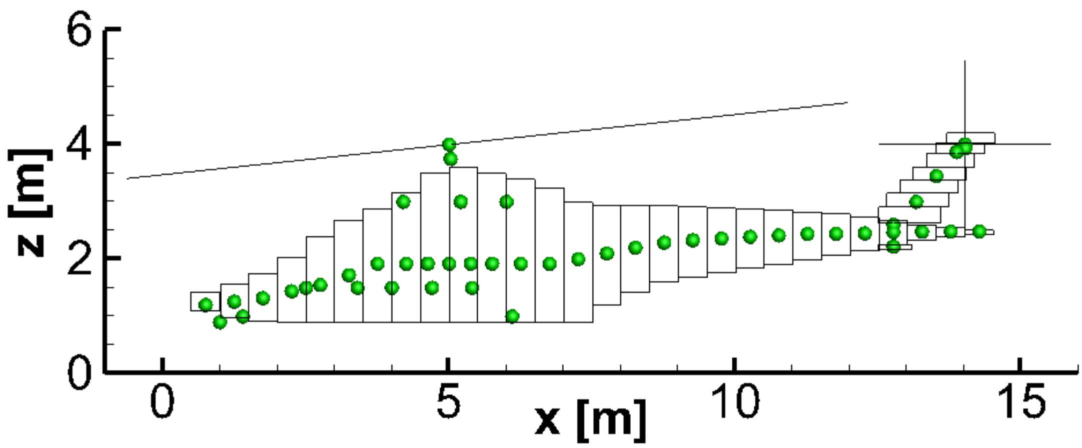

Figure 29. Schematic Representation of Mass State M01, Side View

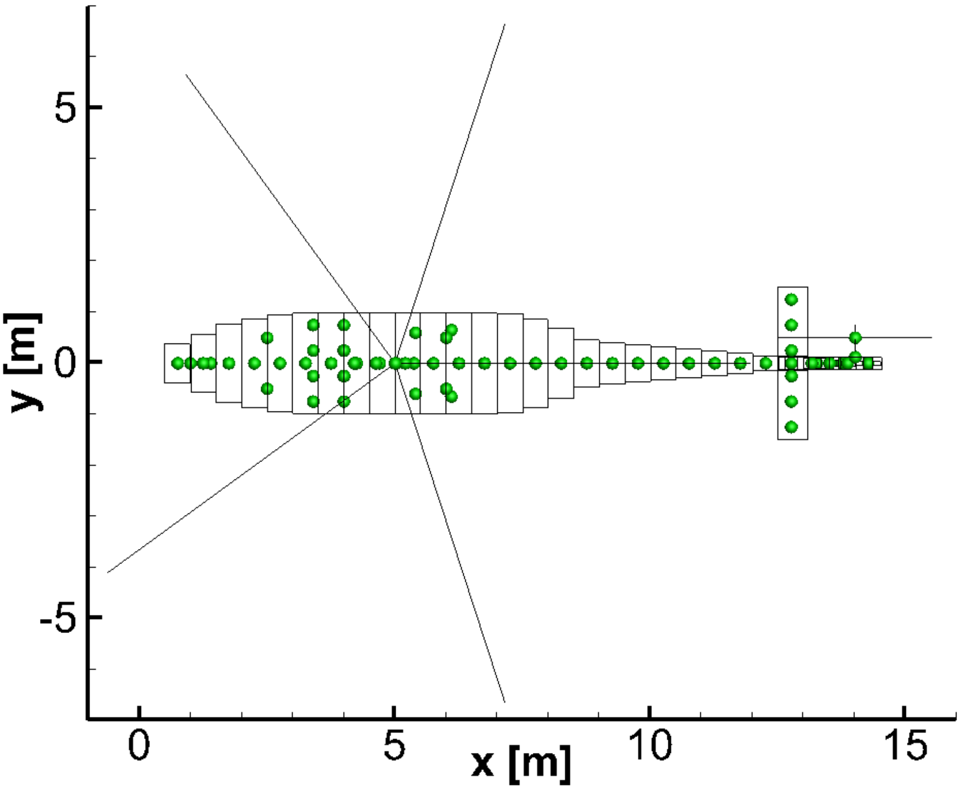

Figure 30. Schematic Representation of Mass State M01, Top View

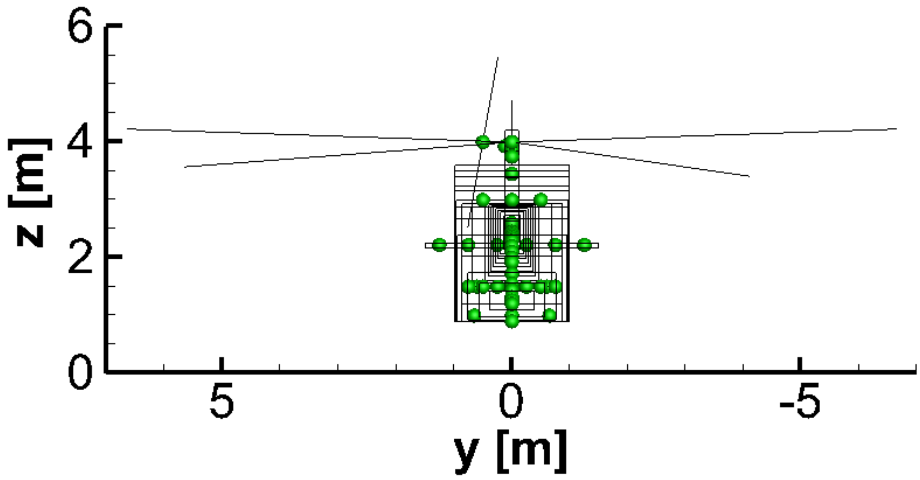

Figure 31. Schematic Representation of Mass State M01, Front View

Table 12. Airframe Mass and Center of Gravity Location for Mass State M01

Mass [kg]	cg_x [m]	cg_y [m]	cg_z [m]
3670	4.929	0.003	1.971

3.2.3.1.2. Monitor Stations

Monitor stations are used to monitor the sectional loads. The forces and moments acting on the rotorcraft fuselage are integrated to these locations and sectional axial force, shear force, torsional moment, and bending moments are obtained. After that, critical flight conditions are chosen based on these loads so that structural analysis can be performed on these critical conditions.

The locations of the monitor stations are chosen based on the fuselage frame locations and the mass items on the rotorcraft. The locations of the frames is an important input to the monitor station locations since critical loading conditions are determined based on the loads at the monitor stations and it is important to know the loading on the frame instead of between the frames, for example. Furthermore, the locations of the heavy mass items in the inertia model is an input to the monitor station locations because the masses generate inertial loading on the fuselage and this results in different forces and moments at cross-sections between the two sides of a mass item. The change in the cross-sectional loads can be captured by using monitor stations at each side of the mass items.

In this thesis, the monitor stations on the rotorcraft are chosen such that the edges of the fuselage structural model and the mass item locations are used. A monitor station is defined for each structural segment edge (given in Table 11) and two monitor stations for each mass item is defined, one for each side of the mass item in the longitudinal direction. These are called as double-stations and they are separated from each other by 2 [mm]. This approach resulted in 55 monitor stations on the fuselage. No monitor station is defined on the horizontal tail and vertical fin since this thesis aims to calculate the loads on the fuselage only. The locations of the monitor stations in LAS are given in Table 13 and schematic representation is presented in Figure 32 to Figure 35. Note that the red dots in these figures represent the monitor stations.

Table 13. Monitor Station Locations

Monitor Station Name	x [m]	y [m]	z [m]
MON_STA_1	0.50000	0.00000	1.20000
MON_STA_2	0.99900	0.00000	1.22988
MON_STA_3	1.00100	0.00000	1.23012
MON_STA_4	1.39900	0.00000	1.27788
MON_STA_5	1.40100	0.00000	1.27812
MON_STA_6	1.50000	0.00000	1.29000
MON_STA_7	2.00000	0.00000	1.38000
MON_STA_8	2.49900	0.00000	1.49478
MON_STA_9	2.50100	0.00000	1.49522
MON_STA_10	3.00000	0.00000	1.63500
MON_STA_11	3.39900	0.00000	1.77960
MON_STA_12	3.40100	0.00000	1.78040
MON_STA_13	3.50000	0.00000	1.82000
MON_STA_14	3.99900	0.00000	1.92000
MON_STA_15	4.00100	0.00000	1.92000
MON_STA_16	4.19900	0.00000	1.92000
MON_STA_17	4.20100	0.00000	1.92000
MON_STA_18	4.50000	0.00000	1.92000
MON_STA_19	4.69900	0.00000	1.92000
MON_STA_20	4.70100	0.00000	1.92000
MON_STA_21	4.75000	0.00000	1.92000
MON_STA_22	5.00000	0.00000	1.92000
MON_STA_23	5.02400	0.00000	1.92000
MON_STA_24	5.02600	0.00000	1.92000
MON_STA_25	5.03900	0.00000	1.92000
MON_STA_26	5.04100	0.00000	1.92000
MON_STA_27	5.19900	0.00000	1.92000
MON_STA_28	5.20100	0.00000	1.92000
MON_STA_29	5.25000	0.00000	1.92000
MON_STA_30	5.39900	0.00000	1.92000
MON_STA_31	5.40100	0.00000	1.92000
MON_STA_32	5.50000	0.00000	1.92000
MON_STA_33	5.99900	0.00000	1.92000
MON_STA_34	6.00100	0.00000	1.92000
MON_STA_35	6.09900	0.00000	1.92000
MON_STA_36	6.10100	0.00000	1.92000
MON_STA_37	6.50000	0.00000	1.92000
MON_STA_38	7.00000	0.00000	1.96000

Table 13 continued

Monitor Station Name	x [m]	y [m]	z [m]
MON_STA_39	7.50000	0.00000	2.05000
MON_STA_40	7.50000	0.00000	2.05000
MON_STA_41	8.00000	0.00000	2.15000
MON_STA_42	8.50000	0.00000	2.24500
MON_STA_43	9.00000	0.00000	2.31000
MON_STA_44	9.50000	0.00000	2.34500
MON_STA_45	10.00000	0.00000	2.37500
MON_STA_46	10.50000	0.00000	2.40250
MON_STA_47	11.00000	0.00000	2.42750
MON_STA_48	11.50000	0.00000	2.44250
MON_STA_49	12.00000	0.00000	2.44750
MON_STA_50	12.45000	0.00000	2.45800
MON_STA_51	13.09900	0.00000	2.47698
MON_STA_52	13.10100	0.00000	2.47702
MON_STA_53	13.50000	0.00000	2.48000
MON_STA_54	14.00000	0.00000	2.48000
MON_STA_55	14.50000	0.00000	2.48000

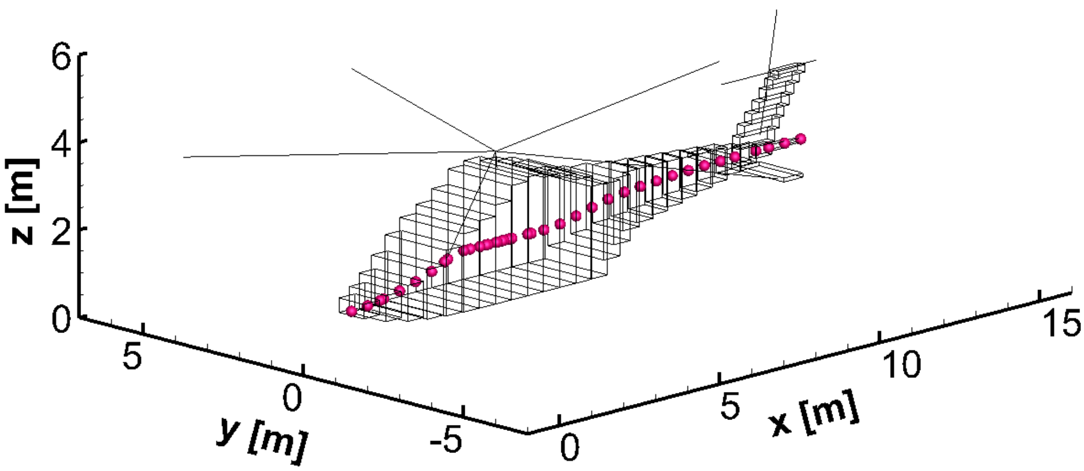

Figure 32. Schematic Representation of Monitor Stations, Isometric View

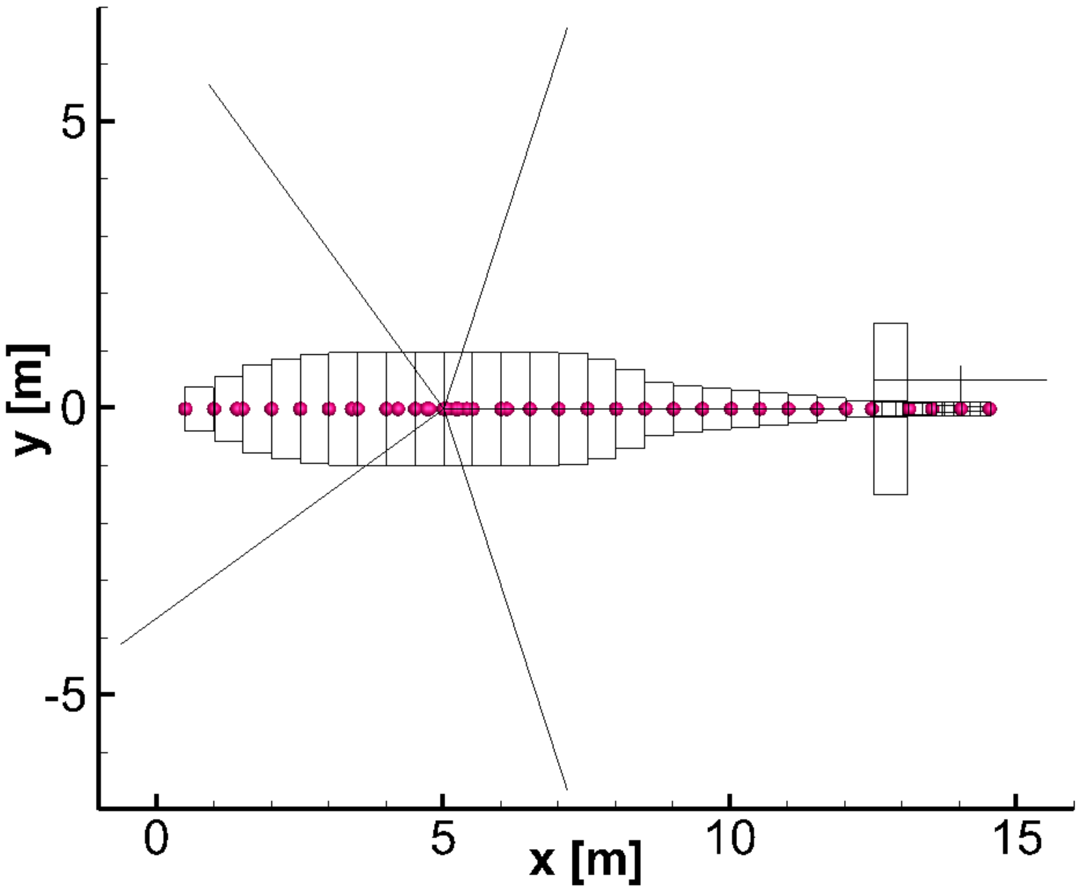

Figure 33. Schematic Representation of Monitor Stations, Top View

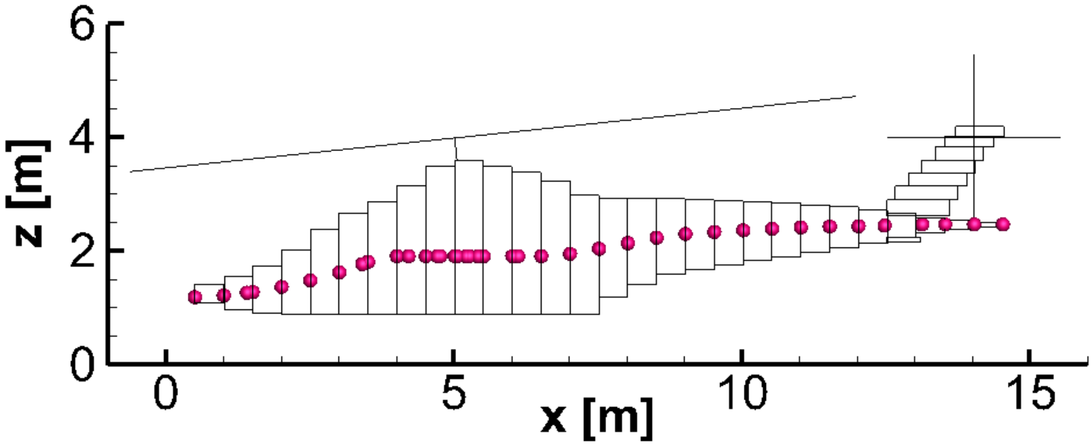

Figure 34. Schematic Representation of Monitor Stations, Side View

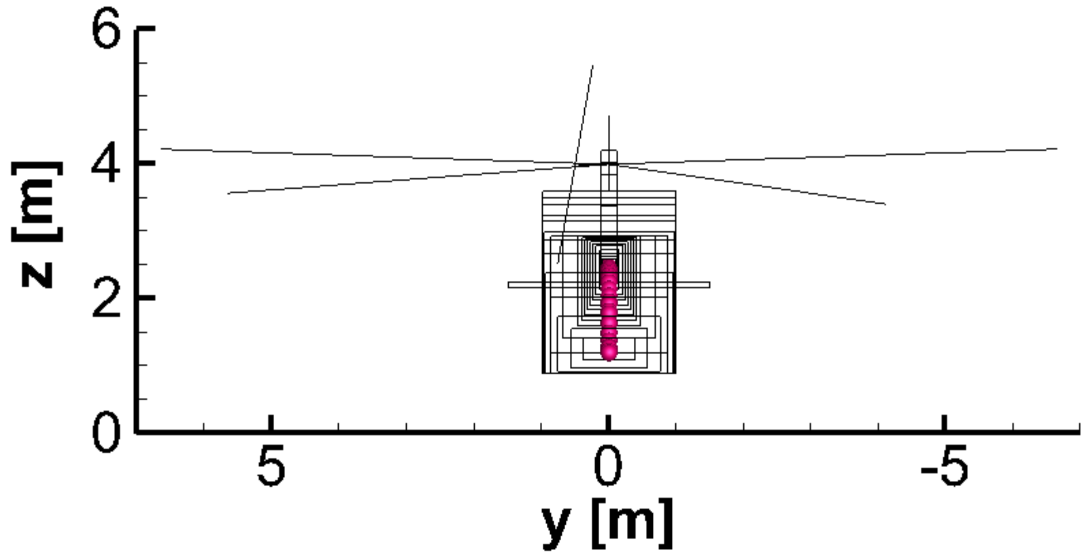

Figure 35. Schematic Representation of Monitor Stations, Front View

Although a high number of monitor stations is used in this thesis, a sensitivity study has been performed by increasing the number of monitor stations and the results are presented in Appendix A. It can be observed that further increasing the number of monitor stations changes only the axial force diagram but the difference is insignificant. The difference is due to the aerodynamic loading since the change in the inertial loading is already captured by the double-stations explained above.

As it can be seen in Table 13 and in Figure 32 to Figure 35, the major change in the monitor station locations is in the longitudinal direction. The vertical position is calculated to be close to the mid-point of the sections and lateral position is always zero. This is due to the fact that the loads on the fuselage sections change in the longitudinal direction more than the other two directions since the fuselage length is higher than the width and height. Although the stress may differ in lateral and vertical directions at a cross-section, the mid-point can be used to have an idea about the loading at that section and to choose the critical conditions.

3.2.3.2. Aerodynamic Model

The aerodynamic model is comprised of pressures on 197179 nodes on the airframe obtained by using ANSYS Fluent for combinations of 12 angle of attack and 31 sideslip angles. No indigenous CFD calculation has been performed in this thesis and the aerodynamic data is taken from an outside source [29].

Since two-dimensional linear interpolation is used for flight dynamics analysis and fuselage loads calculation, the more the number of angle of attack and sideslip angle combinations for pressure distributions exist, the more accurate results can be obtained. The selected angle of attack values are given in Table 14 and the sideslip angle values are given in Table 15.

Table 14. Angle of Attack Values for the Airframe Aerodynamic Model

-90	-70	-40	-24
-15	-6	0	6
15	40	70	90

Table 15. Sideslip Angle Values for the Airframe Aerodynamic Model

-180	-175	-165	-160
-140	-120	-110	-90
-80	-70	-50	-30
-20	-16	-8	0
8	16	20	30
50	70	80	90
110	120	140	160
165	175	180	

The definition and sign convention of angle of attack and sideslip angle are given in Figure 36.

a. Angle of Attack

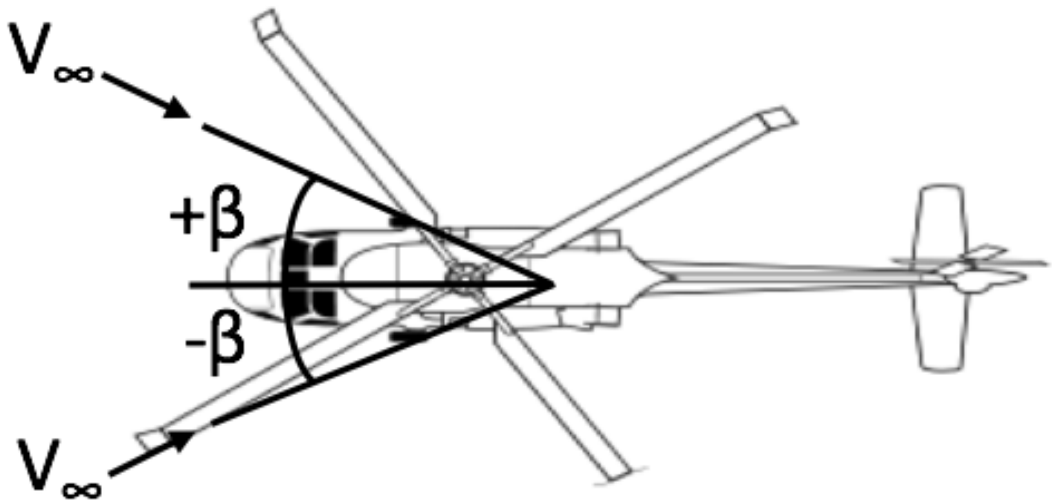

b. Sideslip Angle

Figure 36. Definition and Sign Convention of Angle of Attack and Sideslip Angle

CHAPTER 4

THEORETICAL BACKGROUND

There are different types of loads with different sources acting on a rotorcraft fuselage. These loads are important for both flight dynamics analysis and fuselage loads calculation and they are categorized based on their sources as follows:

1. Aerodynamic Loads
2. Inertial Loads
3. Hub Loads

These loads are calculated for both flight dynamics analysis (for both transient solution and ROFLOT approach) and fuselage loads calculation. However, while flight dynamics analysis requires point loads to solve the equations of the motion of the rotorcraft, fuselage loads calculation requires distributed loads.

4.1. Flight Dynamics Analysis

In order to calculate the loads on a rotorcraft fuselage during flight, the first step is to perform flight dynamics analysis, which refers to both transient solution and ROFLOT analysis, in order to obtain the hub loads acting on the fuselage and the states of the rotorcraft. The states are angular and linear velocities and accelerations of the rotorcraft as well as rotorcraft orientation (Euler angles), angle of attack and sideslip angle.

In order to perform flight dynamics analysis, a mathematical model of the full rotorcraft is established. This model uses integrated (total) parameters which are used to calculate total aerodynamic and inertial loads on the fuselage. Moreover, main rotor and tail rotor hub loads are calculated. After calculating all the point loads on the fuselage, equations of motion of the rotorcraft are solved. Since this thesis aims to calculate the rotorcraft fuselage limit loads and given the fact that it is very difficult to calculate the rotor hub loads with a realistic rotor model, Flightlab [13, 26, 27], explained in Chapter 2.3.5 is used to calculate the hub loads and perform flight dynamics analysis for both transient solution and ROFLOT approach.

4.1.1. Integrated Aerodynamic Loads

Aerodynamic loads are in the form of pressure distribution on a mesh on the rotorcraft airframe. Pressure distributions are obtained for different angle of attack and sideslip angle combinations presented in Chapter 3.2.3.2. The pressure distribution for each angle of attack and sideslip angle combination is integrated to a reference point on the airframe in order to get the forces and moments acting at the reference point and converted to non-dimensional coefficients in body axis system.

The mesh is a triangular mesh as shown in Figure 37. The coordinates of the corners of the triangle are in loads axis system (LAS).

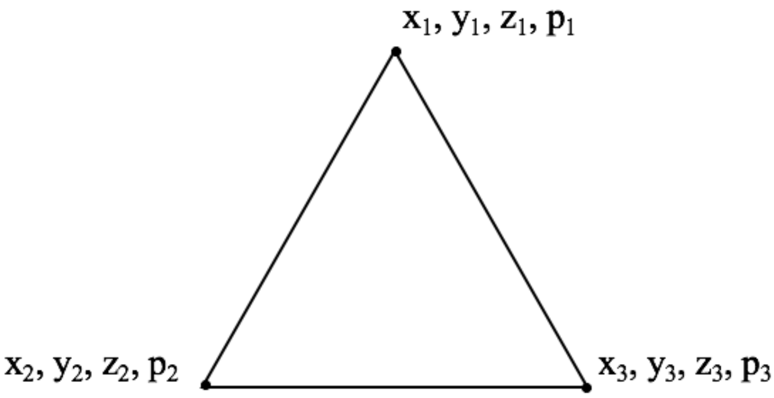

Figure 37. Aerodynamic Pressure on a Triangular Mesh

The pressure on the triangular mesh is the average of the pressure values defined at the nodes as given in Equation 3.

$$P_{mesh} = \frac{1}{3}\sum_{i=1}^{3} P_i \tag{3}$$

The area of the triangular mesh is calculated by using the magnitude of a cross product of any two sides as shown in Equation 4.

$$A_{mesh} = \frac{1}{2}\left\| \begin{Bmatrix} x_1 - x_2 \\ y_1 - y_2 \\ z_1 - z_2 \end{Bmatrix} \times \begin{Bmatrix} x_1 - x_3 \\ y_1 - y_3 \\ z_1 - z_3 \end{Bmatrix} \right\| \tag{4}$$

The total force acting at the geometrical center of the mesh given in Figure 37 is calculated by multiplying the pressure with the area as shown in Equation 5.

$$F_{mesh}^{mesh\_center} = P_{mesh} A_{mesh} \tag{5}$$

The geometrical center is calculated by using Equations 6, 7, and 8.

$$x_c = \frac{1}{3}\sum_{i=1}^{3} x_i \tag{6}$$

$$y_c = \frac{1}{3}\sum_{i=1}^{3} y_i \tag{7}$$

$$z_c = \frac{1}{3}\sum_{i=1}^{3} z_i \tag{8}$$

The direction of the force needs to be determined which is done by calculating the surface normal of the mesh. Creating two vectors from the two sides of the triangular mesh and performing a cross product in clock-wise direction gives the surface normal vector *N* towards the page (since pressure is positive towards the page, as well) in Figure 37 as shown in Equation 9.

$$\begin{Bmatrix} N_{x_{LAS}} \\ N_{y_{LAS}} \\ N_{z_{LAS}} \end{Bmatrix} = \begin{Bmatrix} x_2 - x_3 \\ y_2 - y_3 \\ z_2 - z_3 \end{Bmatrix} \times \begin{Bmatrix} x_1 - x_2 \\ y_1 - y_2 \\ z_1 - z_2 \end{Bmatrix} \tag{9}$$

The normal vector N is divided by its magnitude in order to obtain a unit vector as shown in Equation 10.

$$\begin{Bmatrix} t_{x_{LAS}} \\ t_{y_{LAS}} \\ t_{z_{LAS}} \end{Bmatrix} = \frac{\begin{Bmatrix} N_{x_{LAS}} \\ N_{y_{LAS}} \\ N_{z_{LAS}} \end{Bmatrix}}{\sqrt{N_{x_{LAS}}^2 + N_{y_{LAS}}^2 + N_{z_{LAS}}^2}} \tag{10}$$

So the force calculated in Equation 5 can be converted into a vector as shown in Equation 11.

$$\begin{Bmatrix} F_{x_{LAS}} \\ F_{y_{LAS}} \\ F_{z_{LAS}} \end{Bmatrix}_{mesh}^{mesh\_center} = F_{mesh} \begin{Bmatrix} t_{x_{LAS}} \\ t_{y_{LAS}} \\ t_{z_{LAS}} \end{Bmatrix} \tag{11}$$

Finally, the force vector calculated in Equation 11 is translated to the reference point as shown in Equations 12 and 13. Note that since forces and moments are in LAS, the positions in Equations 12 and 13 are in LAS, as well.

$$\begin{Bmatrix} F_{x_{LAS}} \\ F_{y_{LAS}} \\ F_{z_{LAS}} \end{Bmatrix}_{mesh}^{ref.pt.} = \begin{Bmatrix} F_{x_{LAS}} \\ F_{y_{LAS}} \\ F_{z_{LAS}} \end{Bmatrix}_{mesh}^{mesh\_center} \tag{12}$$

$$\begin{Bmatrix} M_{x_{LAS}} \\ M_{y_{LAS}} \\ M_{z_{LAS}} \end{Bmatrix}_{mesh}^{ref.pt.} = \begin{Bmatrix} r_{x_{LAS}} \\ r_{y_{LAS}} \\ r_{z_{LAS}} \end{Bmatrix}^{c/ref,aero} \times \begin{Bmatrix} F_{x_{LAS}} \\ F_{y_{LAS}} \\ F_{z_{LAS}} \end{Bmatrix}_{mesh}^{mesh\_center} \tag{13}$$

Equations 3 to 13 are presented considering a single mesh. There are hundreds of meshes around the airframe and the same calculations are performed for each mesh. After that, the forces and moments due to each mesh acting at the reference point is added together as shown in Equations 14 and 15.

$$\begin{Bmatrix} F_{x_{LAS}} \\ F_{y_{LAS}} \\ F_{z_{LAS}} \end{Bmatrix}_{aero,database}^{ref.pt.} = \sum_{i=1}^{\#\,of\,mesh} \begin{Bmatrix} F_{x_{LAS}} \\ F_{y_{LAS}} \\ F_{z_{LAS}} \end{Bmatrix}_{mesh,i}^{ref.pt.} \tag{14}$$

$$\begin{Bmatrix} M_{x_{LAS}} \\ M_{y_{LAS}} \\ M_{z_{LAS}} \end{Bmatrix}_{aero,database}^{ref.pt.} = \sum_{i=1}^{\#\,of\,mesh} \begin{Bmatrix} M_{x_{LAS}} \\ M_{y_{LAS}} \\ M_{z_{LAS}} \end{Bmatrix}_{mesh,i}^{ref.pt.} \tag{15}$$

After calculating the aerodynamic forces and moments acting at the aerodynamic reference point in LAS, they are converted to non-dimensional coefficients in body axis system by dividing them by reference area, reference length (only for the moment coefficients) and the dynamic pressure of the aerodynamic solution and multiplying x and z components by -1 as shown in Equations 16, 17, and 18 [30]. These coefficients are then used as input to Flightlab. Based on the angle of attack and sideslip angle of the fuselage, two-dimensional linear interpolation is performed in order to get the aerodynamic force and moment coefficients at the reference point for that particular angle of attack and sideslip angle. After that, the coefficients are multiplied by the corresponding dynamic pressure of the condition, reference area, and reference length in order to get the aerodynamic forces in body axis system as shown in Equations 16, 19, and 20 [30].

$$Q = \frac{1}{2}\rho V^2 \tag{16}$$

$$\begin{Bmatrix} C_{F_{x_{body}}} \\ C_{F_{y_{body}}} \\ C_{F_{z_{body}}} \end{Bmatrix}^{ref.pt.} = \frac{\begin{Bmatrix} -F_{x_{LAS}} \\ F_{y_{LAS}} \\ -F_{z_{LAS}} \end{Bmatrix}^{ref.pt.}_{aero,database}}{Q_{database} S_{ref}} \tag{17}$$

$$\begin{Bmatrix} C_{M_{x_{body}}} \\ C_{M_{y_{body}}} \\ C_{M_{z_{body}}} \end{Bmatrix}^{ref.pt.} = \frac{\begin{Bmatrix} -M_{x_{LAS}} \\ M_{y_{LAS}} \\ -M_{z_{LAS}} \end{Bmatrix}^{ref.pt.}_{aero,database}}{Q_{database} S_{ref} c_{ref}} \tag{18}$$

$$\begin{Bmatrix} F_{x_{body}} \\ F_{y_{body}} \\ F_{z_{body}} \end{Bmatrix}^{ref.pt.}_{aero,condition} = Q_{condition} S_{ref} \begin{Bmatrix} C_{F_{x_{body}}} \\ C_{F_{y_{body}}} \\ C_{F_{z_{body}}} \end{Bmatrix}^{ref.pt.} \tag{19}$$

$$\begin{Bmatrix} M_{x_{body}} \\ M_{y_{body}} \\ M_{z_{body}} \end{Bmatrix}^{ref.pt.}_{aero,condition} = Q_{condition} S_{ref} c_{ref} \begin{Bmatrix} C_{M_{x_{body}}} \\ C_{M_{body}} \\ C_{M_{z_{body}}} \end{Bmatrix}^{ref.pt.} \tag{20}$$

After that, the aerodynamic forces and moments are translated from the aerodynamic reference point to the airframe center of gravity as shown in Equations 21 and 22. Note that since forces and moments are in body axis system, the positions in Equations 21 and 22 are in the body axis system, as well.

$$\begin{Bmatrix} F_{x_{body}} \\ F_{y_{body}} \\ F_{z_{body}} \end{Bmatrix}_{aero,condition}^{cg,airf} = \begin{Bmatrix} F_{x_{body}} \\ F_{y_{body}} \\ F_{z_{body}} \end{Bmatrix}_{aero,condition}^{ref.pt.} \tag{21}$$

$$\begin{Bmatrix} M_{x_{body}} \\ M_{y_{body}} \\ M_{z_{body}} \end{Bmatrix}_{aero,condition}^{cg,airf} = \begin{Bmatrix} r_{x_{body}} \\ r_{y_{body}} \\ r_{z_{body}} \end{Bmatrix}^{ref,aero/cg,airf} \times \begin{Bmatrix} F_{x_{body}} \\ F_{y_{body}} \\ F_{z_{body}} \end{Bmatrix}_{aero,condition}^{ref.pt.} + \begin{Bmatrix} M_{x_{body}} \\ M_{y_{body}} \\ M_{z_{body}} \end{Bmatrix}_{aero,condition}^{ref.pt.} \tag{22}$$

After calculating the aerodynamic forces and moments acting at the airframe center of gravity, the effect of airframe aerodynamics on the flight dynamics can be calculated.

The aerodynamic loads calculated with the method explained above are checked against the aerodynamic loads obtained from Flightlab in order to make sure that they are equal.

4.1.2. Integrated Inertial Loads

The mass items given in Table 11 are used to calculate the airframe mass, center of gravity location, and moment of inertia matrix. These values are used as input to Flightlab in order to perform flight dynamics analysis. The equations governing these calculations are given in Equations 23 through 32. Note that the positions of the mass items are in LAS. Center of gravity and moment of inertia matrix are converted to the body axis system in Equations 24, 26, 30, and 32 by multiplying them by -1.

$$m_{airf} = \sum_{n=1}^{\#\ of\ mp} m_{mp,n} \tag{23}$$

$$x_{cg,airf} = -\sum_{n=1}^{\#\ of\ mp} (x_{cg,mp,n} * m_{mp,n}) \Bigg/ \sum_{n=1}^{\#\ of\ mp} m_{mp,n} \tag{24}$$

$$y_{cg,airf} = \sum_{n=1}^{\#\,of\,mp} (y_{cg,mp,n} * m_{mp,n}) \Bigg/ \sum_{n=1}^{\#\,of\,mp} m_{mp,n} \tag{25}$$

$$z_{cg,airf} = -\sum_{n=1}^{\#\,of\,mp} (z_{cg,mp,n} * m_{mp,n}) \Bigg/ \sum_{n=1}^{\#\,of\,mp} m_{mp,n} \tag{26}$$

$$I_{xx}^{cg,airf} = \sum_{n=1}^{\#\,of\,mp} ((y_{cg,mp,n} - y_{cg,airf})^2 + (z_{cg,mp} - z_{cg,airf})^2)\, m_{mp,n} \tag{27}$$

$$I_{yy}^{cg,airf} = \sum_{n=1}^{\#\,of\,mp} ((x_{cg,mp,n} - x_{cg,airf})^2 + (z_{cg,mp} - z_{cg,airf})^2)\, m_{mp,n} \tag{28}$$

$$I_{zz}^{cg,airf} = \sum_{n=1}^{\#\,of\,mp} ((x_{cg,mp,n} - x_{cg,airf})^2 + (y_{cg,mp} - y_{cg,airf})^2)\, m_{mp,n} \tag{29}$$

$$I_{xy}^{cg,airf} = -\sum_{n=1}^{\#\,of\,mp} \left((x_{cg,mp,n} - x_{cg,airf}\right) * (y_{cg,mp,n} - y_{cg,airf}))\, m_{mp,n} \tag{30}$$

$$I_{xz}^{cg,airf} = \sum_{n=1}^{\#\,of\,mp} \left((x_{cg,mp,n} - x_{cg,airf}\right) * (z_{cg,mp,n} - z_{cg,airf}))\, m_{mp,n} \tag{31}$$

$$I_{yz}^{cg,airf} = -\sum_{n=1}^{\#\,of\,mp} \left((y_{cg,mp,n} - y_{cg,airf}\right) * (z_{cg,mp,n} - z_{cg,airf}))\, m_{mp,n} \tag{32}$$

The gravitational acceleration acts only on the z direction of the inertial axis system (towards the earth center) and it should to be rotated to the body axis system by the roll and pitch angle of the rotorcraft. The equation for this calculation is given in Equation 36. Equations 33, 34, and 35 show how Equation 36 is obtained [31].

$$\begin{Bmatrix} g_{x_{body}} \\ g_{y_{body}} \\ g_{z_{body}} \end{Bmatrix} = f(\phi,\theta) \begin{Bmatrix} 0 \\ 0 \\ g_z \end{Bmatrix} \tag{33}$$

where,

$$f(\phi,\theta) = \begin{bmatrix} 1 & 0 & 0 \\ 0 & \cos(\phi) & \sin(\phi) \\ 0 & -\sin(\phi) & \cos(\phi) \end{bmatrix} * \begin{bmatrix} \cos(\theta) & 0 & -\sin(\theta) \\ 0 & 1 & 0 \\ \sin(\theta) & 0 & \cos(\theta) \end{bmatrix} \tag{34}$$

which is equal to,

$$f(\phi,\theta) = \begin{bmatrix} \cos(\theta) & 0 & -\sin(\theta) \\ \sin(\phi)\sin(\theta) & \cos(\phi) & \sin(\phi)\cos(\theta) \\ \cos(\phi)\sin(\theta) & -\sin(\phi) & \cos(\phi)\cos(\theta) \end{bmatrix} \tag{35}$$

So,

$$\begin{Bmatrix} g_{x_{body}} \\ g_{y_{body}} \\ g_{z_{body}} \end{Bmatrix} = \begin{bmatrix} \cos(\theta) & 0 & -\sin(\theta) \\ \sin(\phi)\sin(\theta) & \cos(\phi) & \sin(\phi)\cos(\theta) \\ \cos(\phi)\sin(\theta) & -\sin(\phi) & \cos(\phi)\cos(\theta) \end{bmatrix} \begin{Bmatrix} 0 \\ 0 \\ g_{z_{inertial}} \end{Bmatrix} \tag{36}$$

After calculating the components of the gravitational acceleration on the body axis system, the inertial force acting on the airframe can be calculated by using mass of the airframe, gravitational acceleration, and body acceleration by using Equation 41. Equations 37, 38, 39, and 40 show how Equation 41 is obtained.

$$\begin{Bmatrix} F_{x_{body}} \\ F_{y_{body}} \\ F_{z_{body}} \end{Bmatrix}_{total}^{cg,airf} = m_{airf} \left(\begin{Bmatrix} a_{x_{body}} \\ a_{y_{body}} \\ a_{z_{body}} \end{Bmatrix}^{cg,airf} \right) \tag{37}$$

Expanding the total force term,

$$\begin{Bmatrix} F_{x_{body}} \\ F_{y_{body}} \\ F_{z_{body}} \end{Bmatrix}_{external}^{cg,airf} + \begin{Bmatrix} F_{x_{body}} \\ F_{y_{body}} \\ F_{z_{body}} \end{Bmatrix}_{weight}^{cg,airf} = m_{airf} \left(\begin{Bmatrix} a_{x_{body}} \\ a_{y_{body}} \\ a_{z_{body}} \end{Bmatrix}^{cg,airf} \right) \tag{38}$$

where,

$$\begin{Bmatrix} F_{x_{body}} \\ F_{y_{body}} \\ F_{z_{body}} \end{Bmatrix}_{weight}^{cg,airf} = m_{airf} \begin{Bmatrix} g_{x_{body}} \\ g_{y_{body}} \\ g_{z_{body}} \end{Bmatrix} \tag{39}$$

and,

$$\begin{Bmatrix} F_{x_{body}} \\ F_{y_{body}} \\ F_{z_{body}} \end{Bmatrix}_{inertial}^{cg,airf} = -\begin{Bmatrix} F_{x_{body}} \\ F_{y_{body}} \\ F_{z_{body}} \end{Bmatrix}_{external}^{cg,airf} \tag{40}$$

So, Equation 38 becomes,

$$\begin{Bmatrix} F_{x_{body}} \\ F_{y_{body}} \\ F_{z_{body}} \end{Bmatrix}_{inertial}^{cg,airf} = m_{airf}\left(\begin{Bmatrix} g_{x_{body}} \\ g_{y_{body}} \\ g_{z_{body}} \end{Bmatrix} - \begin{Bmatrix} a_{x_{body}} \\ a_{y_{body}} \\ a_{z_{body}} \end{Bmatrix}^{cg,airf}\right) \tag{41}$$

Note that the term load factor is often used in the loads analysis of the maneuvers. It is denoted by 'n' and obtained by dividing Equation 41 by the weight of the airframe as shown in Equation 42.

$$\begin{Bmatrix} n_{x_{body}} \\ n_{y_{body}} \\ n_{z_{body}} \end{Bmatrix}^{cg,airf} = \frac{1}{g}\left[\begin{Bmatrix} g_{x_{body}} \\ g_{y_{body}} \\ g_{z_{body}} \end{Bmatrix} - \begin{Bmatrix} a_{x_{body}} \\ a_{y_{body}} \\ a_{z_{body}} \end{Bmatrix}^{cg,airf}\right] \tag{42}$$

In order to calculate the inertial moments acting at the airframe center of gravity, moment of inertia matrix, angular accelerations, and angular velocities are used as shown in Equation 43 [32].

$$\begin{Bmatrix} M_{x_{body}} \\ M_{y_{body}} \\ M_{z_{body}} \end{Bmatrix}_{inertial}^{cg,airf} = -\left[[I]^{cg,airf}\begin{Bmatrix} \dot{p} \\ \dot{q} \\ \dot{r} \end{Bmatrix} + \begin{Bmatrix} p \\ q \\ r \end{Bmatrix} \times \left([I]^{cg,airf}\begin{Bmatrix} p \\ q \\ r \end{Bmatrix}\right)\right] \tag{43}$$

where,

$$[I]^{cg,airf} = \begin{bmatrix} I_{xx}^{cg,airf} & -I_{xy}^{cg,airf} & -I_{xz}^{cg,airf} \\ -I_{xy}^{cg,airf} & I_{yy}^{cg,airf} & -I_{yz}^{cg,airf} \\ -I_{xz}^{cg,airf} & -I_{yz}^{cg,airf} & I_{zz}^{cg,airf} \end{bmatrix} \tag{44}$$

After expanding Equation 43, Equations 45, 46, and 47 are obtained.

$$M_{x_{body},inertial}^{cg,airf} = -(I_{xx}^{cg,airf}(\dot{p}) + I_{xy}^{cg,airf}(pr - \dot{q}) - I_{xz}^{cg,airf}(pq + \dot{r}) + I_{yz}^{cg,airf}(r^2 - q^2) + (I_{zz}^{cg,airf} - I_{yy}^{cg,airf})(qr)) \tag{45}$$

$$M_{y_{body},inertial}^{cg,airf} = -(I_{yy}^{cg,airf}(\dot{q}) - I_{xy}^{cg,airf}(qr + \dot{p}) + I_{yz}^{cg,airf}(pq - \dot{r}) + I_{xz}^{cg,airf}(p^2 - r^2) + (I_{xx}^{cg,airf} - I_{zz}^{cg,airf})(pr)) \tag{46}$$

$$M_{z_{body},inertial}^{cg,airf} = -(I_{zz}^{cg,airf}(\dot{r}) - I_{yz}^{cg,airf}(pr + \dot{q}) + I_{xz}^{cg,airf}(qr - \dot{p}) + I_{xy}^{cg,airf}(q^2 - p^2) + (I_{yy}^{cg,airf} - I_{xx}^{cg,airf})(pq)) \tag{47}$$

The total inertial loads calculated with the method explained above are checked against the inertial loads obtained from Flightlab in order to make sure that they are equal.

4.1.3. Hub Loads

Hub loads are the loads produced by the main rotor and tail rotor acting at the hub locations, which are given in Table 4 and Table 7. These loads are the results of the solutions of complicated dynamic and aerodynamic equations of the rotors. Flightlab is used to obtain these loads. After the hub loads are obtained, they are first rotated from the corresponding hub axis system to the body axis system and then translated to the airframe center of gravity location. The equations for the rotation are given in Equations 48, 49, and 50.

$$\begin{Bmatrix} F_{x_{body}} \\ F_{y_{body}} \\ F_{z_{body}} \end{Bmatrix}_{hub,mr}^{hub,mr} = [f(\phi_{mr}, \theta_{mr}, \psi_{mr})]^{-1} \begin{Bmatrix} F_{x_{mrhub}} \\ F_{y_{mrhub}} \\ F_{z_{mrhub}} \end{Bmatrix}_{hub,mr}^{hub,mr} \tag{48}$$

$$\begin{Bmatrix} M_{x_{body}} \\ M_{y_{body}} \\ M_{z_{body}} \end{Bmatrix}_{hub,mr}^{hub,mr} = [f(\phi_{mr}, \theta_{mr}, \psi_{mr})]^{-1} \begin{Bmatrix} M_{x_{mrhub}} \\ M_{y_{mrhub}} \\ M_{z_{mrhub}} \end{Bmatrix}_{hub,mr}^{hub,mr} \tag{49}$$

Where, $\phi_{hub,mr}$, $\theta_{hub,mr}$, $\psi_{hub,mr}$ angles represent the rotor orientation with respect to the body axis system. The values of these angles for main rotor and tail rotor are given in Table 4 and Table 7, respectively. The rotation matrix is given in Equation 50 [31].

$$f(\phi_{mr}, \theta_{mr}, \psi_{mr}) = \begin{bmatrix} 1 & 0 & 0 \\ 0 & \cos(\phi_{mr}) & \sin(\phi_{mr}) \\ 0 & -\sin(\phi_{mr}) & \cos(\phi_{mr}) \end{bmatrix} * \begin{bmatrix} \cos(\theta_{mr}) & 0 & -\sin(\theta_{mr}) \\ 0 & 1 & 0 \\ \sin(\theta_{mr}) & 0 & \cos(\theta_{mr}) \end{bmatrix} * \begin{bmatrix} \cos(\psi_{mr}) & \sin(\psi_{mr}) & 0 \\ -\sin(\psi_{mr}) & \cos(\psi_{mr}) & 0 \\ 0 & 0 & 1 \end{bmatrix} \tag{50}$$

After the rotation, the equations for translating the hub forces and moments to the airframe center of gravity is given in Equations 51 and 52.

$$\begin{Bmatrix} F_{x_{body}} \\ F_{y_{body}} \\ F_{z_{body}} \end{Bmatrix}_{hub,mr}^{cg,airf} = \begin{Bmatrix} F_{x_{body}} \\ F_{y_{body}} \\ F_{z_{body}} \end{Bmatrix}_{hub,mr}^{hub,mr} \tag{51}$$

$$\begin{Bmatrix} M_{x_{body}} \\ M_{y_{body}} \\ M_{z_{body}} \end{Bmatrix}_{hub,mr}^{cg,airf} = \begin{Bmatrix} r_{x_{body}} \\ r_{y_{body}} \\ r_{z_{body}} \end{Bmatrix}^{hub,mr/cg,airf} \times \begin{Bmatrix} F_{x_{body}} \\ F_{y_{body}} \\ F_{z_{body}} \end{Bmatrix}_{hub,mr}^{hub,mr} + \begin{Bmatrix} M_{x_{body}} \\ M_{y_{body}} \\ M_{z_{body}} \end{Bmatrix}_{hub,mr}^{hub,mr} \tag{52}$$

Note that since forces and moments are in body axis system, the positions in Equations 51 and 52 are in the body axis system, as well. Moreover, although Equations 48, 49, 51, and 52 are written for the main rotor, the same equations also apply for the tail rotor with corresponding rotor orientation angles and hub positions.

Sum of all the forces and moments acting at the airframe center of gravity location, or any other location, should be equal to zero in order for the rotorcraft to be mathematically balanced as shown in Equations 53 and 54.

$$\begin{Bmatrix} F_{x_{body}} \\ F_{y_{body}} \\ F_{z_{body}} \end{Bmatrix}_{aero,condition}^{cg,airf} + \begin{Bmatrix} F_{x_{body}} \\ F_{y_{body}} \\ F_{z_{body}} \end{Bmatrix}_{inertial}^{cg,airf} + \begin{Bmatrix} F_{x_{body}} \\ F_{y_{body}} \\ F_{z_{body}} \end{Bmatrix}_{hub,mr}^{cg,airf} + \begin{Bmatrix} F_{x_{body}} \\ F_{y_{body}} \\ F_{z_{body}} \end{Bmatrix}_{hub,tr}^{cg,airf} = \begin{Bmatrix} 0 \\ 0 \\ 0 \end{Bmatrix} \tag{53}$$

$$\begin{Bmatrix} M_{x_{body}} \\ M_{y_{body}} \\ M_{z_{body}} \end{Bmatrix}_{aero,condition}^{cg,airf} + \begin{Bmatrix} M_{x_{body}} \\ M_{y_{body}} \\ M_{z_{body}} \end{Bmatrix}_{inertial}^{cg,airf} + \begin{Bmatrix} M_{x_{body}} \\ M_{y_{body}} \\ M_{z_{body}} \end{Bmatrix}_{hub,mr}^{cg,airf} + \begin{Bmatrix} M_{x_{body}} \\ M_{y_{body}} \\ M_{z_{body}} \end{Bmatrix}_{hub,tr}^{cg,airf} = \begin{Bmatrix} 0 \\ 0 \\ 0 \end{Bmatrix} \tag{54}$$

4.2. Fuselage Loads Calculation

After the flight dynamics analysis is completed, the second step is to calculate the fuselage loads. In order to do this, main rotor and tail rotor hub loads and some of the rotorcraft states are used. The states that are used for the fuselage loads calculation are as follows:

1. Angle of Attack and Sideslip Angle
2. Rotorcraft Orientation (Euler Angles)
3. Linear and Angular Velocities in Body Axis System
4. Linear and Angular Accelerations in Body Axis System

Total linear velocity and angle of attack and sideslip angle are used to calculate the distributed aerodynamic loads and rotorcraft orientation, angular velocities, and linear and angular accelerations are used to calculate the distributed inertial loads.

4.2.1. Distributed Aerodynamic Loads

Once the pressure distributions on the airframe for different angle of attack and sideslip angle combinations are at hand, they are integrated to the pre-determined monitor stations by using Equations 3 to 15. However, Equations 14 and 15 cannot be used as they are since not all the meshes are to be used this time.

In order to decide which mesh to be included in Equations 3 to 15 for the calculation of aerodynamic forces and moments acting at the monitor stations, a method called integration direction is used. The meshes shown by the integration direction arrow which is drawn from the corresponding monitor station are included in the calculations. Moreover, using two integration directions is useful to perform calculations faster. In this thesis, two integration directions are used as shown in Figure 38. The integration direction changes at x = 7.5 [m].

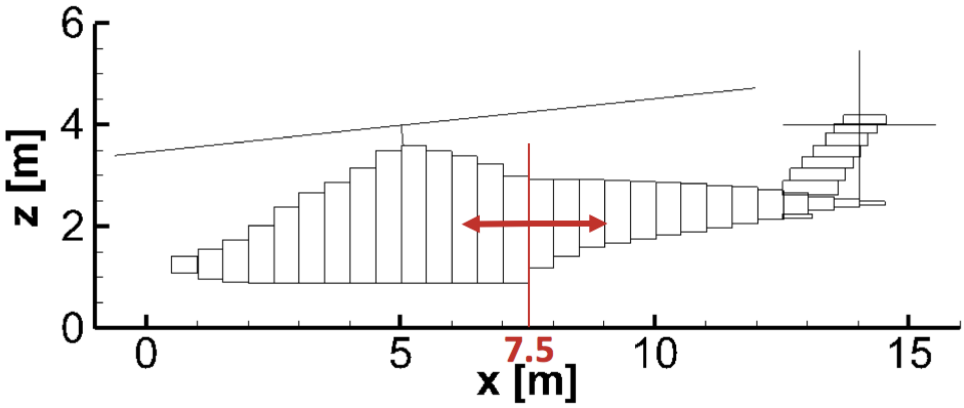

Figure 38. Integration Directions on the Airframe

The calculations for the aerodynamic loads are performed only once, not for each condition, and a database is created which includes the aerodynamic load information at the monitor stations for a known dynamic pressure and for different angle of attack and sideslip angle combinations. When a specific condition is analyzed, two-dimensional linear interpolation based on the angle of attack and sideslip angle is performed on the aerodynamic loads at each monitor station and the loads are multiplied by a factor based on the dynamic pressure for that specific condition as shown in Equations 55 and 56.

$$\begin{Bmatrix} F_{x_{LAS}} \\ F_{y_{LAS}} \\ F_{z_{LAS}} \end{Bmatrix}_{aero,condition}^{monitor\_station} = \frac{Q_{condition}}{Q_{database}} \begin{Bmatrix} F_{x_{LAS}} \\ F_{y_{LAS}} \\ F_{z_{LAS}} \end{Bmatrix}_{aero,database}^{monitor\_station} \tag{55}$$

$$\begin{Bmatrix} M_{x_{LAS}} \\ M_{y_{LAS}} \\ M_{z_{LAS}} \end{Bmatrix}_{aero,condition}^{monitor\_station} = \frac{Q_{condition}}{Q_{database}} \begin{Bmatrix} M_{x_{LAS}} \\ M_{y_{LAS}} \\ M_{z_{LAS}} \end{Bmatrix}_{aero,database}^{monitor\_station} \tag{56}$$

4.2.2. Distributed Inertial Loads

Inertial loads acting on each mass item given in Table 11 are calculated based on the linear and angular accelerations and angular velocities of the rotorcraft. Equations 36, 41, 45, 46, and 47 are used to calculate the inertial load on each mass item with corresponding mass and moment of inertia value. The acceleration term in Equation 41 can be further expressed as shown in Equation 57 [32].

$$\begin{Bmatrix} a_{x_{body}} \\ a_{y_{body}} \\ a_{z_{body}} \end{Bmatrix}^{cg,mp} = \left[\begin{Bmatrix} a_{x_{body}} \\ a_{y_{body}} \\ a_{z_{body}} \end{Bmatrix}^{cg,airf} + \begin{Bmatrix} a_{x_{body}} \\ a_{y_{body}} \\ a_{z_{body}} \end{Bmatrix}^{mp/cg,airf} \right] \tag{57}$$

Equation 57 can be further expressed as shown in Equation 58 [32].

$$\begin{Bmatrix} a_{x_{body}} \\ a_{y_{body}} \\ a_{z_{body}} \end{Bmatrix}^{cg,mp} = \left[\begin{Bmatrix} a_{x_{body}} \\ a_{y_{body}} \\ a_{z_{body}} \end{Bmatrix}^{cg,airf} + \begin{Bmatrix} \dot{p} \\ \dot{q} \\ \dot{r} \end{Bmatrix} \times \begin{Bmatrix} r_{x_{body}} \\ r_{y_{body}} \\ r_{z_{body}} \end{Bmatrix}^{cg,mp/cg,airf} \right. \\ \left. + \begin{Bmatrix} p \\ q \\ r \end{Bmatrix} \times \left[\begin{Bmatrix} p \\ q \\ r \end{Bmatrix} \times \begin{Bmatrix} r_{x_{body}} \\ r_{y_{body}} \\ r_{z_{body}} \end{Bmatrix}^{cg,mp/cg,airf} \right] \right] \tag{58}$$

After calculating the inertial forces and moments acting at the center of gravity of each mass item in body axis system, they are converted to LAS and then translated to the monitor stations by using Equations 59 and 60. Note that since forces and moments are in LAS, the positions in Equations 59 and 60 are in LAS, as well.

$$\begin{Bmatrix} F_{x_{LAS}} \\ F_{y_{LAS}} \\ F_{z_{LAS}} \end{Bmatrix}_{inertial}^{monitor\_station} = \begin{Bmatrix} -F_{x_{body}} \\ F_{y_{body}} \\ -F_{z_{body}} \end{Bmatrix}_{inertial}^{cg,mp} \tag{59}$$

$$\begin{Bmatrix} M_{x_{LAS}} \\ M_{y_{LAS}} \\ M_{z_{LAS}} \end{Bmatrix}_{inertial}^{monitor\_station} = \\ \begin{Bmatrix} r_{x_{LAS}} \\ r_{y_{LAS}} \\ r_{z_{LAS}} \end{Bmatrix}^{cg,mp/monitor\_station} \times \begin{Bmatrix} -F_{x_{body}} \\ F_{y_{body}} \\ -F_{z_{body}} \end{Bmatrix}_{inertial}^{cg,mp} + \begin{Bmatrix} -M_{x_{body}} \\ M_{y_{body}} \\ -M_{z_{body}} \end{Bmatrix}_{inertial}^{cg,mp} \tag{60}$$

The integration direction method used for the aerodynamic loads is used for the inertial loads, as well. Integration direction for the inertial loads changes at x = 7.5 [m] which is the same point used for the aerodynamic loads. Just like the aerodynamic mesh, the mass points shown by the integration direction arrow which is drawn from the corresponding monitor station are included in the monitor station force and moment calculation.

Unlike the calculation of aerodynamic loads at the monitor stations, this calculation needs to be done for each condition which means for each trim and each time instant in the transient analysis.

4.2.3. Hub Loads

The hub loads obtained from Flightlab are treated as external point loads acting on the airframe. They are rotated from the corresponding hub axis system to the body axis system by using Equations 48, 49, and 50. After that, these forces and moments are converted to LAS and then translated to each of the monitor station by using Equations 61 and 62. Note that since forces and moments are in LAS, the positions in Equations 61 and 62 are in LAS, as well.

$$\begin{Bmatrix} F_{x_{LAS}} \\ F_{y_{LAS}} \\ F_{z_{LAS}} \end{Bmatrix}_{hub,mr}^{monitor\_station} = \begin{Bmatrix} -F_{x_{body}} \\ F_{y_{body}} \\ -F_{z_{body}} \end{Bmatrix}_{hub,mr}^{hub,mr} \tag{61}$$

$$\begin{Bmatrix} M_{x_{LAS}} \\ M_{y_{LAS}} \\ M_{z_{LAS}} \end{Bmatrix}_{hub,mr}^{monitor\_station} = \begin{Bmatrix} r_{x_{LAS}} \\ r_{y_{LAS}} \\ r_{z_{LAS}} \end{Bmatrix}^{hub,mr/monitor\_station} \times \begin{Bmatrix} -F_{x_{body}} \\ F_{y_{body}} \\ -F_{z_{body}} \end{Bmatrix}_{hub,mr}^{hub,mr} + \begin{Bmatrix} -M_{x_{body}} \\ M_{y_{body}} \\ -M_{z_{body}} \end{Bmatrix}_{hub,mr}^{hub,mr} \tag{62}$$

Although Equations 61 and 62 are written for the main rotor, the same equations also apply for the tail rotor with corresponding hub positions.

The next step in the calculation of the forces and moments acting at the monitor stations is to sum all the forces and moments due to aerodynamics, inertia, and hub loads as shown in Equations 63 and 64.

$$\begin{Bmatrix} F_{x_{LAS}} \\ F_{y_{LAS}} \\ F_{z_{LAS}} \end{Bmatrix}_{total}^{monitor\_station} = \begin{Bmatrix} F_{x_{LAS}} \\ F_{y_{LAS}} \\ F_{z_{LAS}} \end{Bmatrix}_{aero}^{monitor\_station} + \begin{Bmatrix} F_{x_{LAS}} \\ F_{y_{LAS}} \\ F_{z_{LAS}} \end{Bmatrix}_{inertial}^{monitor\_station} + \begin{Bmatrix} F_{x_{LAS}} \\ F_{y_{LAS}} \\ F_{z_{LAS}} \end{Bmatrix}_{hub,mr}^{monitor\_station} + \begin{Bmatrix} F_{x_{LAS}} \\ F_{y_{LAS}} \\ F_{z_{LAS}} \end{Bmatrix}_{hub,tr}^{monitor\_station} \quad (63)$$

$$\begin{Bmatrix} M_{x_{LAS}} \\ M_{y_{LAS}} \\ M_{z_{LAS}} \end{Bmatrix}_{total}^{monitor\_station} = \begin{Bmatrix} M_{x_{LAS}} \\ M_{y_{LAS}} \\ M_{z_{LAS}} \end{Bmatrix}_{aero}^{monitor\_station} + \begin{Bmatrix} M_{x_{LAS}} \\ M_{y_{LAS}} \\ M_{z_{LAS}} \end{Bmatrix}_{inertial}^{monitor\_station} + \begin{Bmatrix} M_{x_{LAS}} \\ M_{y_{LAS}} \\ M_{z_{LAS}} \end{Bmatrix}_{hub,mr}^{monitor\_station} + \begin{Bmatrix} M_{x_{LAS}} \\ M_{y_{LAS}} \\ M_{z_{LAS}} \end{Bmatrix}_{hub,tr}^{monitor\_station} \quad (64)$$

CHAPTER 5

SOFTWARE and METHODOLOGY

5.1. Software

Two different software have been used in order to calculate the rotorcraft fuselage loads. The first one is Flightlab and the scripts to run Flightlab and the second one is to calculate the fuselage sectional forces and moments for a given maneuver.

5.1.1. Flight Dynamics Analysis

Flight dynamics analysis have been performed by using Flightlab, as explained before. Although Flightlab has a graphical user interface (GUI), it is not suitable to perform several analysis automatically and to collect the inputs required automatically for the fuselage loads calculation. It is rather used for quick checks. Therefore, it is not possible to obtain the inputs required for the rotorcraft fuselage loads calculation with the GUI provided since each condition and each output requires a manual intervention.

In order to perform flight dynamics analysis and get the outputs in a specific format automatically for as many conditions as required, scripts that Flightlab can read has been prepared. These scripts are used to specify the maneuver type, rotorcraft configuration, and flight condition, perform trim or transient analysis and collect the required outputs. Matlab has been used to develop a software to both create an alternative GUI for Flightlab and to call Flightlab by altering the scripts mentioned above based on the user input. This software has been named as LOFD (Loads-Flight Dynamics) and the GUI created can be seen in Figure 39.

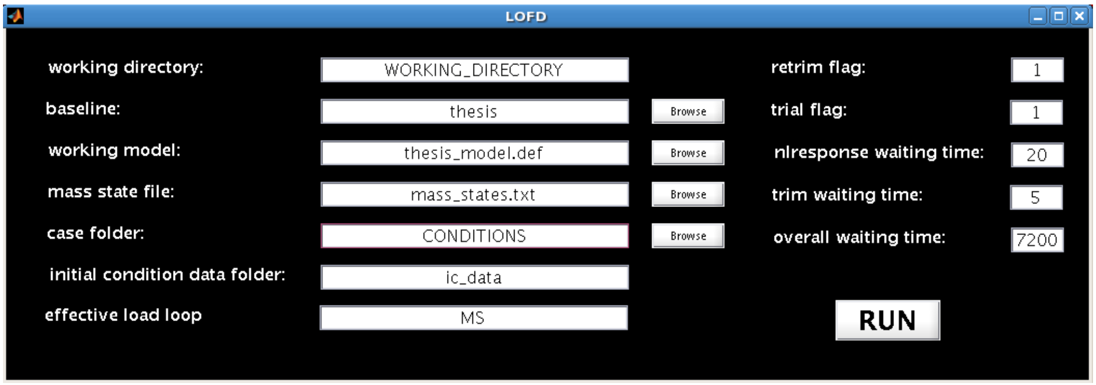

Figure 39. Graphical User Interface of LOFD

LOFD enables the user to perform many trim or transient analysis automatically. The conditions are defined in text files. Every input required to perform a trim or transient analysis can be defined. The inputs can be defined includes, but not limited to, velocity, altitude, temperature, required load factor for pull-up and push-over trims, trim variables, trim targets, transient gust profiles, transient pilot inputs, etc.

Other scripts that work together with LOFD have also been developed in order to perform trims for pull-up, push-over, and yaw maneuvers and gust conditions the methods of which are explained in Chapters 5.2.1.2, 5.2.2.2, 5.2.3.2, and 5.2.4.2.

5.1.2. Fuselage Loads Calculation

Fuselage loads calculations have been performed by employing the methods explained in Chapter 4.2. The loads model of the rotorcraft consisting of airframe inertia model, explained in Chapter 3.2.3.1.1, monitor stations, explained in Chapter 3.2.3.1.2, airframe aerodynamic model, explained in Chapter 3.2.3.2, and rotorcraft states and hub loads are used as inputs to this software. As outputs, fuselage sectional loads are generated. Furthermore, loads cards for structural analysis purposes are generated. Load cards of the conditions determined to be critical based on the sectional loads at the monitor stations are transferred to structural analysis group in order to perform the sizing of the fuselage.

5.2. Methodology

In this chapter, the methodology applied to calculate the rotorcraft fuselage loads for both the transient solution and ROFLOT approach is explained. This section governs the first step of the loads calculation, flight dynamics analysis. It is aimed to explain how transient analyses normally performed for calculation of the rotorcraft fuselage loads encountered during maneuvers and gust conditions are replaced by trim point(s) with ROFLOT approach.

5.2.1. Pull-up Maneuver

In pull-up maneuver, high load factor in vertical direction occurs. There is a direct relationship between the load factor, pitch rate, and the time derivative of the vertical velocity. This relationship is shown in Equation 69 and Equations 65, 66, 67, and 68 show how Equation 69 is obtained.

The equation of motion of the rotorcraft in z_{body} direction is given in Equation 65.

$$\sum F_{z_{body}} = m_{airf} a_{z_{body}} \tag{65}$$

Where the acceleration term can be further expressed as in Equation 66 [33].

$$\sum F_{z_{body}} = m_{airf}(\dot{w} + pv - qu) \tag{66}$$

In order to obtain the relationship mentioned above and since pull-up maneuver is a symmetric maneuver, the roll rate and lateral velocity can be assumed to be zero.

$$p = v = 0$$

Equation 67 is obtained.

$$\sum F_{z_{body}} = m_{airf}(\dot{w} - qu) \tag{67}$$

Considering the definition of load factor shown in Equation 42, Equation 68 is obtained.

$$n_{z_{body}} = \frac{1}{g}\left(g_{z_{body}} - \dot{w} + qu\right) \tag{68}$$

Assuming the roll and pitch angles are small and based on Equation 36,

$$g_{z_{body}} \cong g$$

Equation 69 can be obtained.

$$n_{z_{body}} = 1 + \left(\frac{-\dot{w} + qu}{g}\right) \tag{69}$$

According to Equation 69, a load factor value greater than 1 is possible with either a positive pitch rate or negative velocity derivative in z_{body} direction, or a combination of both. In the actual maneuver, when the load factor is the highest, the velocity derivative in the vertical direction is close to zero and the pitch rate is the highest. Since the pitch rate is the highest, the pitch acceleration is also close to zero.

Pull-up maneuver has been performed by employing both transient analysis and ROFLOT approach. Under ROFLOT approach, two different methods have been developed. While high negative vertical velocity derivative in z_{body} direction is created on the airframe with zero pitch rate in one of the methods, non-zero pitch rate is generated with zero vertical velocity derivative in the second method. The methodology for both the transient solution and ROFLOT approach is explained in this chapter.

5.2.1.1. Transient Analysis

First, the rotorcraft is trimmed in forward flight condition by using the trim variables and the trim targets shown in Table 16.

The trim variables and the trim targets mentioned above are the variables and the targets used in the trim algorithm. Newton-Raphson method [34] is used as the trim algorithm for every trim performed in this thesis. In trim, the trim variables are altered in order to obtain the required trim targets. The equation that is used in the Newton-Raphson method is given in Equation 70.

$$x_{n+1} = x_n - \frac{f(x_n)}{f'(x_n)} \tag{70}$$

Table 16. Trim Variables and Targets Used for the Forward Flight Trim

Trim variables	ϕ, θ, S_c, S_b, S_a, S_p
Trim targets	$\dot{u}=0$, $\dot{v}=0$, $\dot{w}=0$ $\dot{p}=0$, $\dot{q}=0$, $\dot{r}=0$

The transient analysis follows the forward flight trim solution explained above. A prescribed longitudinal cyclic and collective input are used for the transient analysis of the pull-up maneuver. The rotorcraft is first allowed to dive by pushing the longitudinal cyclic stick forward. After sufficiently large dive angle is achieved, with negative pitch and flight path angles, longitudinal cyclic stick is pulled aft suddenly, with the rise time of 0.2 [s], together with some collective control in order to achieve the desired load factor.

Low rise time is used in order to generate high pitching moment on the rotorcraft. The time history of the longitudinal cyclic stick position used for the pull-up transient analysis performed in 80 [knot] is given in Figure 40. Collective control is used as required in order to generate a load factor of 3.5 in a rational manner.

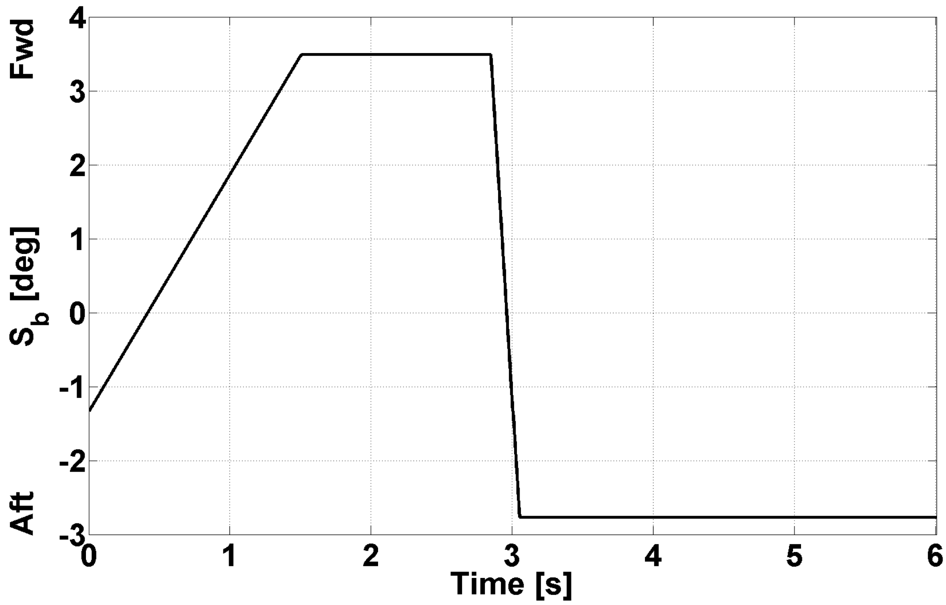

Figure 40. Time History of the Longitudinal Cyclic Position for the Transient Analysis of Pull-up Maneuver in 80 [knot]

Performing transient analysis of a pull-up maneuver is not only computationally expensive; it also requires a lot of engineering effort since each analysis requires a trial-and-error procedure in order to obtain the desired load factor. Furthermore, the transient analysis requires a stability augmentation system model in order to keep the rotorcraft roll and yaw attitudes (ϕ and ψ angles) in their trim values. Because of high coupling between roll, pitch, and yaw motions of a rotorcraft, it is very difficult to perform a transient analysis of the pull-up maneuver without using a stability augmentation system, if not impossible.

5.2.1.2. ROFLOT Approach

Pull-up maneuver is represented by two trim points under ROFLOT approach. The first point is the start of the pull-up maneuver which is a forward flight trim. The second point is to represent the high vertical load factor. Two different methods have been developed for the second trim. Explanations of the methodology for each of the methods are given in this chapter. The fuselage loads have been obtained by using both of the methods separately and the results are compared in Chapter 6.1.

5.2.1.2.1. Pull-up Trim Method

This method aims to trim the rotorcraft in the required vertical load factor with positive pitch rate and with zero velocity time derivative in the z_{body} direction. In other words, it is aimed to catch the time instant of the transient analysis where the maximum load factor occurs. First, the rotorcraft is trimmed in a forward flight condition which is the same trim performed for the first step of the transient analysis. Then, some of the trim variables and trim targets are modified as shown in Table 17 [35].

Table 17. Trim Variables and Targets Used for the Pull-up Trim

Trim variables	ϕ, θ, S_b, S_a, S_p
Trim targets	$\dot{v}$=0, $\dot{w}$=0 $\dot{p}$=0, $\dot{q}$=0, $\dot{r}$=0

As it can be seen from Table 17, the collective stick position is no longer a trim variable and $\dot{u}$ (time derivative of velocity in x_{body} direction) is no longer a trim target. This approach emerges from the fact that in the transient analysis of the pull-up maneuver, $\dot{u}$ is not zero at the time instant when the maximum load factor occurs. Time history of $\dot{u}$ in the pull-up transient analysis performed in 80 [knot] is given in Figure 41.

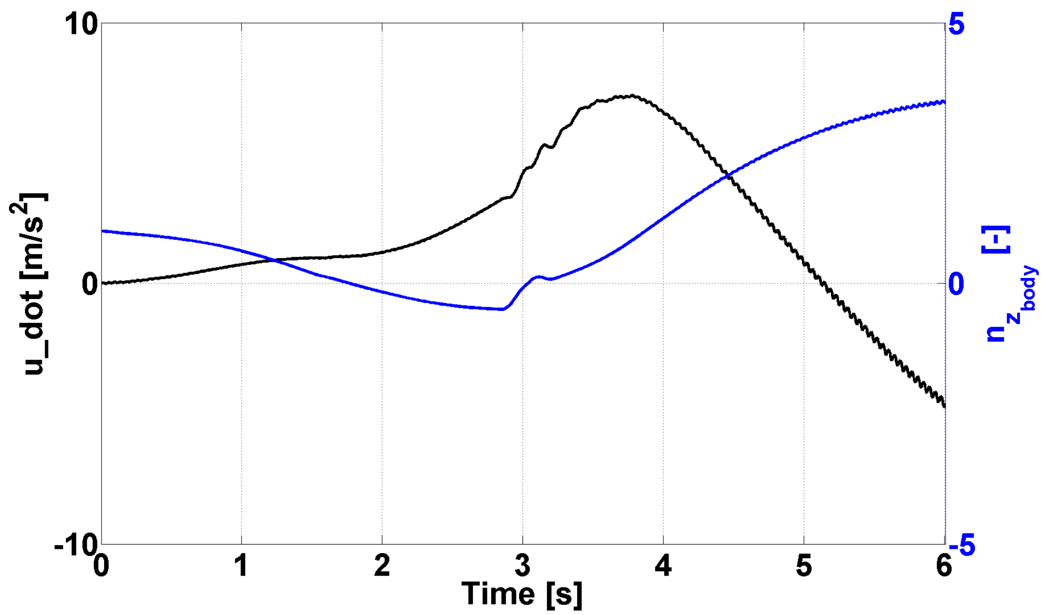

Figure 41. Time History of the Time Derivative of the Velocity in x_{body} Direction for the Pull-up Maneuver Transient Analysis in 80 [knot]

Usually trim is referred to a state of the rotorcraft when the linear and angular accelerations are zero. However, mathematically, trim can also be a point when there is non-zero acceleration on the rotorcraft. In other words, the trim targets can be set free or a non-zero value may be aimed in the Newton-Raphson trim iteration. In such a case, trim actually becomes a ‘dynamic trim’.

After the modification of the trim variables and the trim targets, by using LOFD combined with a script specifically developed for this task, the rotorcraft is given a non-zero pitch rate increment until the load factor is reached to the desired load factor. Whenever the collective value is not enough to provide the load factor associated with the given pitch rate, it is increased in an outer loop so that the pitch rate, and automatically the load factor, can be further increased.

This method eliminates the trial-and-error procedure employed for the transient analysis of the pull-up maneuver which reduces the engineering effort significantly. The computation time is also reduced since the maneuver is represented by a single trim point. Finally, the need for a stability augmentation system is eliminated.

5.2.1.2.2. High-g Forward Flight Trim Method

This method aims to apply a high vertical force on the fuselage in the negative z_{body} direction with zero pitch rate and non-zero time derivative of the velocity in the z_{body} direction.

First, the rotorcraft is trimmed in the forward flight condition with the trim variables and the trim targets shown in Table 16 and one more trim is performed. Then, the trim variables and the trim targets are modified as shown in Table 18.

Table 18. Trim Variables and Targets Used for the High-g Forward Flight Trim

Trim variables	S_c, S_b, S_a, S_p
Trim targets	$\dot{w}$=based on Equation 68 $\dot{p}=0$, $\dot{q}=0$, $\dot{r}=0$

The roll and pitch angles of the rotorcraft are no longer trim variables and they are kept constant at their forward flight trim values. Because of that, the rotorcraft can no longer sustain a flight with zero $\dot{u}$ and $\dot{w}$. That is the reason why they are no longer trim targets. This trim can also be called as a dynamic trim.

As explained before in Chapter 2.1.1, this condition is mentioned to be a bookcase [6] so an artificial state of the rotorcraft can be created for the sake of calculating the fuselage loads in a high vertical load factor condition. This analysis is performed automatically by using LOFD and a script to modify the trim variables and the trim targets.

Like the pull-up maneuver explained in Chapter 5.2.1.2.1, this method also eliminates the trial-and-error procedure and reduces the computation time. Furthermore, this method is faster than the pull-up trim method in terms of flight dynamics analysis since no collective and pitch rate loops are used in this method. In other words, single trim is performed after the forward flight trim in order to reach the desired load factor.

5.2.2. Push-over Maneuver

Push-over maneuver is very similar to the pull-up maneuver but this time, load factor is less than 1. Equation 69 is valid for the push-over maneuver, as well.

According to Equation 69, a load factor value less than 1 is possible with either a negative pitch rate or positive velocity derivative in z_{body} direction, or a combination of both. In the actual maneuver, when the absolute value of the load factor is the highest, the velocity derivative in the vertical direction is close to zero and the absolute value of the pitch rate is the highest.

Similar to the pull-up maneuver, push-over has been performed by employing both transient analysis and ROFLOT approach. Two different types of trims have been performed under ROFLOT approach. While high positive vertical velocity derivative in z_{body} direction is created on the airframe with zero pitch rate in one of the trim methods, non-zero pitch rate is generated with zero vertical velocity derivative in the other method. The methodology for both the transient solution and ROFLOT approach are explained in this chapter.

5.2.2.1. Transient Analysis

In order to perform the transient analysis, the rotorcraft is first trimmed in a climb condition by using the trim variables and the trim targets shown in Table 19.

Table 19. Trim Variables and Targets Used for the Climb Trim

Trim variables	ϕ, S_c, S_b, S_a, S_p
Trim targets	$\dot{v}=0$, $\dot{w}=0$ $\dot{p}=0$, $\dot{q}=0$, $\dot{r}=0$

The transient analysis follows the forward flight trim solution explained above. Similar to the pull-up maneuver, a prescribed longitudinal cyclic and collective input are used for the transient analysis of the push-over maneuver. Longitudinal cyclic stick is pulled aft suddenly, with the rise time of 0.2 [s], together with some collective control in order to achieve the desired load factor.

Again, low rise time is used in order to generate high negative pitching moment on the rotorcraft. The time history of the longitudinal cyclic stick position used for the push-over transient analysis performed in 120 [knot] is given in Figure 40. Collective control is used as required in order to generate a load factor of -1 in a rational manner.

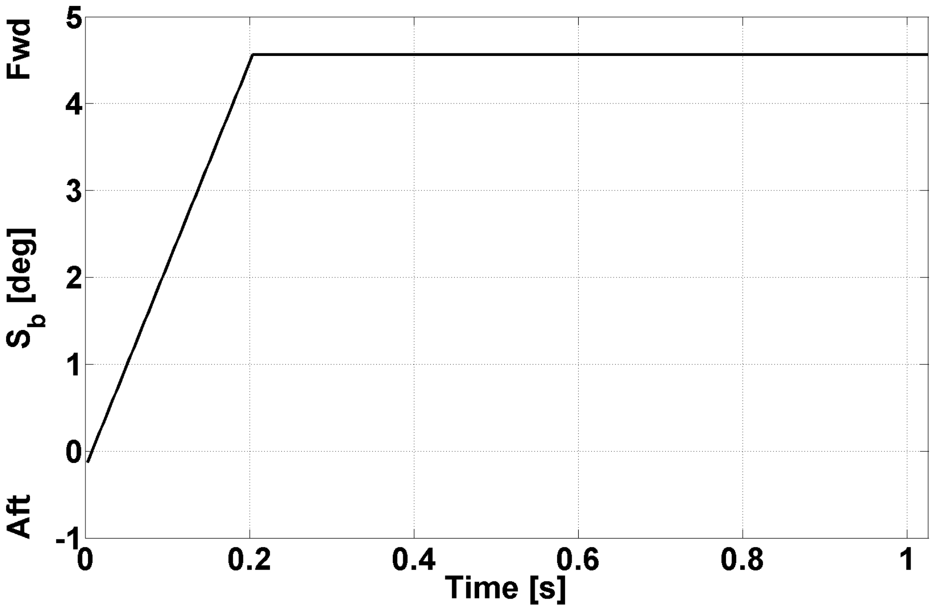

Figure 42. Time History of the Longitudinal Cyclic Position for the Transient Analysis of Push-over Maneuver in 120 [knot]

Similar to the pull-up maneuver, transient analysis of a push-over maneuver is also computationally expensive and it requires a trial-and-error procedure in order to obtain the desired load factor. A stability augmentation system model is required for the push-over maneuver as well in order to keep the rotorcraft roll and yaw attitudes (ϕ and ψ angles) in their trim values.

5.2.2.2. ROFLOT Approach

Similar to the pull-up maneuver, push-over maneuver is represented by two different trim points under ROFLOT approach. For the second trim point, two methods have been developed. The fuselage loads have been obtained by using both of the methods and the results are compared in Chapter 6.2.

5.2.2.2.1. Push-over Trim Method

This method is very similar to the pull-up trim method explained in Chapter 5.2.1.2.1. After a forward flight trim, the trim variables and targets are modified as shown in Table 17. $\dot{u}$ is no longer a trim target since it is non-zero when the load factor in the negative z_{body} direction is the highest in the transient analysis as shown in Figure 43.

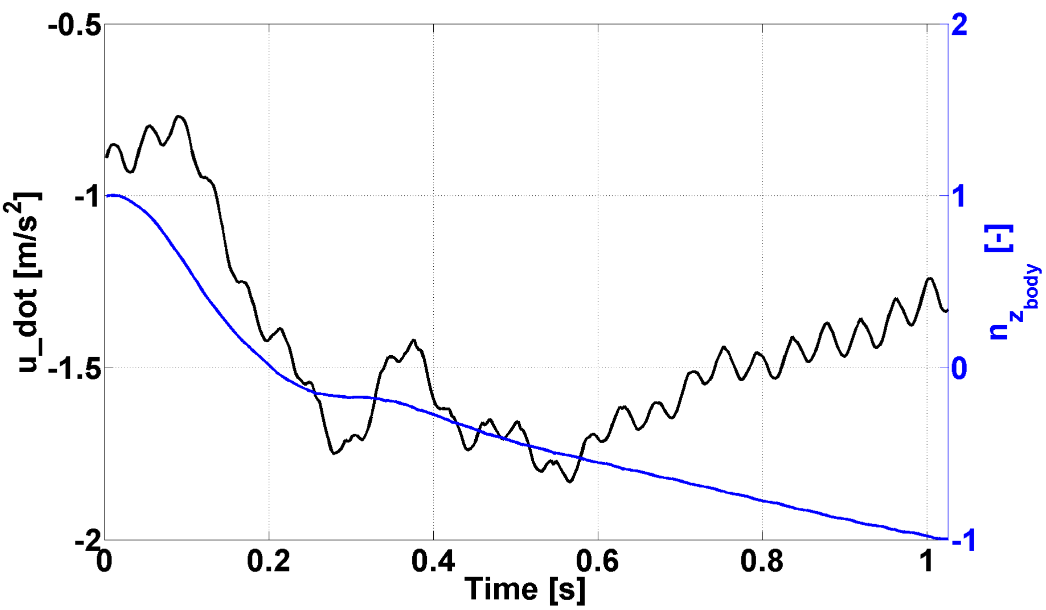

Figure 43. Time History of the Time Derivative of the Velocity in x_{body} Direction for the Push-over Maneuver Transient Analysis in 120 [knot]

This trim is also a dynamic trim. The same script developed for the pull-up maneuver is used for the push-over maneuver. However, this time, the pitch rate increment is negative and collective is decreased in an outer loop until the desired load factor is reached. The benefits achieved by using ROFLOT approach for the pull-up maneuver is also achieved for the push-over maneuver.

5.2.2.2.2. Low-g Forward Flight Trim Method

This method is the same as the high-g forward flight trim method explained in 5.2.1.2.2. Since this condition can be considered to be a bookcase [6], an artificial state of the rotorcraft is created for the sake of calculating the fuselage loads in a high negative g condition by applying high vertical force on the fuselage in the z_{body} direction. This trim is performed after a forward flight trim by using the trim variables and the trim targets shown in Table 18 and by using the same script developed for the high-g forward flight trim.

Similar to the pull-up maneuver, this method is faster than the push-over trim method in terms of flight dynamics analysis since single trim is performed after the forward flight trim in order to achieve the desired load factor.

5.2.3. Yaw Maneuver

Yaw maneuver has been analyzed by using both transient analysis and ROFLOT approach. The methodology for the transient solution and ROFLOT approach are explained in this chapter. Note that both the entry phase and the return phase have been analyzed in this thesis.

5.2.3.1. Transient Analysis

Entry phase of the transient analysis of the yaw maneuver is performed by applying sudden pedal input with the rise time of 0.2 [s] after a forward flight trim with the trim variables and targets shown in Table 16. The amplitude of the pedal input required is determined by using the outputs of another trim. In this second trim, the rotorcraft flies with the steady-state sideslip angle determined from Figure 2 based on the flight velocity. The trim variables and targets shown in Table 20 are used for this trim.

Table 20. Trim Variables and Targets Used for High Sideslip Angle Trim

Trim variables	θ, S_c, S_b, S_a, β
Trim targets	$\dot{u}=0$, $\dot{w}=0$ $\dot{p}=0$, $\dot{q}=0$, $\dot{r}=0$

The pedal value is set to 100% in this trim. The resulting sideslip angle is checked and if it is higher than the value defined in Figure 2, another trim is performed with the trim variables and targets shown in Table 21. In this trim, the sideslip angle is set to the value defined in Figure 2.

Table 21. Trim Variables and Targets Used for the Second High Sideslip Angle Trim

Trim variables	θ, S_c, S_b, S_a, S_p
Trim targets	$\dot{u}=0$, $\dot{w}=0$ $\dot{p}=0$, $\dot{q}=0$, $\dot{r}=0$

This way, the pedal required for the yaw maneuver can be determined. If the resulting sideslip angle of the first high sideslip angle trim is less than the value defined in Figure 2, then the pedal is taken as 100%. If not, the pedal input required is determined from the second trim with high sideslip angle.

The pedal is kept constant until the rotorcraft reaches the maximum transient sideslip angle or to the value defined in Figure 2, whichever is less. The time instants after that point are removed from the data for fuselage loads calculation. The time history of the pedal input used for the yaw to port condition in 80 [knot] is given in Figure 44.

In order to perform transient analysis for the return phase of the yaw maneuver, the pedal is suddenly returned to its initial position (forward flight position) after the steady-state sideslip angle trim explained above. Then, the rotorcraft is allowed to stabilize at zero sideslip angle.

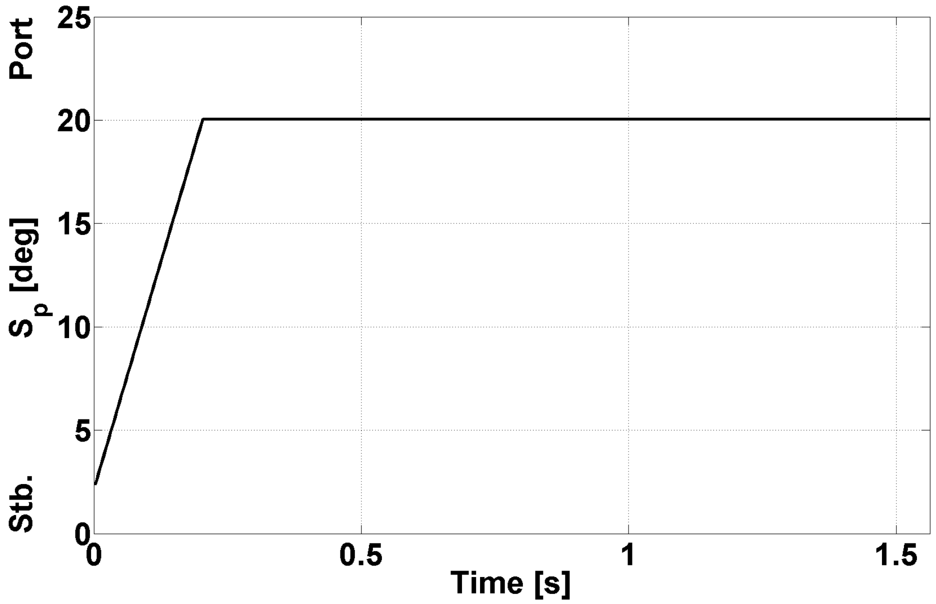

Figure 44. Time History of the Pedal Input Used for the Transient Analysis of the Yaw Maneuver in 80 [knot]

Similar to the transient analysis of pull-up and push-over maneuvers, calculating the fuselage loads for the whole maneuver is computationally expensive. Instead, critical time instants of a transient analysis can be determined and fuselage loads can be calculated by using ROFLOT approach. Moreover, like the transient analysis of pull-up and push-over maneuvers, yaw maneuver also requires a stability augmentation system model. This time, it is required to keep the roll and pitch angles at their trim values.

5.2.3.2. ROFLOT Approach

In this method, four different trim points are used. These points are maximum tail rotor force case, maximum yaw velocity with sideslip angle case, maximum transient sideslip angle (determined from Figure 2) with yaw velocity case, and return phase. The first point, maximum tail rotor force case, is used to generate high F_y and M_z on the fuselage. The second and third points are for generating high F_x on the airframe because of the combination of high inertial loading and high aerodynamic loading. The last point is to generate high F_y and M_z in the opposite direction of the entry phase of the maneuver.

After the forward flight trim with the trim variables and the trim targets shown in Table 16, maximum tail rotor force trim is performed by modifying the trim variable and trim target list as shown in Table 22.

Table 22. Trim Variables and Targets Used for Maximum Tail Rotor Force Trim

Trim variables	S_c, S_b, S_a
Trim targets	$\dot{w}=0$, $\dot{p}=0$, $\dot{q}=0$

As it can be seen, S_p is no longer a trim variable. The same steady-state sideslip angle trims explained in Table 20 and Table 21 are performed also here to determine the pedal input required. Then, S_p is set to the pedal value determined and the rotorcraft is allowed to have a yaw acceleration ($\dot{r}$) by removing it from the trim targets. Furthermore, since roll and pitch angles are kept at their trim values, the rotorcraft can no longer sustain a flight with zero $\dot{u}$ and $\dot{v}$.

In order to estimate the maximum yaw velocity with the corresponding sideslip angle and maximum transient sideslip angle with the corresponding yaw velocity, an approach is required. It is known that the rotorcraft initially flies in a forward flight condition. Then, in 0.2 [s], high yaw acceleration, the value of which is known from the maximum tail rotor force trim, develops. It is assumed that the yaw acceleration changes linearly with time and the maximum transient sideslip angle occurs in t_2 seconds. The assumed time history of the yaw acceleration can be seen in Figure 45.

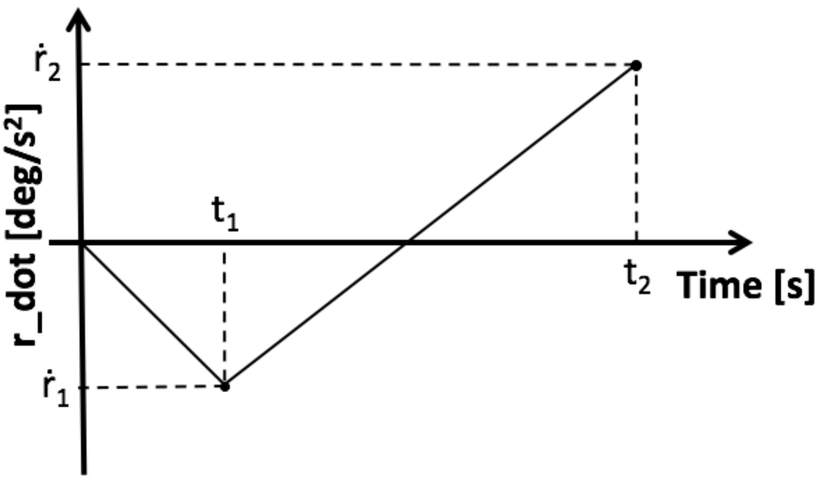

Figure 45. Assumed Yaw Acceleration

The values of t_2 and the corresponding final yaw acceleration ($\dot{r}_2$) are not known. In order to estimate them, it is assumed that the maximum transient sideslip angle is 30% higher than the steady-state sideslip angle determined before. Since the sideslip angle is maximum at t_2, the yaw velocity must be equal to zero. Therefore, two unknowns can be calculated with two equations which are first and second integrals of the yaw acceleration. The piecewise linear function for the yaw acceleration is given in Equation 71. Note that although the starting yaw acceleration ($\dot{r}_1$) and the corresponding time (t_1) are known, they are shown symbolically in Equations 71, 72, and 73.

$$\dot{r} = \begin{cases} \dfrac{\dot{r}_1 t}{t_1} & if\ t_1 \geq t \geq 0 \\ (t - t_1)\dfrac{(\dot{r}_2 - \dot{r}_1)}{(t_2 - t_1)} + \dot{r}_1 & if\ t_2 \geq t > t_1 \end{cases} \tag{71}$$

The yaw velocity is the first integral of the yaw acceleration in time. Integrating yaw acceleration from $t = 0$ to $t = t_2$, Equation 72 is obtained. Note that Equation 72 should be equal to zero since maximum transient sideslip angle is achieved at $t = t_2$ and this can only be possible if the yaw velocity is equal to zero at $t = t_2$.

$$\int_0^{t_2} \dot{r}dt = \left(\frac{t_2^2}{2} - t_1 t_2\right)\frac{\dot{r}_2 - \dot{r}_1}{t_2 - t_1} + \dot{r}_1 t_2 - \left(-\frac{t_1^2}{2}\frac{\dot{r}_2 - \dot{r}_1}{t_2 - t_1} + \dot{r}_1 t_1\right) + \dot{r}_1 \frac{t_1}{2} = 0 \tag{72}$$

The sideslip angle (β) is the second integral of the yaw acceleration in time. Integrating yaw acceleration from $t = 0$ to $t = t_2$ twice, Equation 73 is obtained. Note that Equation 73 should be equal to the maximum transient sideslip angle.

$$\iint_{0}^{t_2} \dot{r}\,dt\,dt = \left(\left(\frac{t_2^3}{6} - t_1\frac{t_2^2}{2}\right)\frac{\dot{r}_2 - \dot{r}_1}{t_2 - t_1} + \dot{r}_1\frac{t_2^2}{2} - t_2\left(-\frac{t_1^2}{2}\frac{\dot{r}_2 - \dot{r}_1}{t_2 - t_1} + \dot{r}_1 t_1\right) + \left(\dot{r}_1 t_1 \frac{t_2}{2}\right)\right) - \left(\left(-\frac{t_1^3}{3}\right)\frac{\dot{r}_2 - \dot{r}_1}{t_2 - t_1} + \dot{r}_1\frac{t_1^2}{2} - t_1\left(-\frac{t_1^2}{2}\frac{\dot{r}_2 - \dot{r}_1}{t_2 - t_1} + \dot{r}_1 t_1\right) + \left(\dot{r}_1\frac{t_1^2}{2}\right)\right) + \dot{r}_1\frac{t_1^2}{6} = 1.3\beta_{steady-state} \tag{73}$$

Simultaneous solution of Equations 72 and 73 is performed numerically to calculate the values of the unknowns t_2 and $\dot{r}_2$. The yaw acceleration, yaw velocity and sideslip angle calculated by using the approach explained above and the corresponding values obtained from the transient analysis are compared in Figure 46, Figure 47, and Figure 48 for yaw-to-port maneuver in 80 [knot], 120 [knot], and 160 [knot], respectively.

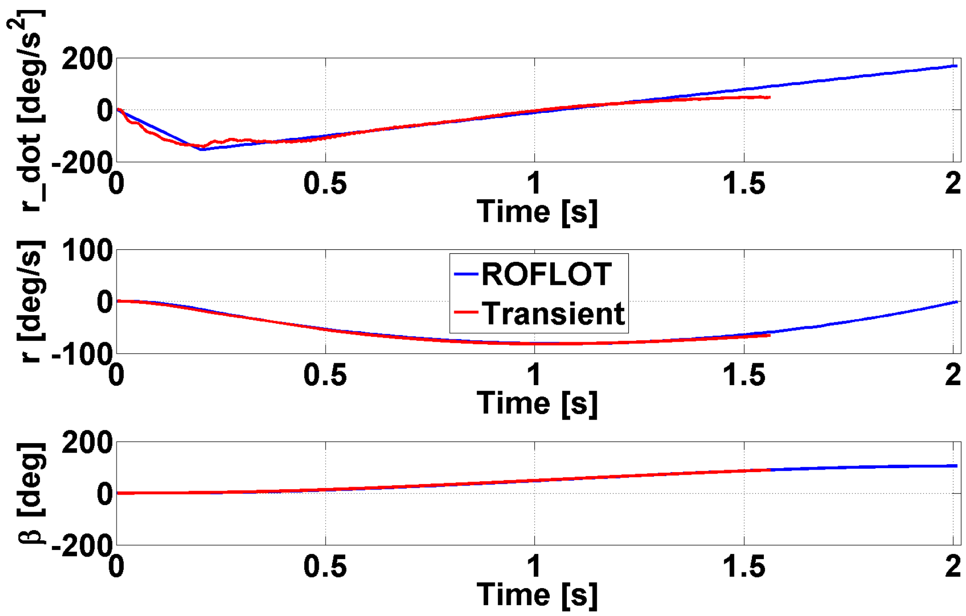

Figure 46. Comparison of the Yaw Acceleration, Yaw Velocity and Sideslip Angle Estimated and Obtained from the Transient Analysis of Yaw to Port Maneuver in 80 [knot]

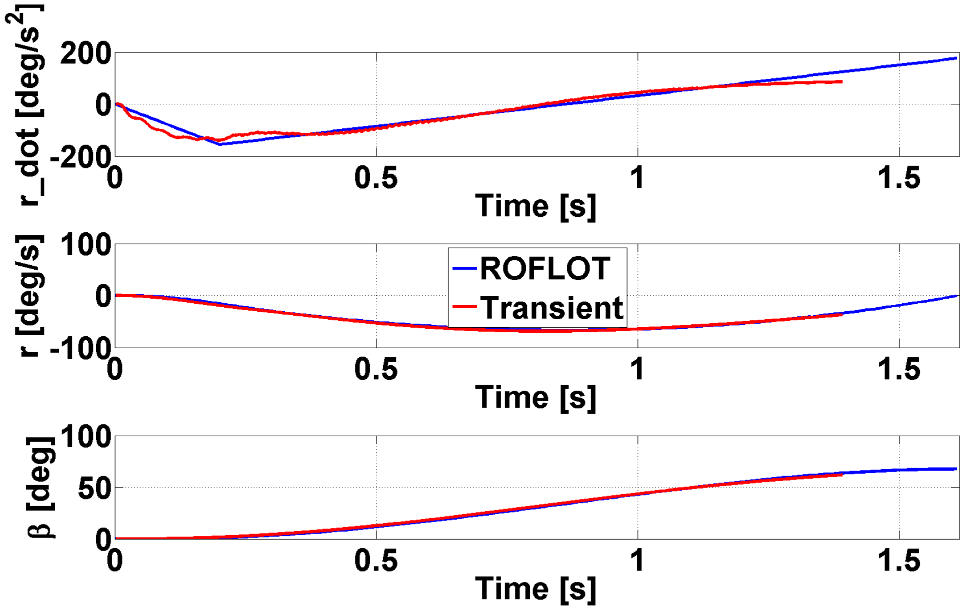

Figure 47. Comparison of the Yaw Acceleration, Yaw Velocity and Sideslip Angle Estimated and Obtained from the Transient Analysis of Yaw to Port Maneuver in 120 [knot]

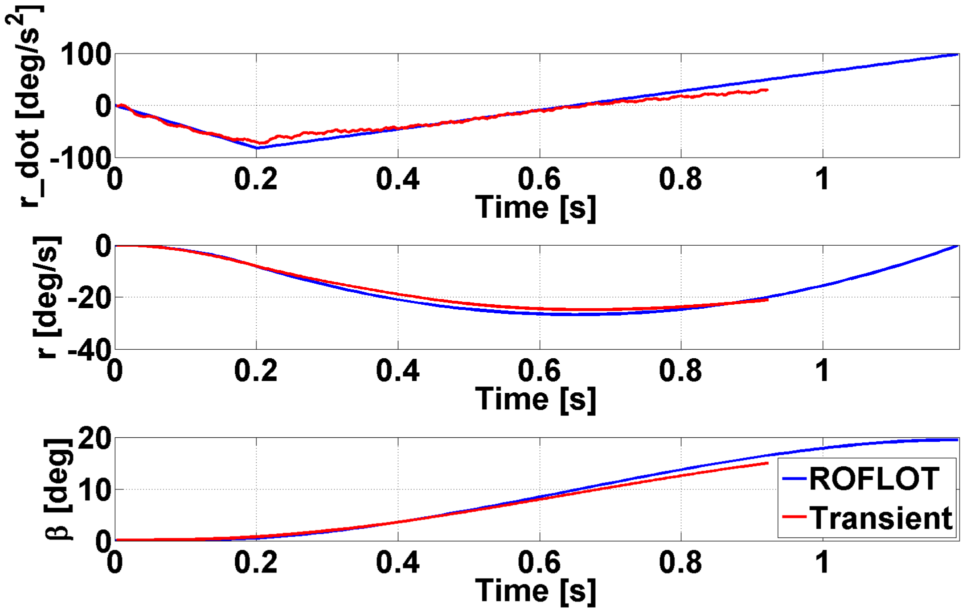

Figure 48. Comparison of the Yaw Acceleration, Yaw Velocity and Sideslip Angle Estimated and Obtained from the Transient Analysis of Yaw to Port Maneuver in 160 [knot]

As it can be seen from Figure 46, Figure 47, and Figure 48, the yaw velocity and sideslip angles can be estimated well with the approach developed. This way, the critical time instants of a yaw maneuver can be solved by using trim points.

The last trim point is for the return phase of the yaw maneuver. The rotorcraft is trimmed at the steady-state sideslip angle explained above and the trim variables and trim targets are altered very similar to the maximum tail rotor thrust trim. This time, the pedal is set to its forward flight position.

All the trims mentioned above are performed with scripts specifically developed for this task.

5.2.4. Gust Conditions

Gust conditions have been analyzed by employing both transient analysis and ROFLOT approach. Gusts conditions from forward, rear, up, down, left, and right have been analyzed but the methodology is the same regardless of the gust direction. The methodology for both the transient solution and ROFLOT approach are explained in this chapter.

5.2.4.1. Transient Analysis

For the transient analysis of the gust conditions, first, the rotorcraft is trimmed in a forward flight condition by using the trim variables and the trim targets shown in Table 16. After that, starting from this forward flight condition, transient analysis is performed by defining a gust profile based on the gust condition by using LOFD. The rotorcraft enters the sharp-edged gust field immediately after the forward flight trim. After the rotorcraft flies a distance of three times the radius of the main rotor blades, it exits the gust field. However, for the hover condition, since the rotorcraft does not move, 2 [s] is used for the gradient time of the gust profile as shown in Figure 49.

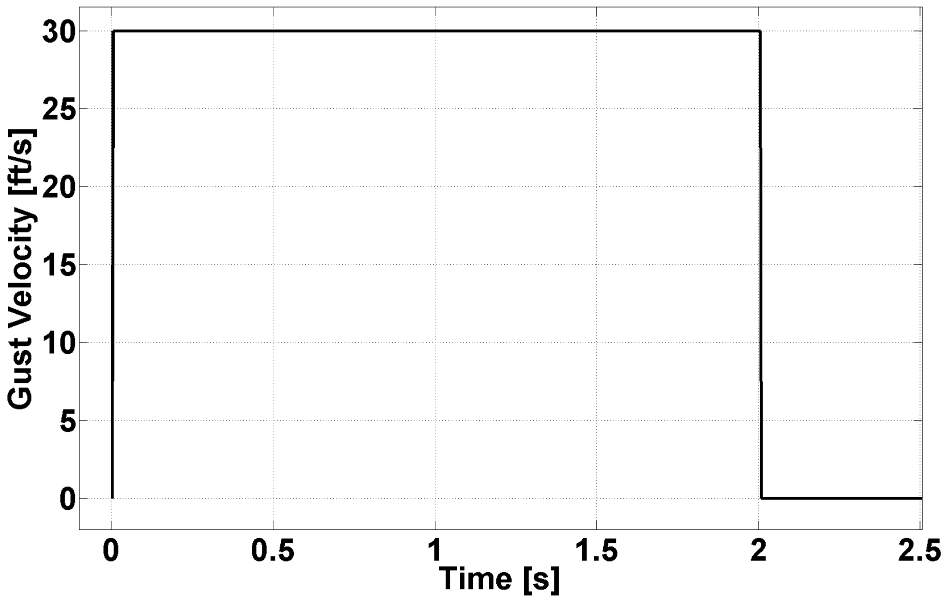

Figure 49. Gust Profile Used for the Transient Analysis of the Gust Conditions in Hover

Performing gust transient analyses and calculating the fuselage loads for different mass states, velocities, densities is computationally expensive. As an example, considering six mass states, five flight speeds, two rotor speeds, four densities, and six gust conditions in order to cover gusts from forward, rear, up, down, left, and right directions makes a total of almost one thousand and five hundred conditions.

5.2.4.2. ROFLOT Approach

In this method, the gust condition is represented by a single point. Like the transient analysis, first, the rotorcraft is trimmed in a forward flight condition by using the trim variables and the trim targets shown in Table 16. After that, all the trim variables are kept constant at their trim values. In other words, the stick positions, pedal position, roll and pitch angles shown in Table 16 are set to the values obtained from the forward flight trim. Furthermore, the trim targets are set free which means that linear and angular accelerations in all the directions are allowed.

The velocity of the gust (30 [fps]) is defined and the velocity field on both main rotor and tail rotor and the airframe is changed. This method can also be called as a dynamic trim but this time no iteration is performed since there is no trim variable and trim target for the Newton-Raphson method.

LOFD combined with a script specifically developed for this task has been used to perform the gust analyses in all the directions after a single forward flight trim is performed. In other words, the velocity field on main rotor, tail rotor, and airframe is changed depending on the gust condition and analysis is performed for each gust direction by using the stick positions and rotorcraft attitude obtained from the forward flight condition.

In this method, no angular velocity is developed on the airframe. However, angular accelerations and linear accelerations do occur since the forward flight trim is no longer preserved.

CHAPTER 6

RESULTS & COMPARISONS

In this chapter, the fuselage loads obtained by using the transient solution and ROFLOT approach are compared. Both case-by-case and overall comparisons are provided. Note that the x axis in the force and moment diagrams is from the most forward (0 [m]) to the most aft (14 [m]) of the fuselage.

6.1. Pull-up Maneuver

Comparison of maximum and minimum axial force, shear forces, torsional moment, and bending moments obtained by using ROFLOT approach and transient solution for a 3.5 [g] pull-up maneuver performed in flight speeds of 80 [knot] and 120 [knot] are given in Figure 50 to Figure 55.

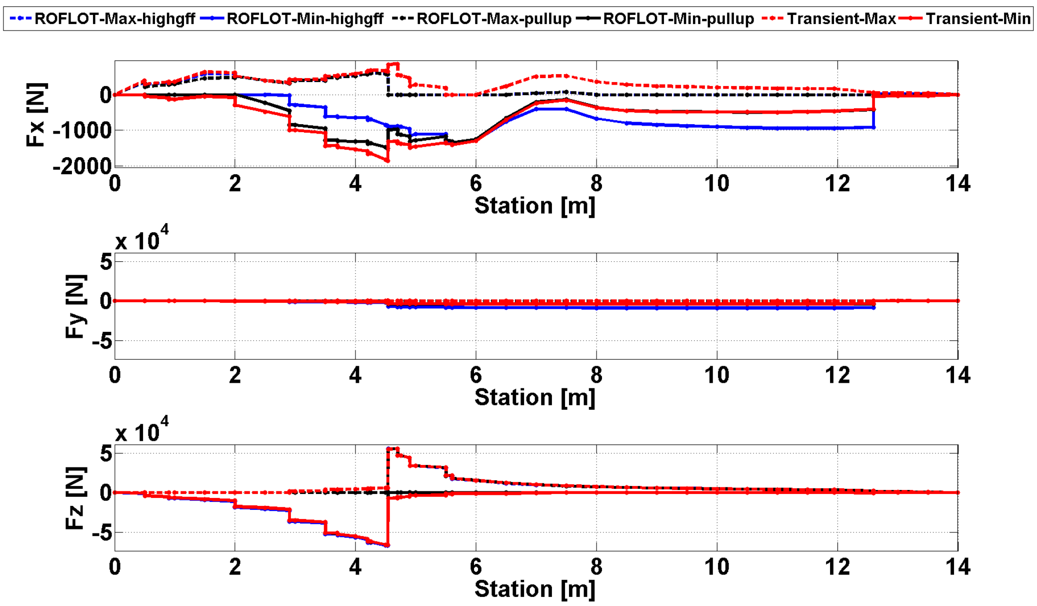

Figure 50. Comparison of Trim and Transient Solution Axial and Shear Forces for Sea Level, ISA -55 C^0, 80 [knot], 3.5 [g] Pull-up Maneuver

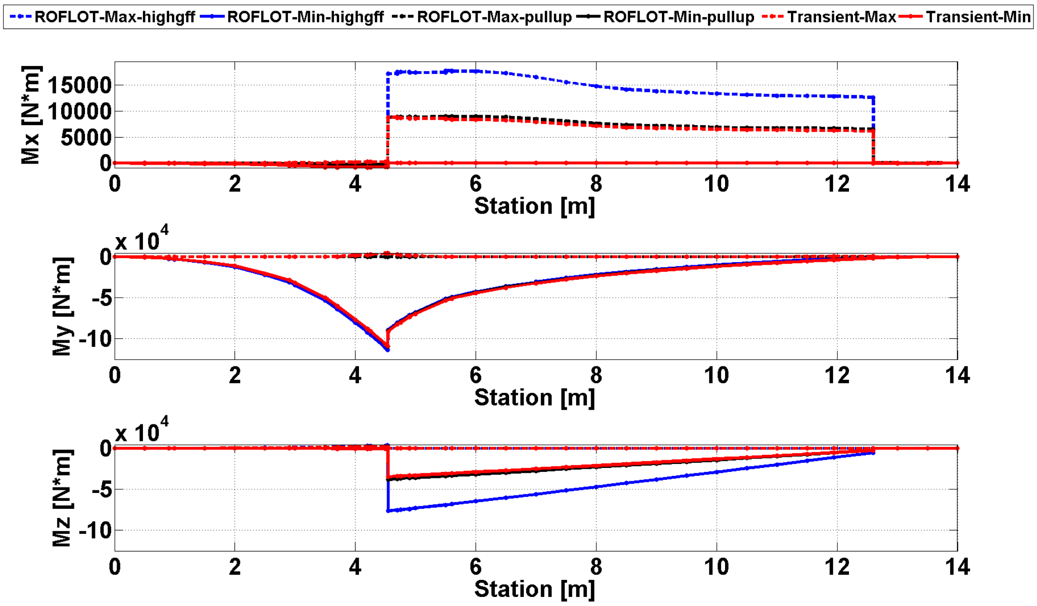

Figure 51. Comparison of Trim and Transient Solution Torsional and Bending Moments for Sea Level, ISA -55 C^0, 80 [knot], 3.5 [g] Pull-up Maneuver

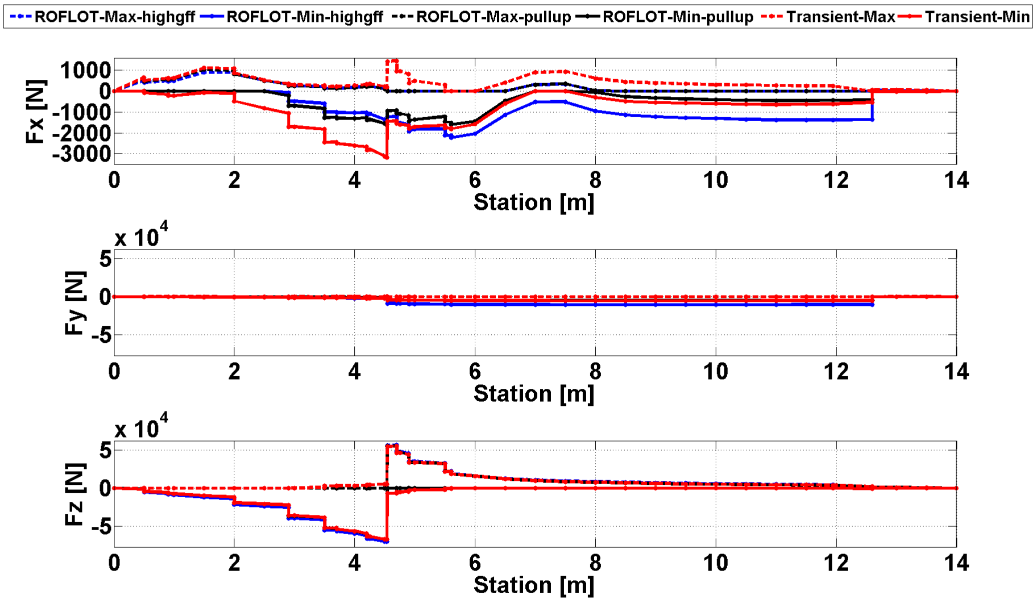

Figure 52. Comparison of Trim and Transient Solution Axial and Shear Forces for Sea Level, ISA -55 C^0, 120 [knot], 3.5 [g] Pull-up Maneuver

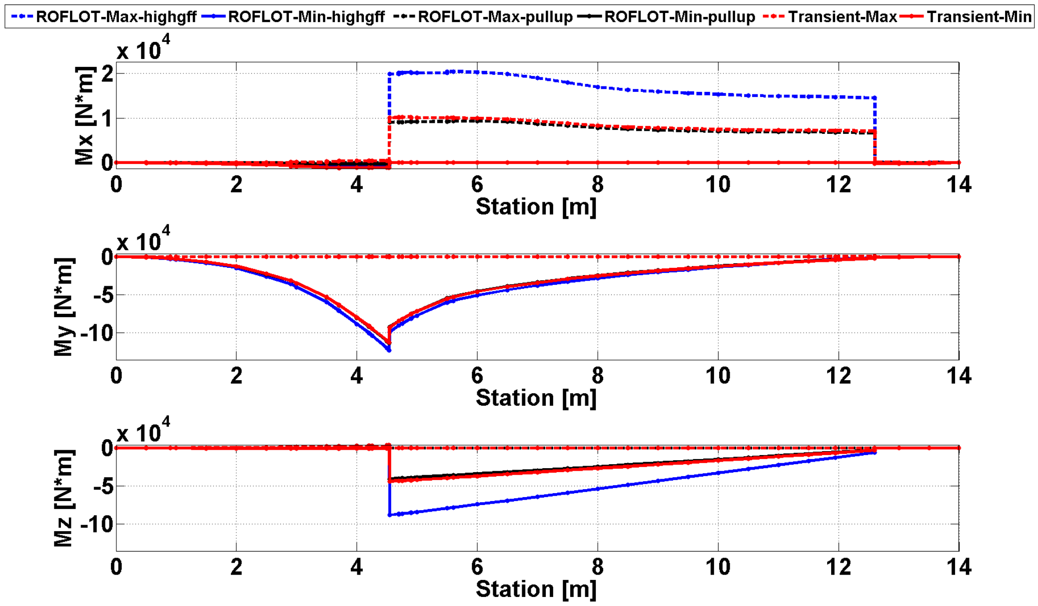

Figure 53. Comparison of Trim and Transient Solution Torsional and Bending Moments for Sea Level, ISA -55 C^0, 120 [knot], 3.5 [g] Pull-up Maneuver

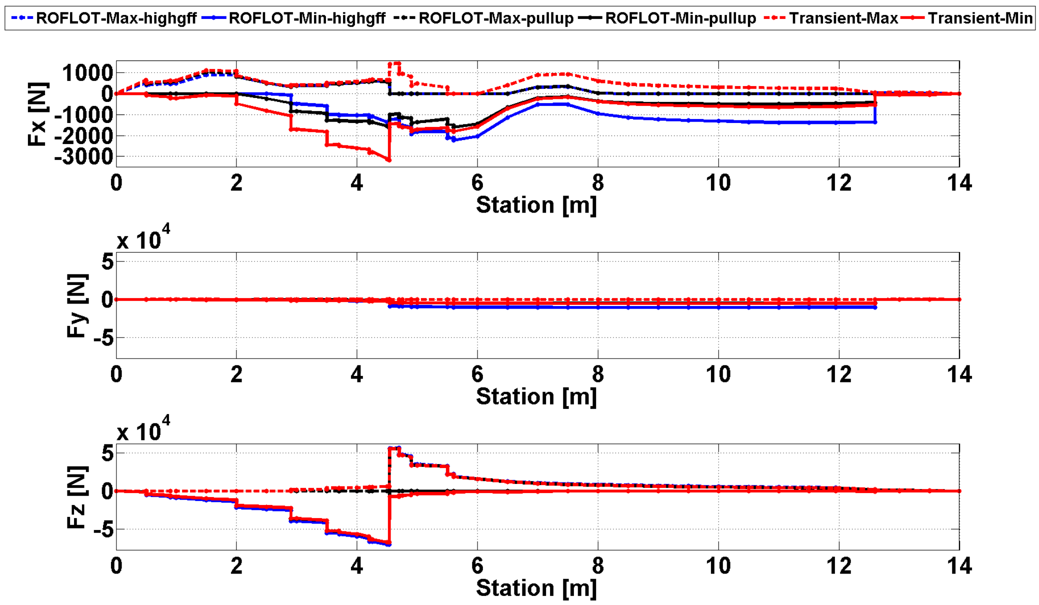

Figure 54. Comparison of Trim and Transient Solution Overall Maximum and Minimum Axial and Shear Forces of the Pull-up Maneuvers

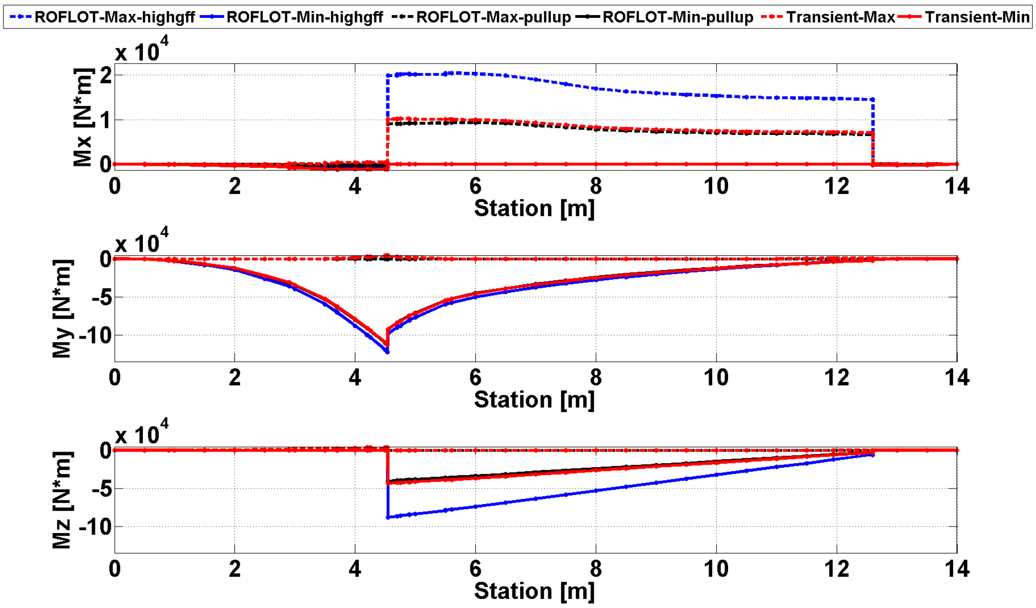

Figure 55. Comparison of Trim and Transient Solution Overall Maximum and Minimum Torsional and Bending Moments of the Pull-up Maneuvers

It can be seen in Figure 50 to Figure 55 that the pull-up trim method can estimate the maximum and minimum loads encountered in a pull-up maneuver very well except from F_x in terms of negative values which is generally underestimated especially for the sections between the nose and 5.5 [m]. The high-g forward flight method can estimate F_z and M_y well but it overestimates M_x and M_z. The reason behind this is the main rotor torque difference in the analysis results. The high torque requires high tail rotor thrust and main rotor generates high side force to compensate for the high tail rotor thrust. Furthermore, since the main rotor has a shaft tilt angle, the rotor torque has components on both x_{LAS} and z_{LAS} directions. As a result, high M_x and M_z occur. Moreover, F_x is underestimated for the sections towards the nose and overestimated for the sections towards the tail for the high-g forward flight trim method.

The aerodynamic loading on the fuselage for the high-g forward flight trim method is different than that of the transient analysis. However, since F_z and M_y are close to the transient solution, it can be stated that the aerodynamic load difference is not significant in these directions when compared to the inertial loads. Furthermore, it can be observed that the effect of inertial loading due to pitch rate (centrifugal force) on F_z and M_y is not significant.

6.2. Push-over Maneuver

Comparison of maximum and minimum axial force, shear forces, torsional moment, and bending moments obtained by using ROFLOT approach and transient solution for a -1 [g] push-over maneuver performed in flight speeds of 80 [knot] and 120 [knot] are given in Figure 56 to Figure 61.

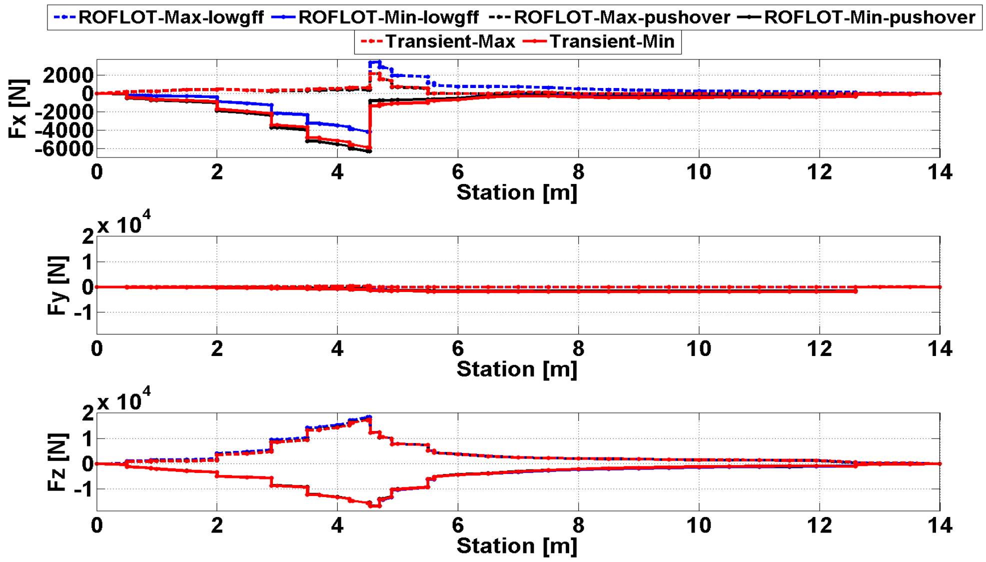

Figure 56. Comparison of Trim and Transient Solution Axial and Shear Forces for Sea Level, ISA -55 C^0, 80 [knot], -1 [g] Push-over Maneuver

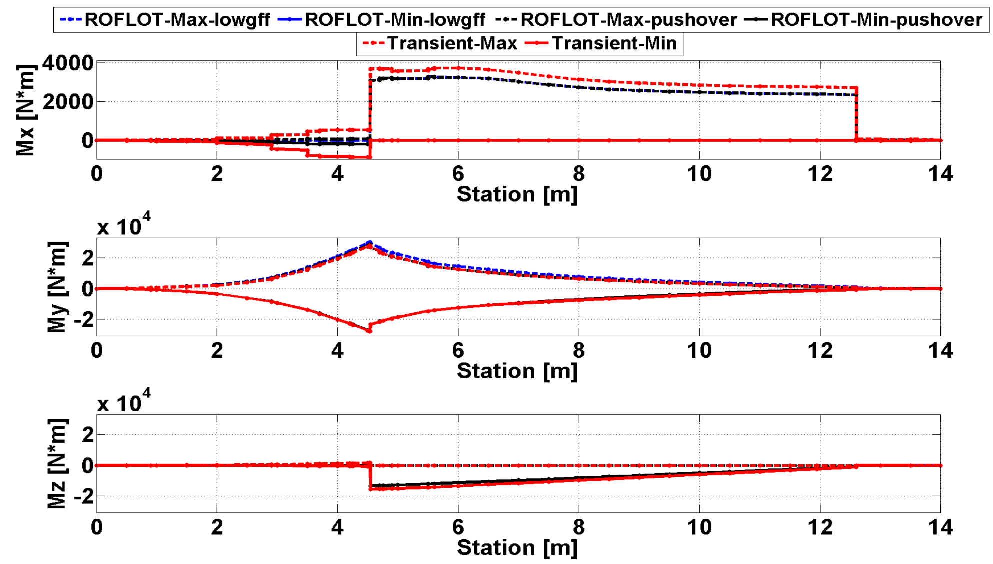

Figure 57. Comparison of Trim and Transient Solution Torsional and Bending Moments for Sea Level, ISA -55 C^0, 80 [knot], -1 [g] Push-over Maneuver

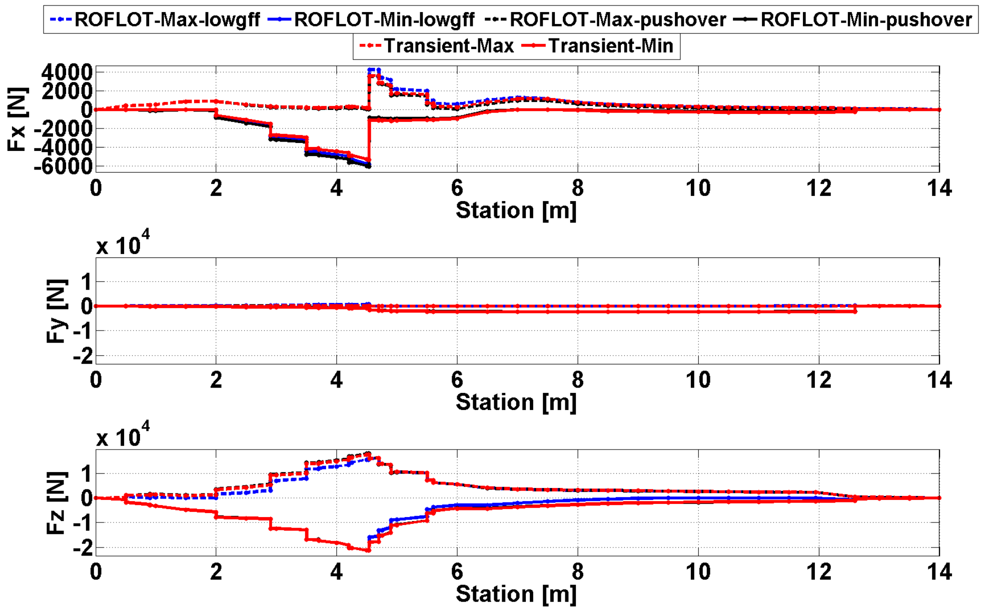

Figure 58. Comparison of Trim and Transient Solution Axial and Shear Forces for Sea Level, ISA -55 C^0, 120 [knot], -1 [g] Push-over Maneuver

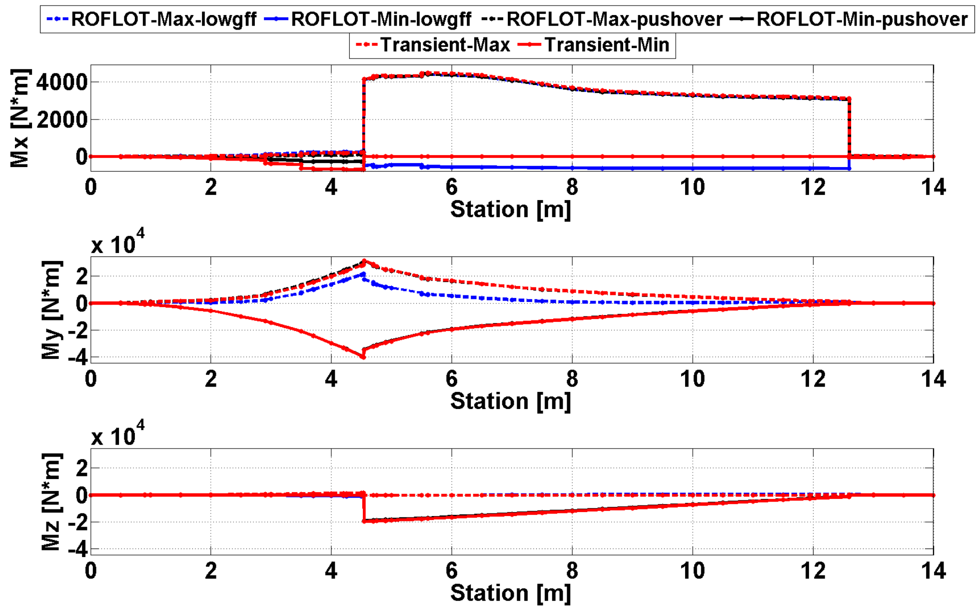

Figure 59. Comparison of Trim and Transient Solution Torsional and Bending Moments for Sea Level, ISA -55 C^0, 120 [knot], -1 [g] Push-over Maneuver

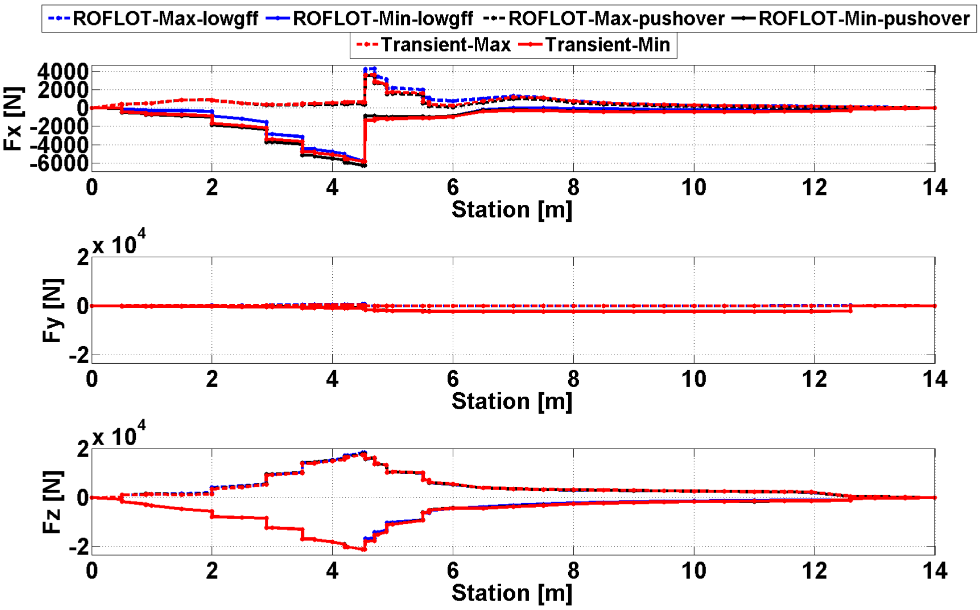

Figure 60. Comparison of Trim and Transient Solution Overall Maximum and Minimum Axial and Shear Forces of the Push-over Maneuvers

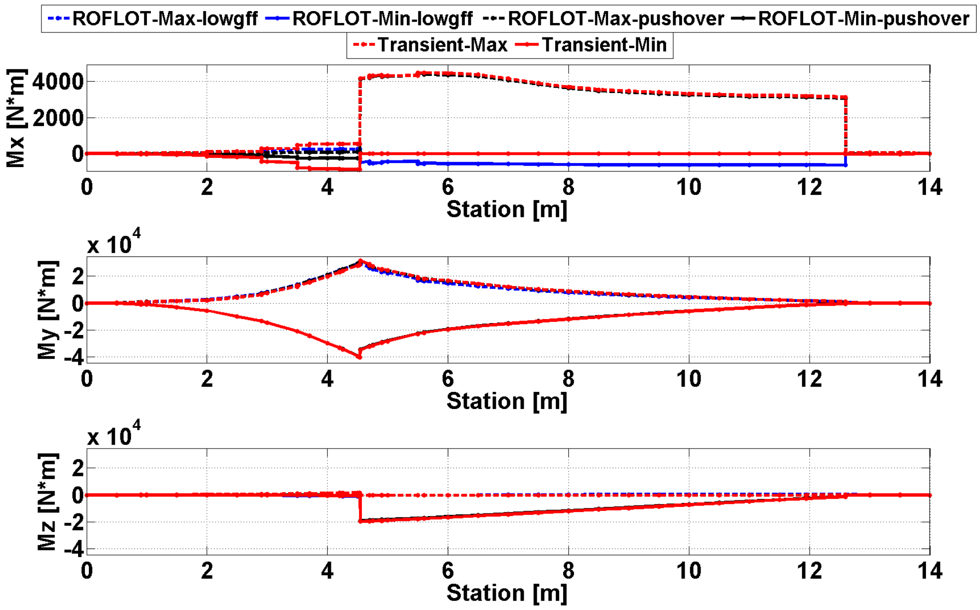

Figure 61. Comparison of Trim and Transient Solution Overall Maximum and Minimum Torsional and Bending Moments of the Push-over Maneuvers

It can be seen in Figure 56 to Figure 61 that positive F_z before the main rotor hub and negative F_z after occurs in the push-over maneuver. Furthermore, positive M_y occurs due to the negative load factor.

The loads obtained by using the push-over trim method are generally very close to the transient analysis loads. Furthermore, low-g forward flight trim method results are satisfactorily close to the transient solution results for 80 [knot] case except from F_x. However, the same agreement is not observed for the 120 [knot] case. F_z and M_y for the 120 [knot] case are lower than the transient solution because of the difference in the aerodynamic loading. However, the overall maximum and minimum loads presented in Figure 60 and Figure 61 show good agreement between the results of transient analysis and ROFLOT approach since high positive F_z and M_y are already achieved in the 80 [knot] case.

6.3. Yaw Maneuver

Comparison of maximum and minimum axial force, shear forces, torsional moment, and bending moments obtained by using ROFLOT approach and transient solution for yaw to port maneuver, both entry and return, performed in flight speeds of 80 [knot], 120 [knot], and 160 [knot] are given in Figure 62 to Figure 69.

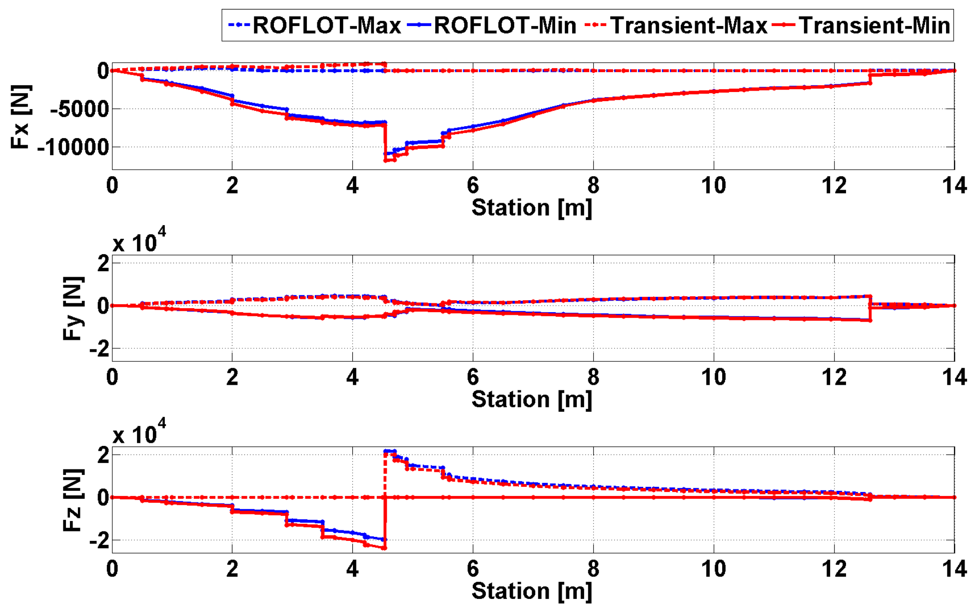

Figure 62. Comparison of Trim and Transient Solution Axial and Shear Forces for Sea Level, 80 [knot], Yaw to Port Maneuver

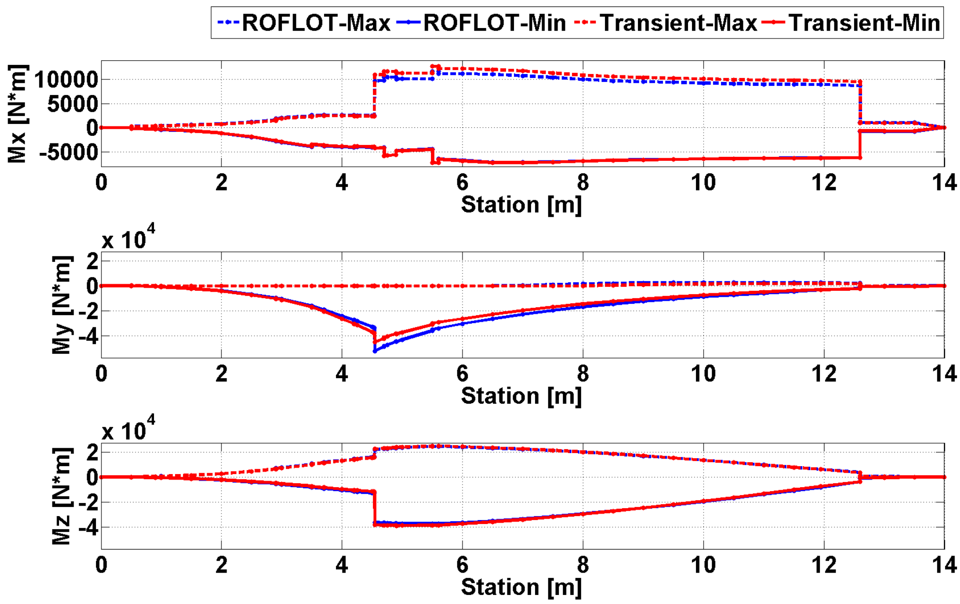

Figure 63. Comparison of Trim and Transient Solution Torsional and Bending Moments for Sea Level, 80 [knot], Yaw to Port Maneuver

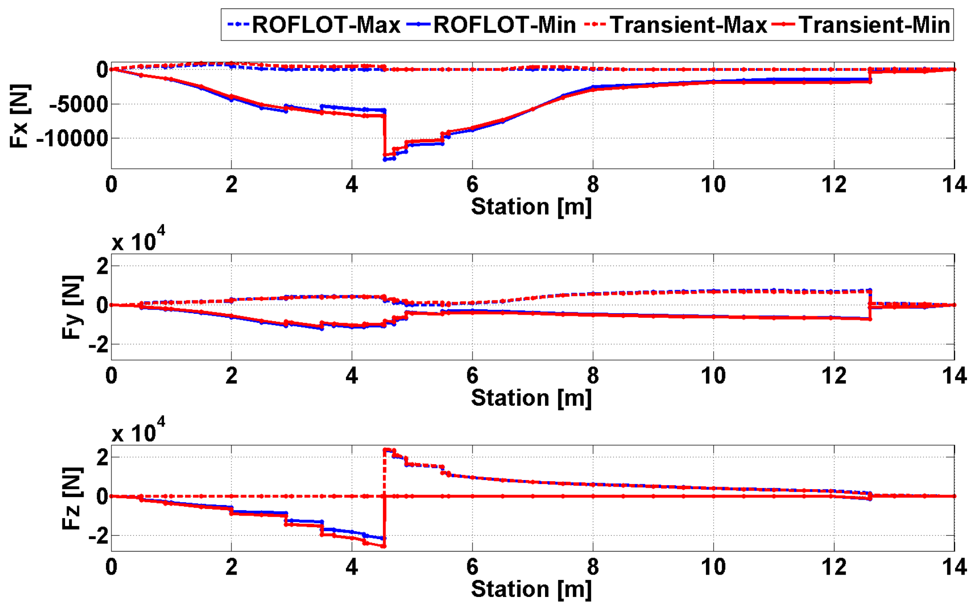

Figure 64. Comparison of Trim and Transient Solution Axial and Shear Forces for Sea Level, 120 [knot], Yaw to Port Maneuver

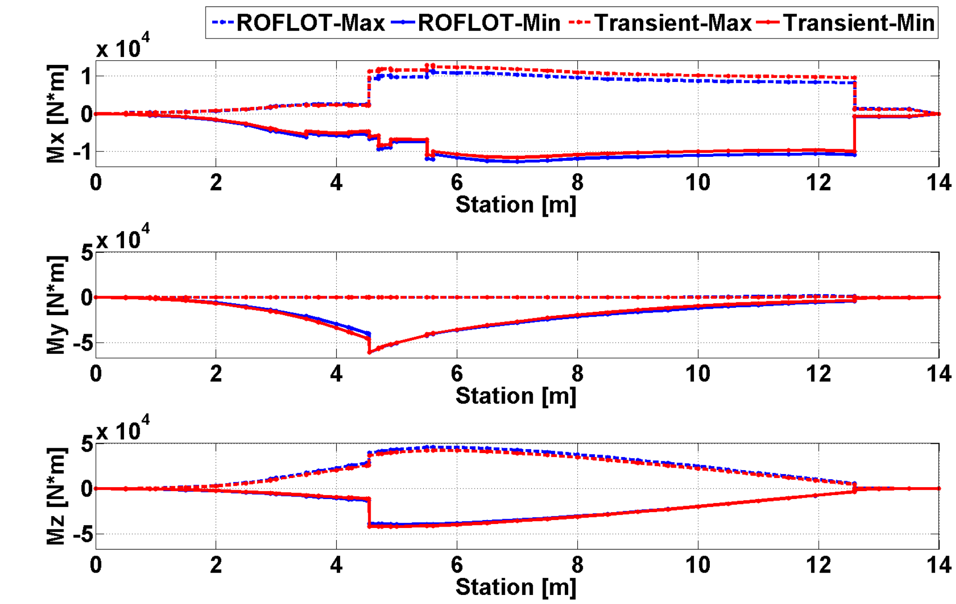

Figure 65. Comparison of Trim and Transient Solution Torsional and Bending Moments for Sea Level, 120 [knot], Yaw to Port Maneuver

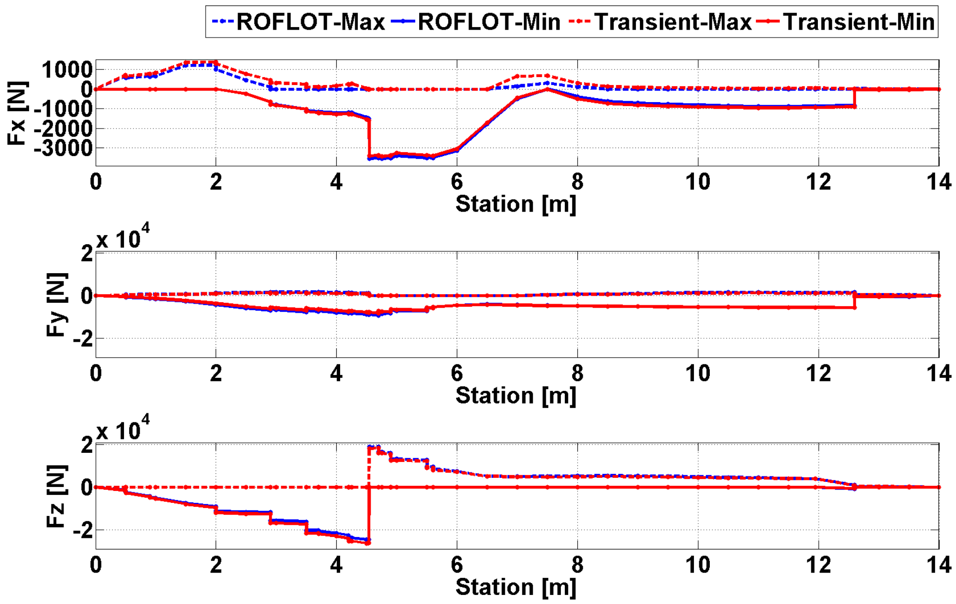

Figure 66. Comparison of Trim and Transient Solution Axial and Shear Forces for Sea Level, 160 [knot], Yaw to Port Maneuver

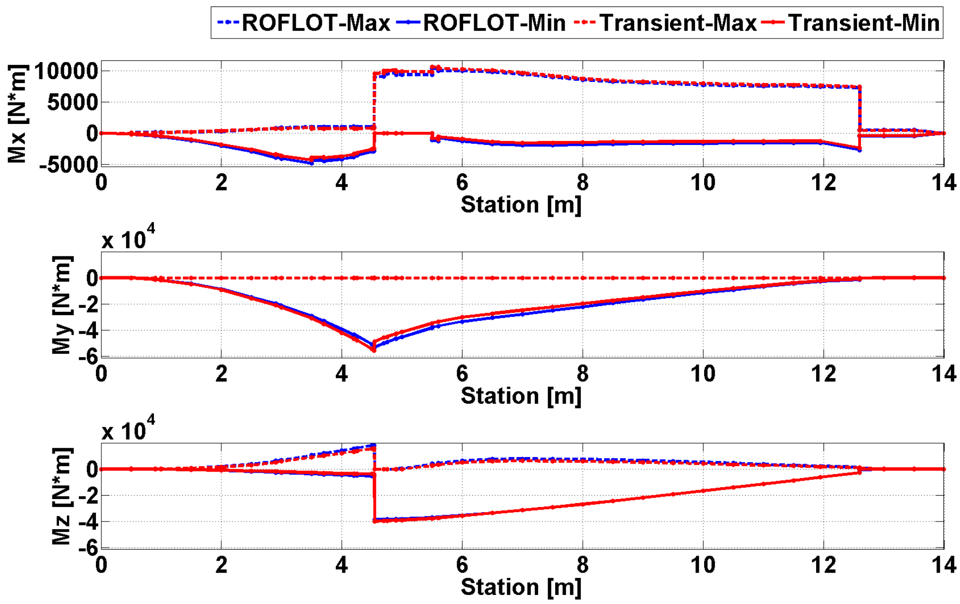

Figure 67. Comparison of Trim and Transient Solution Torsional and Bending Moments for Sea Level, 160 [knot], Yaw to Port Maneuver

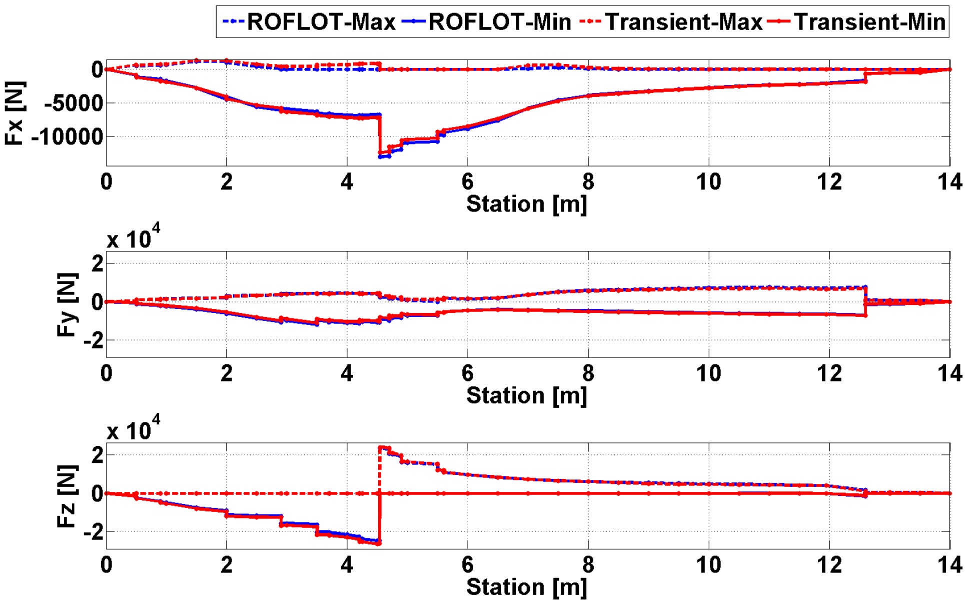

Figure 68. Comparison of Trim and Transient Solution Overall Maximum and Minimum Axial and Shear Forces of the Yaw Maneuvers

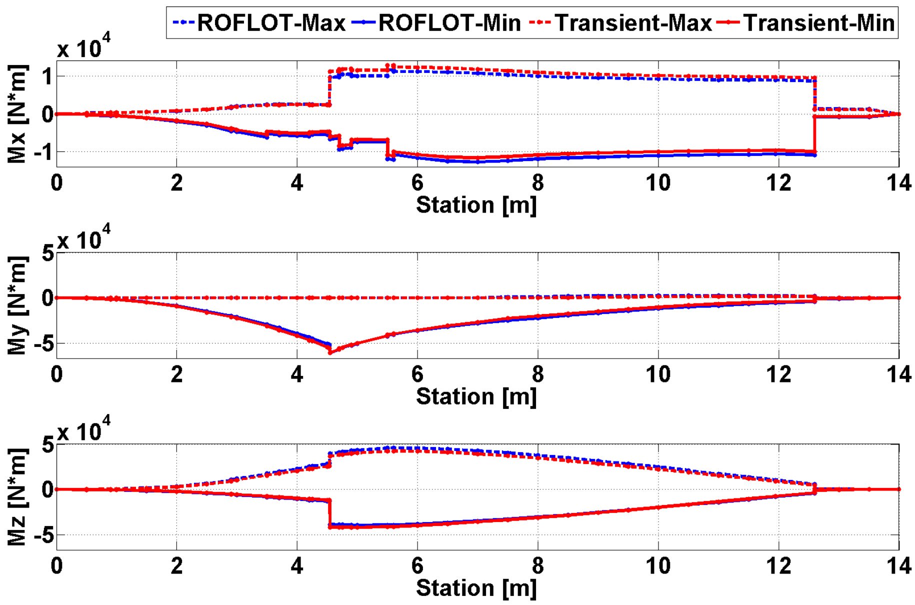

Figure 69. Comparison of Trim and Transient Solution Overall Maximum and Minimum Torsional and Bending Moments of the Yaw Maneuvers

It can be seen in Figure 62 to Figure 69 that the loads calculated by using ROFLOT approach and transient analysis are very close. High F_x occurs on the fuselage due to the combination of high yaw rate and high sideslip angle. Furthermore, high M_z in the negative direction occurs due to high tail rotor thrust in the entry part of the maneuver and high M_z in the positive direction occurs due to the return part.

6.4. Gust Conditions

Gust conditions are divided into sub chapters based on the direction of the gust. Gusts from forward, rear, up, down, left, and right have been analyzed.

6.3.1. Gust From Forward Condition

Comparison of maximum and minimum axial force, shear forces, torsional moment, and bending moments obtained by using ROFLOT approach and transient solution for gust from forward condition in hover, 80 [knot], and 160 [knot] are given in Figure 70 to Figure 75.

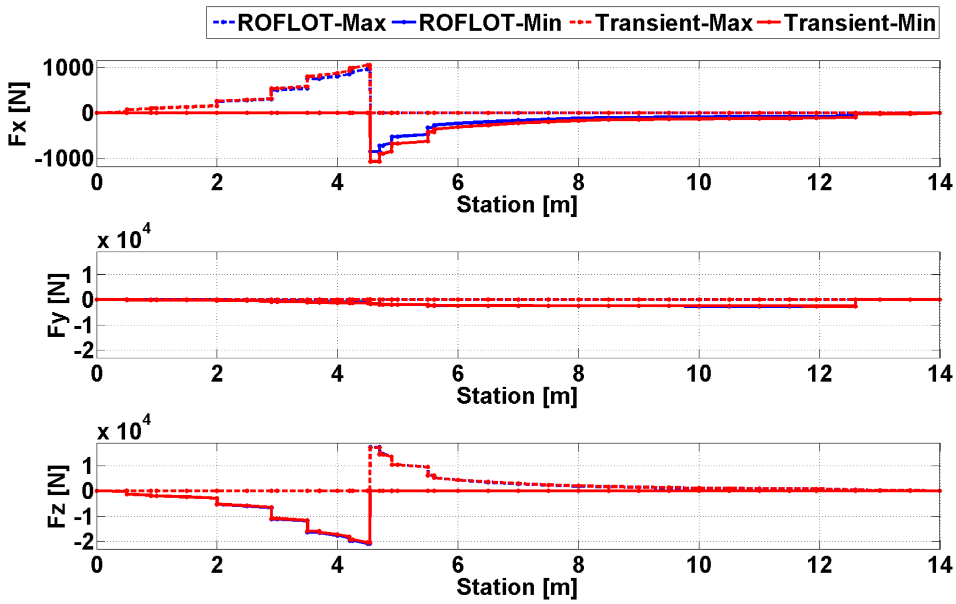

Figure 70. Comparison of Trim and Transient Solution Axial and Shear Forces for Sea Level, Hover, Gust From Forward Condition

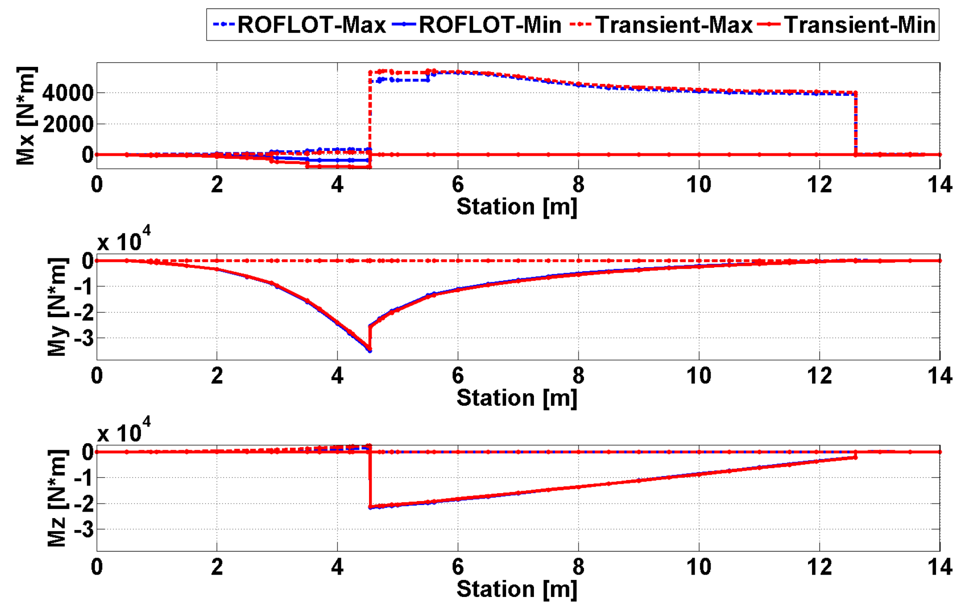

Figure 71. Comparison of Trim and Transient Solution Torsional and Bending Moments for Sea Level, Hover, Gust From Forward Condition

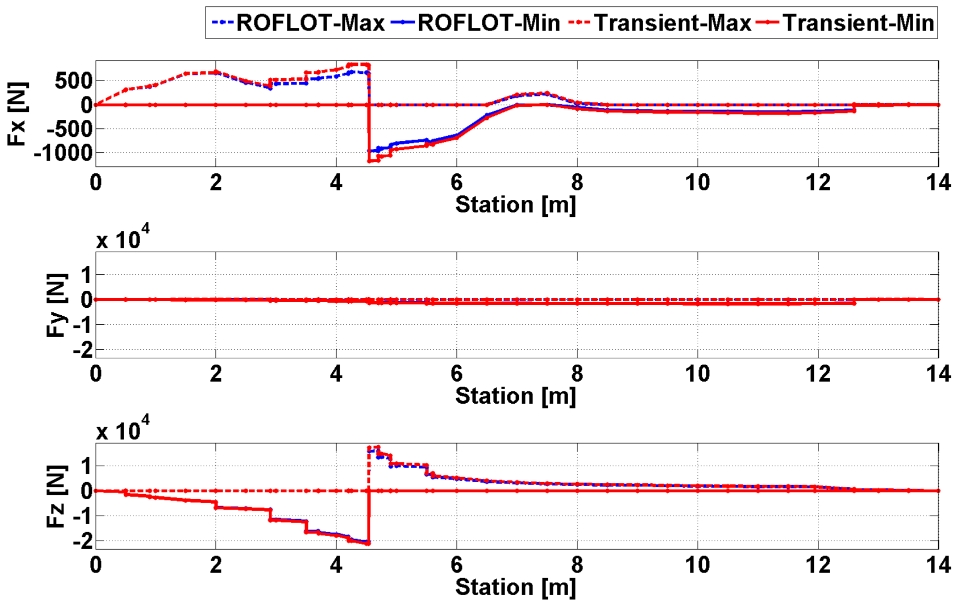

Figure 72. Comparison of Trim and Transient Solution Axial and Shear Forces for Sea Level, 80 [knot] Forward Flight, Gust From Forward Condition

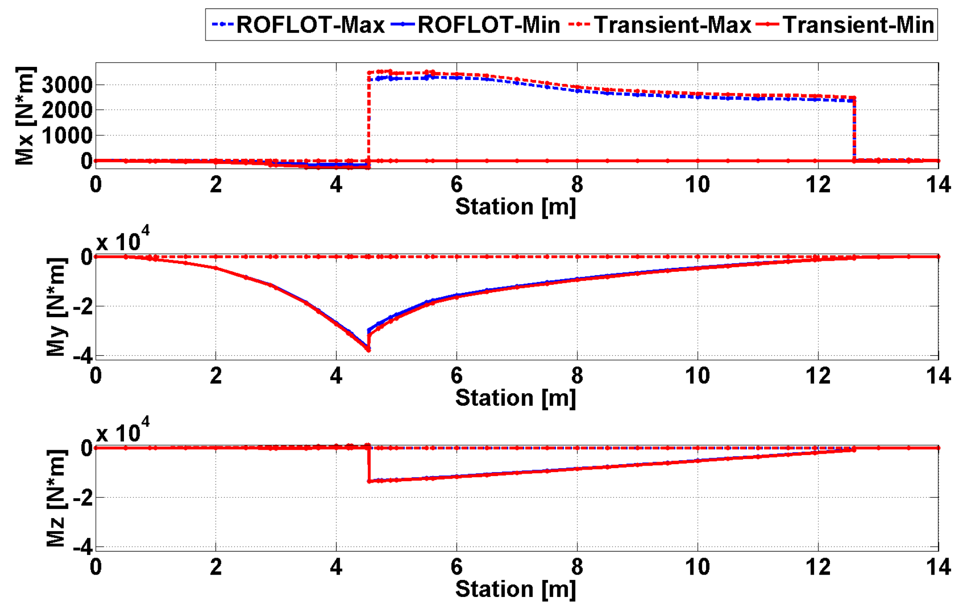

Figure 73. Comparison of Trim and Transient Solution Torsional and Bending Moments for Sea Level, 80 [knot] Forward Flight, Gust From Forward Condition

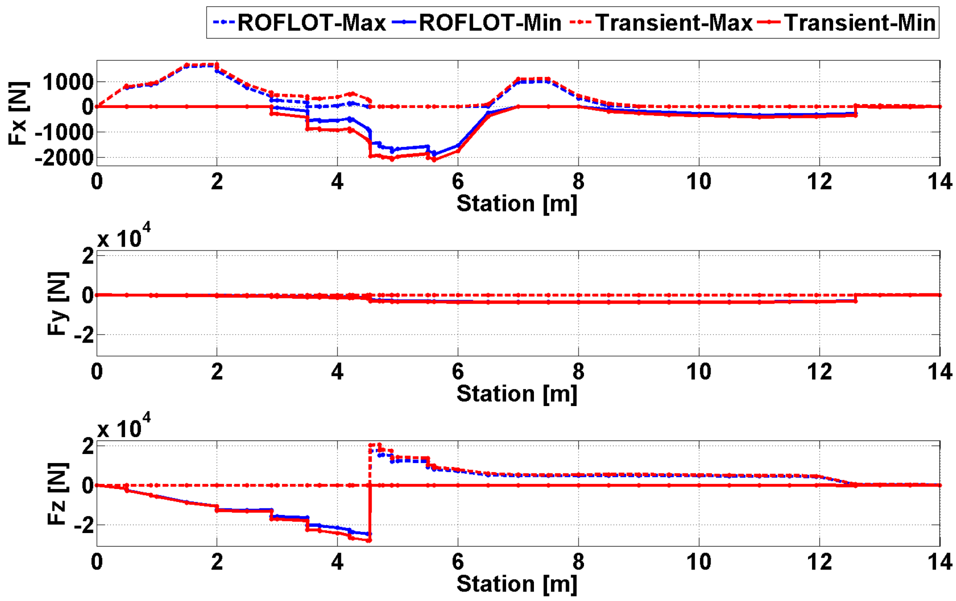

Figure 74. Comparison of Trim and Transient Solution Axial and Shear Forces for Sea Level, 160 [knot] Forward Flight, Gust From Forward Condition

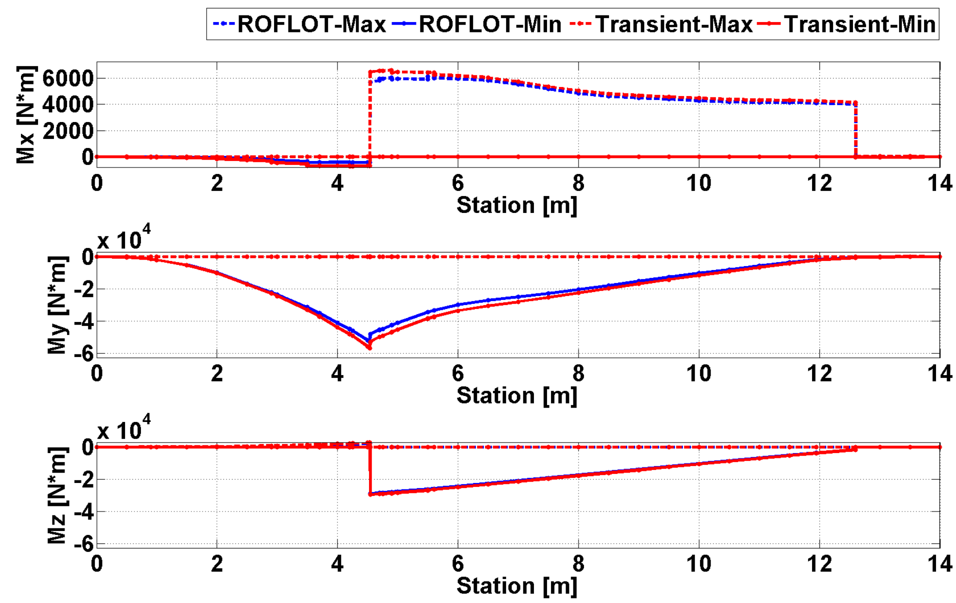

Figure 75. Comparison of Trim and Transient Solution Torsional and Bending Moments for Sea Level, 160 [knot] Forward Flight, Gust From Forward Condition

It can be seen in Figure 70 to Figure 75 that the loads calculated by using ROFLOT approach and transient analysis are very close for the hover and 80 [knot] cases except from F_x which is slightly underestimated. For the 160 [knot] case, M_y is also slightly underestimated by using ROFLOT approach.

6.3.2. Gust From Rear Condition

Comparison of maximum and minimum axial force, shear forces, torsional moment, and bending moments obtained by using ROFLOT approach and transient solution for gust from rear condition in hover, 80 [knot], and 160 [knot] are given in Figure 76 to Figure 81.

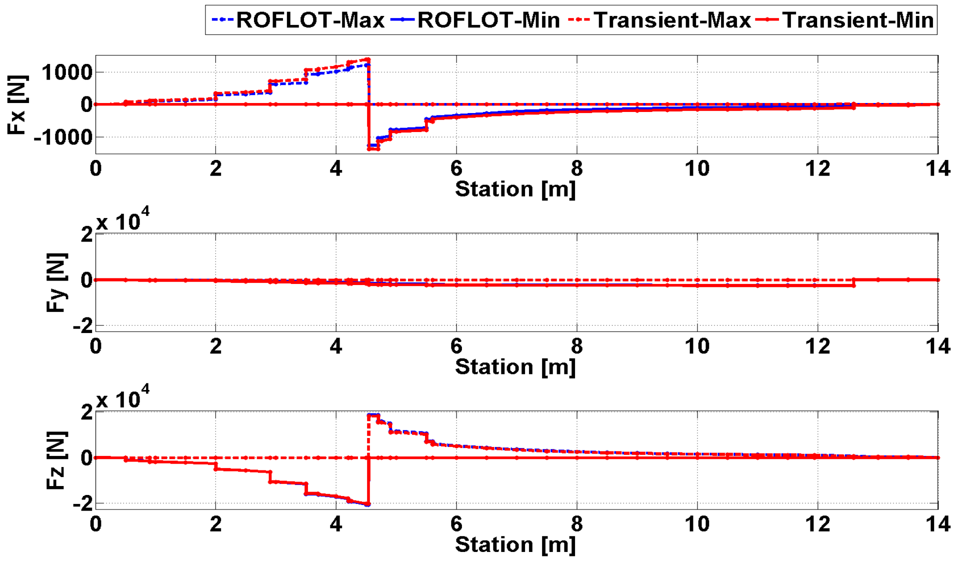

Figure 76. Comparison of Trim and Transient Solution Axial and Shear Forces for Sea Level, Hover, Gust From Rear Condition

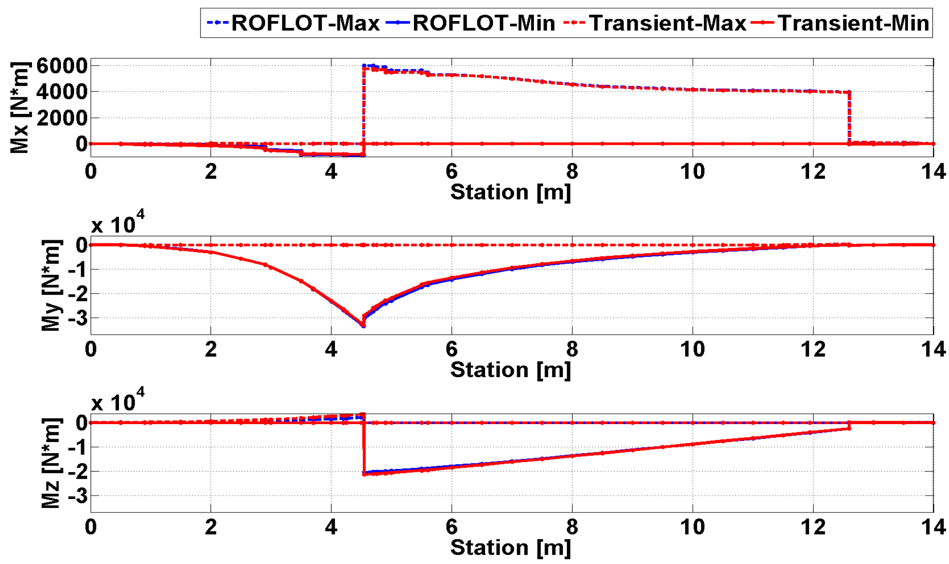

Figure 77. Comparison of Trim and Transient Solution Torsional and Bending Moments for Sea Level, Hover, Gust From Rear Condition

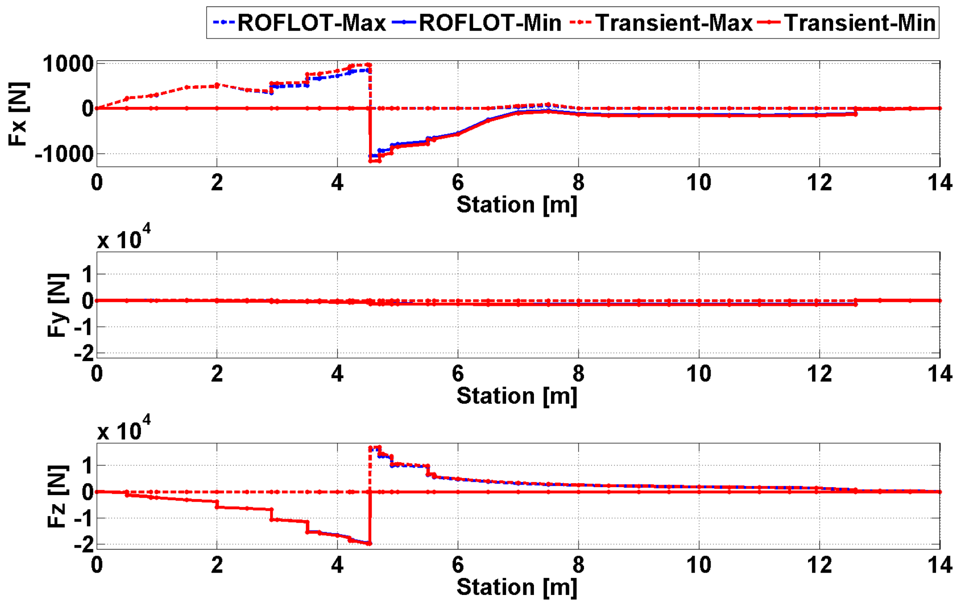

Figure 78. Comparison of Trim and Transient Solution Axial and Shear Forces for Sea Level, 80 [knot] Forward Flight, Gust From Rear Condition

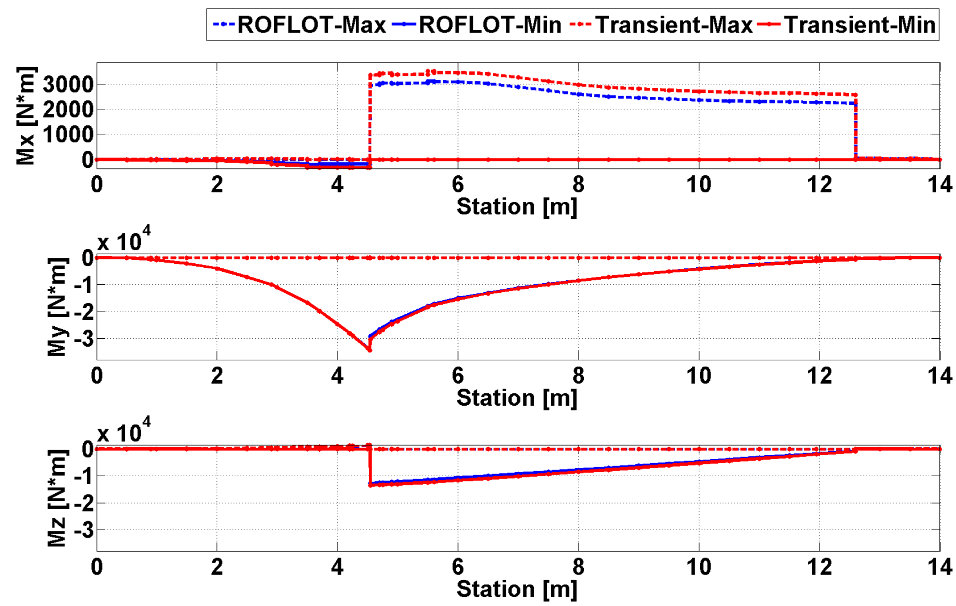

Figure 79. Comparison of Trim and Transient Solution Torsional and Bending Moments for Sea Level, 80 [knot] Forward Flight, Gust From Rear Condition

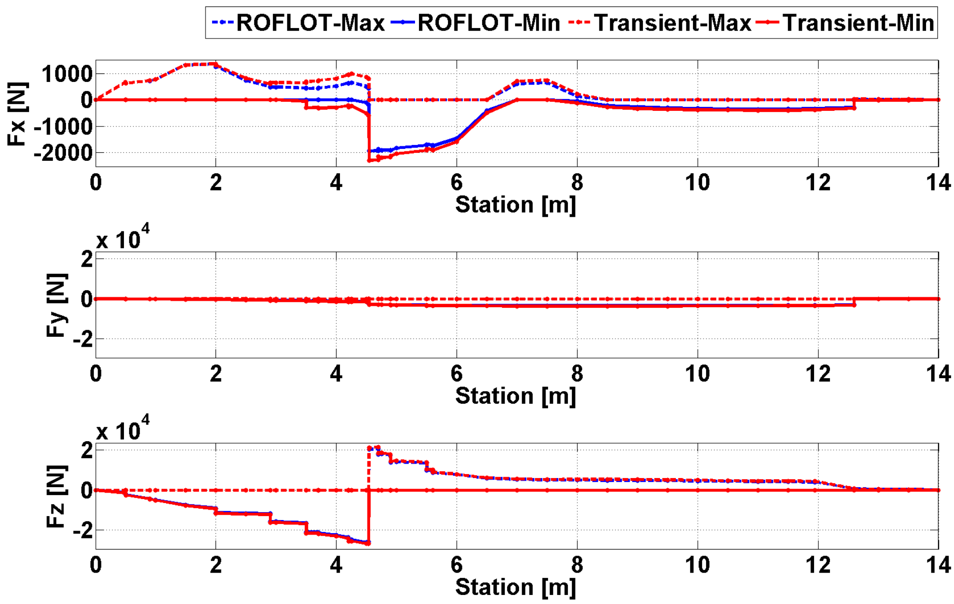

Figure 80. Comparison of Trim and Transient Solution Axial and Shear Forces for Sea Level, 160 [knot] Forward Flight, Gust From Rear Condition

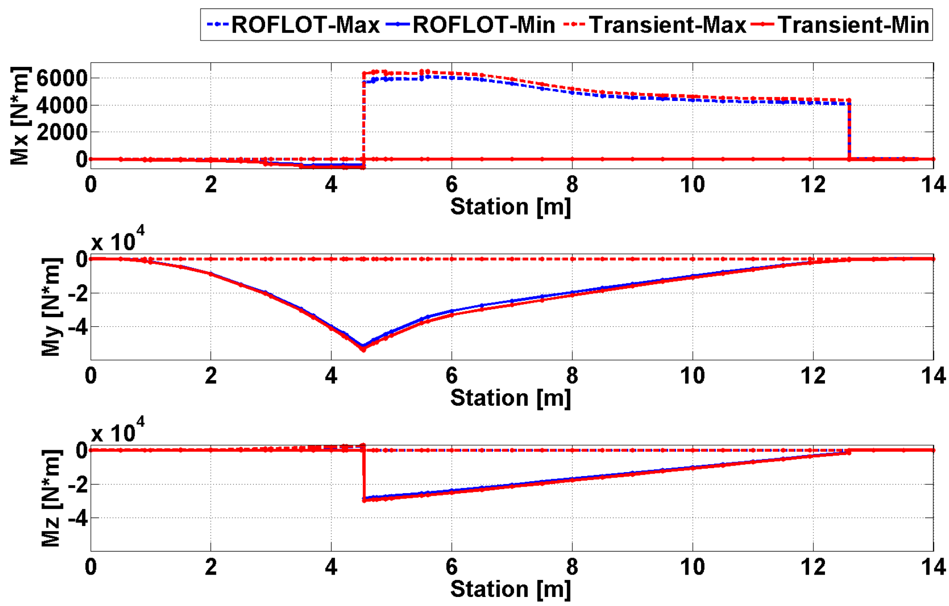

Figure 81. Comparison of Trim and Transient Solution Torsional and Bending Moments for Sea Level, 160 [knot] Forward Flight, Gust From Rear Condition

It can be seen in Figure 76 to Figure 81 that the loads calculated by using ROFLOT approach and transient analysis are generally in good agreement.

6.3.3. Gust From Up Condition

Comparison of maximum and minimum axial force, shear forces, torsional moment, and bending moments obtained by using ROFLOT approach and transient solution for gust from up condition in hover, 80 [knot], and 160 [knot] are given in Figure 82 to Figure 87.

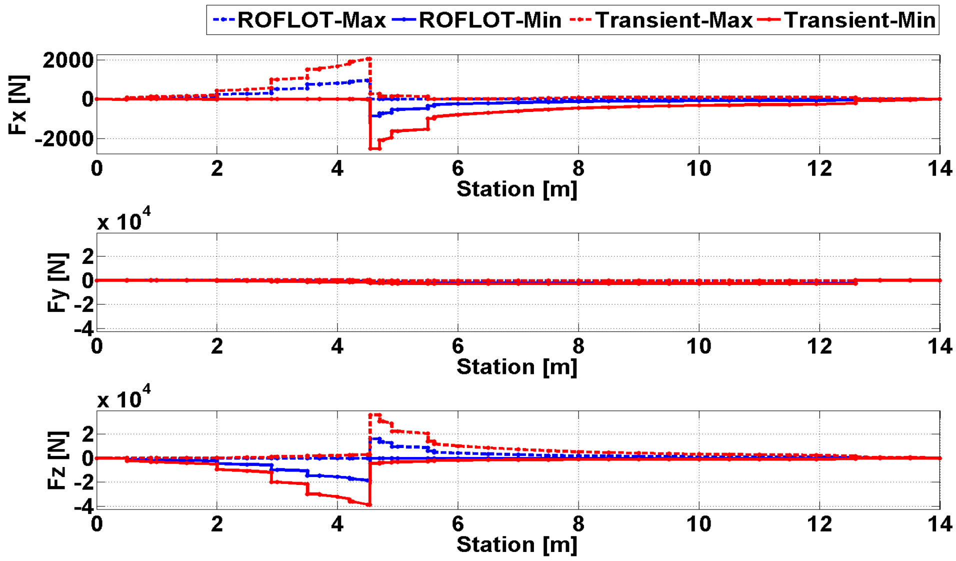

Figure 82. Comparison of Trim and Transient Solution Axial and Shear Forces for Sea Level, Hover, Gust From Up Condition

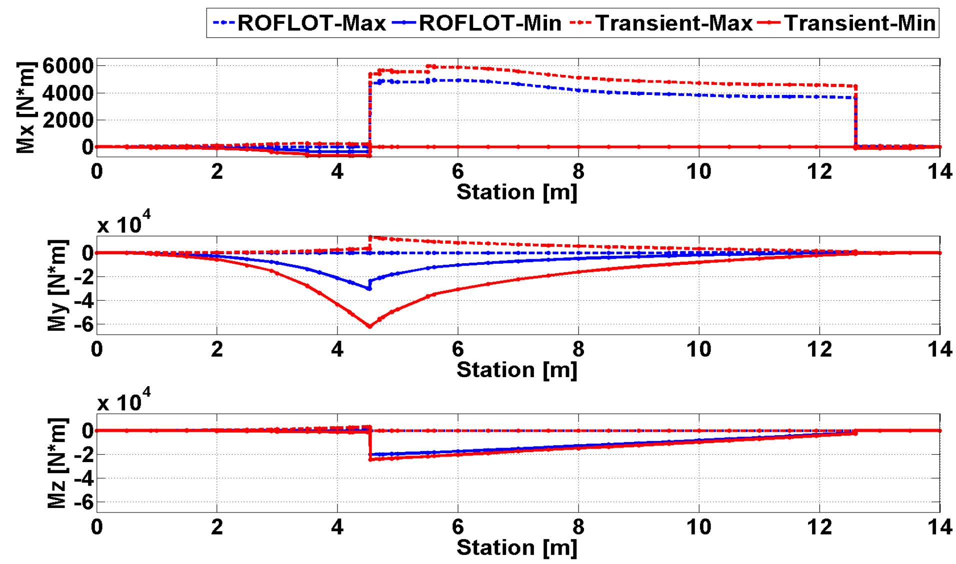

Figure 83. Comparison of Trim and Transient Solution Torsional and Bending Moments for Sea Level, Hover, Gust From Up Condition

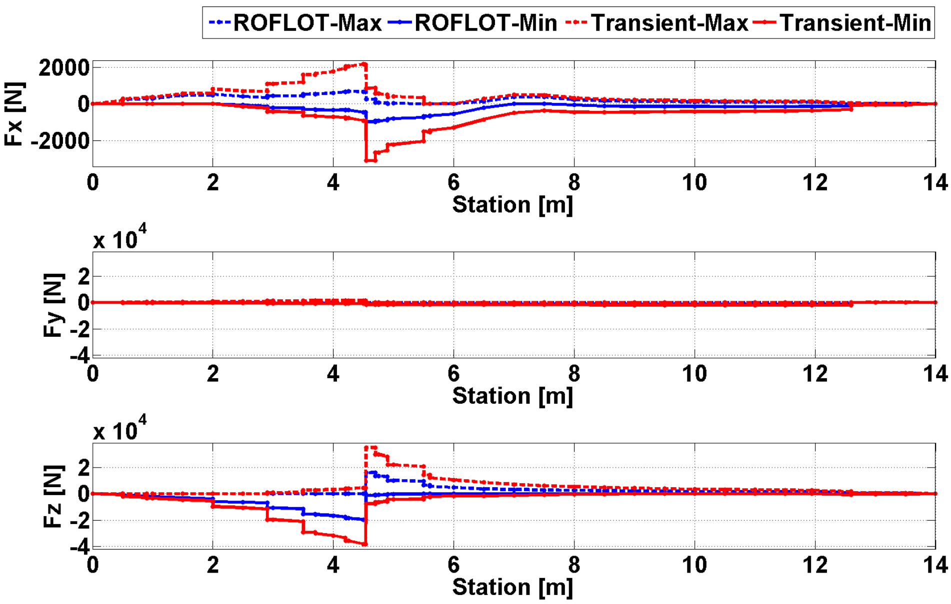

Figure 84. Comparison of Trim and Transient Solution Axial and Shear Forces for Sea Level, 80 [knot] Forward Flight, Gust From Up Condition

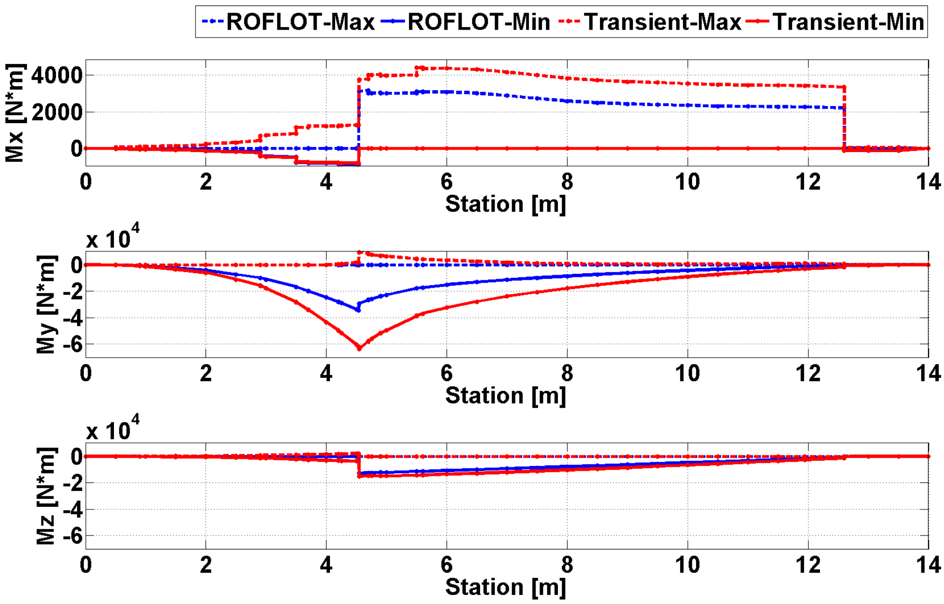

Figure 85. Comparison of Trim and Transient Solution Torsional and Bending Moments for Sea Level, 80 [knot] Forward Flight, Gust From Up Condition

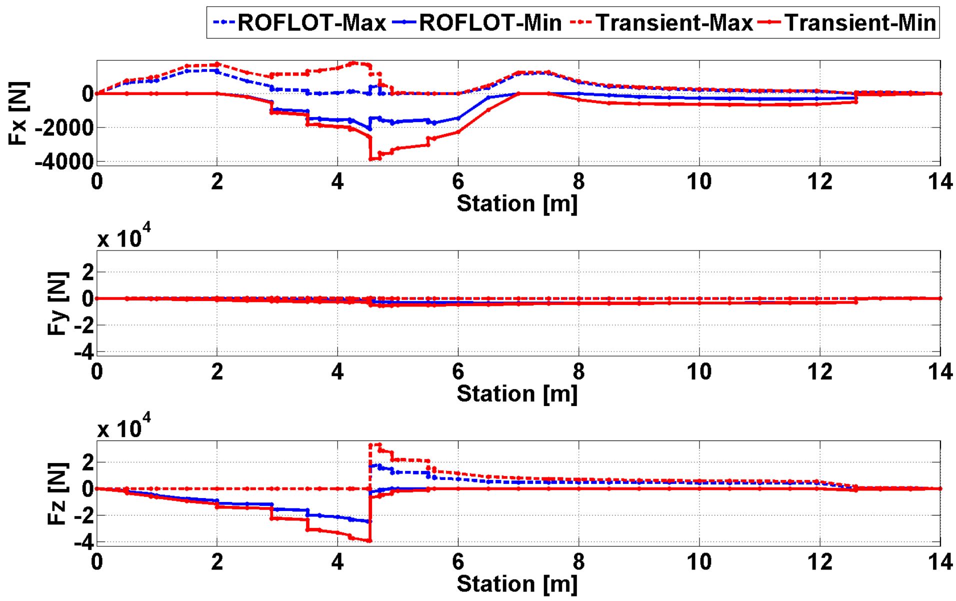

Figure 86. Comparison of Trim and Transient Solution Axial and Shear Forces for Sea Level, 160 [knot] Forward Flight, Gust From Up Condition

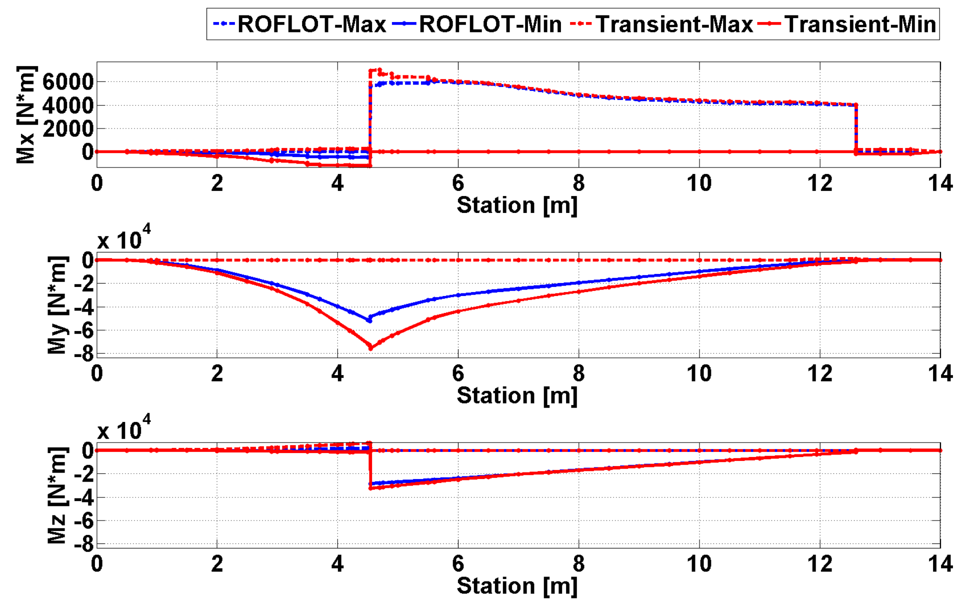

Figure 87. Comparison of Trim and Transient Solution Torsional and Bending Moments for Sea Level, 160 [knot] Forward Flight, Gust From Up Condition

It can be seen in Figure 82 to Figure 87 that the loads are usually underestimated by using ROFLOT approach when compared to the loads obtained by using transient analysis except from M_z. The agreement of the loads for the 160 [knot] case is slightly better than the hover and 80 [knot] cases.

6.3.4. Gust From Down Condition

Comparison of maximum and minimum axial force, shear forces, torsional moment, and bending moments obtained by using ROFLOT approach and transient solution for gust from down condition in hover, 80 [knot], and 160 [knot] are given in Figure 88 to Figure 93.

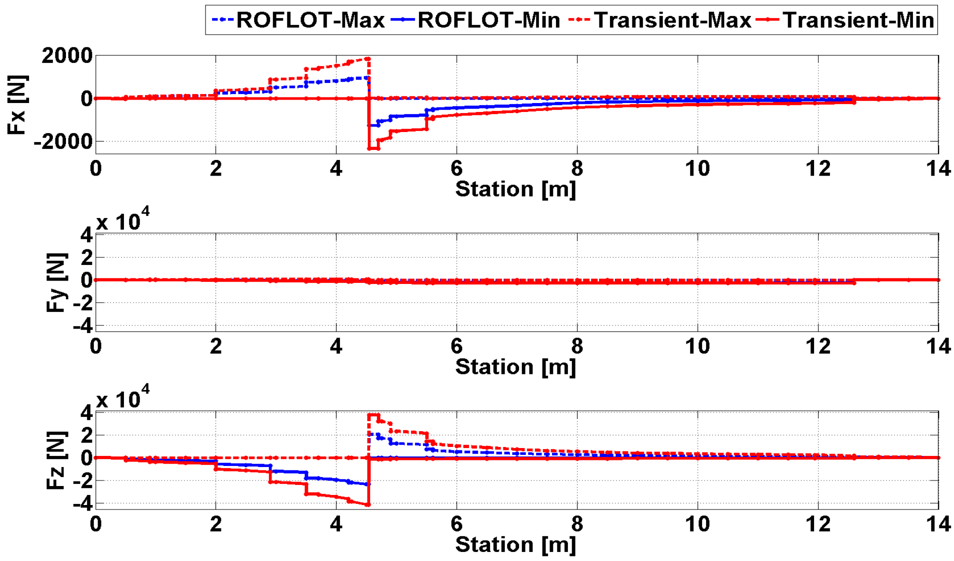

Figure 88. Comparison of Trim and Transient Solution Axial and Shear Forces for Sea Level, Hover, Gust From Down Condition

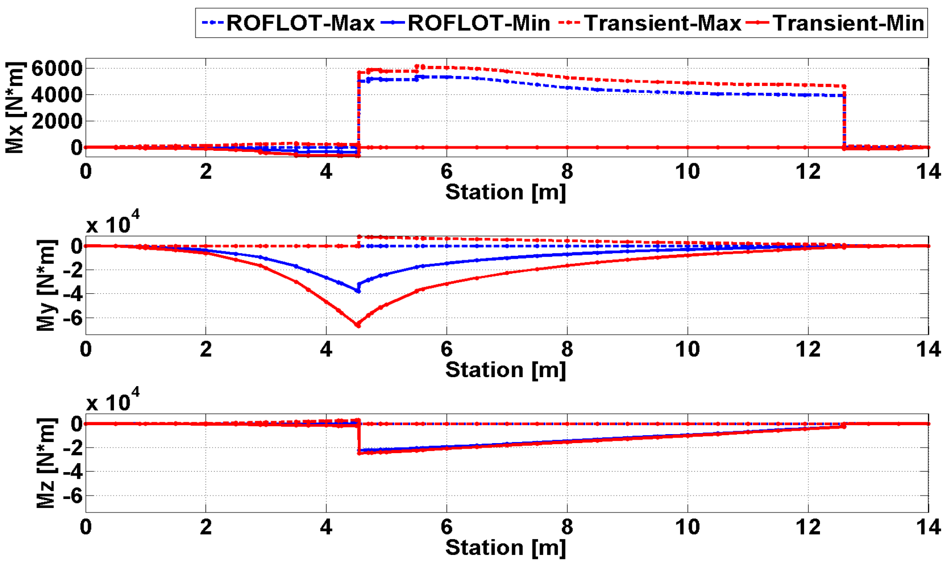

Figure 89. Comparison of Trim and Transient Solution Torsional and Bending Moments for Sea Level, Hover, Gust From Down Condition

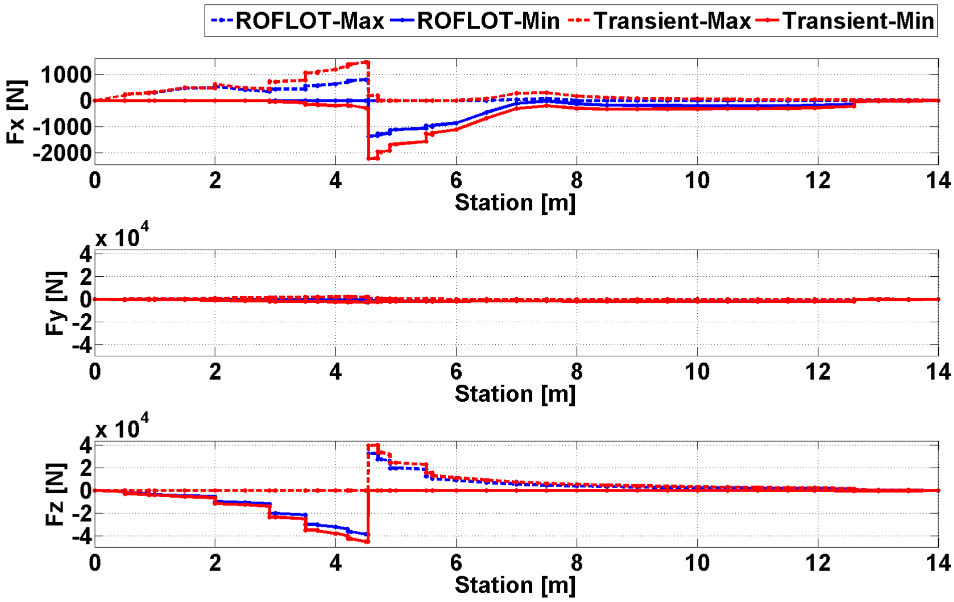

Figure 90. Comparison of Trim and Transient Solution Axial and Shear Forces for Sea Level, 80 [knot] Forward Flight, Gust From Down Condition

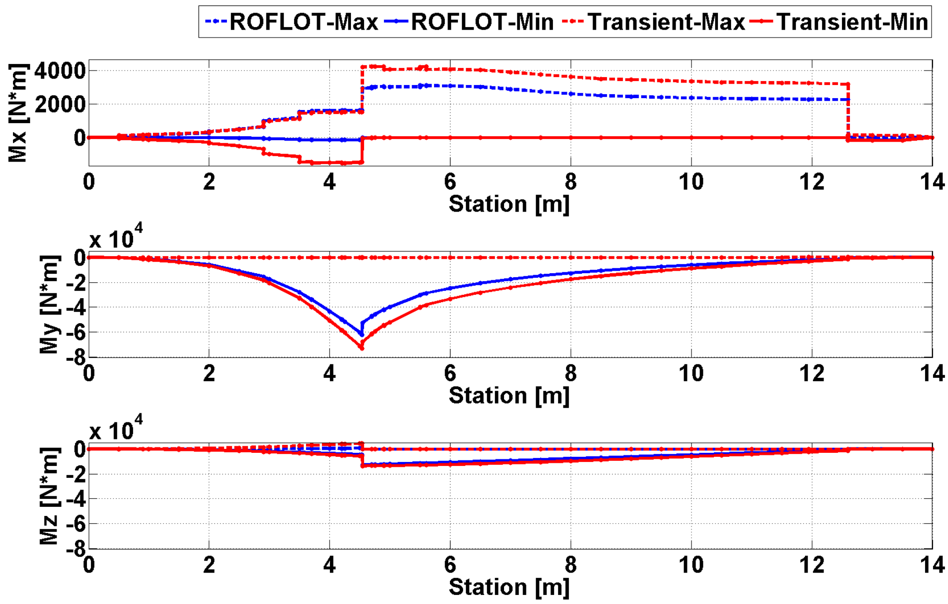

Figure 91. Comparison of Trim and Transient Solution Torsional and Bending Moments for Sea Level, 80 [knot] Forward Flight, Gust From Down Condition

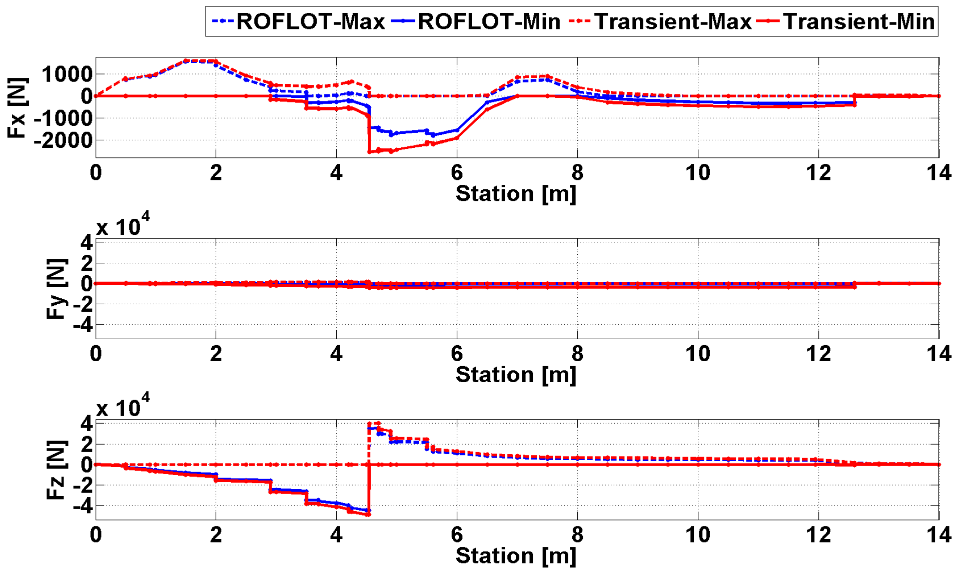

Figure 92. Comparison of Trim and Transient Solution Axial and Shear Forces for Sea Level, 160 [knot] Forward Flight, Gust From Down Condition

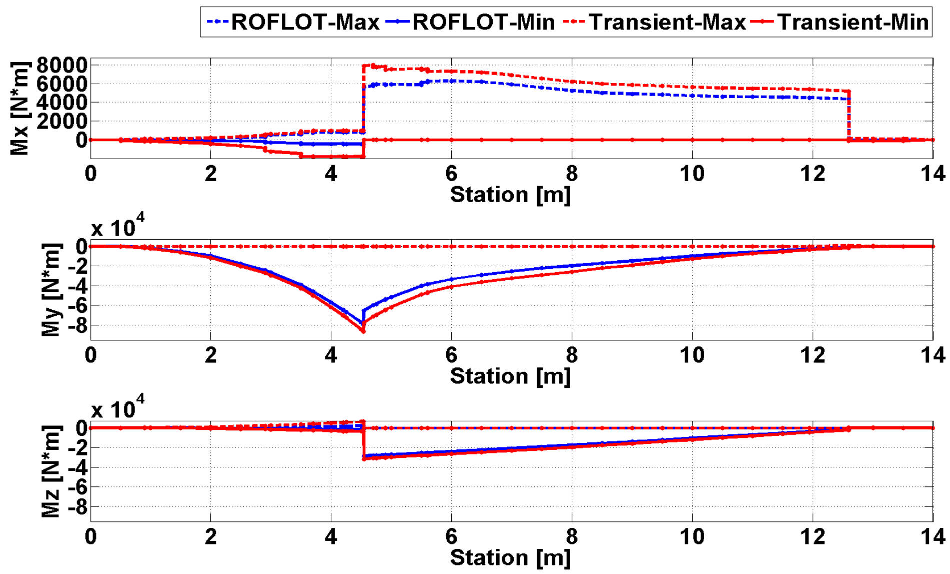

Figure 93. Comparison of Trim and Transient Solution Torsional and Bending Moments for Sea Level, 160 [knot] Forward Flight, Gust From Down Condition

It can be seen in Figure 88 to Figure 93 that the loads are generally underestimated by using ROFLOT approach when compared to the loads obtained by using transient analysis. However, as the flight speed increases, ROFLOT approach results in closer loads to the transient analysis loads which is important since highest loads occur when the flight speed is 160 [knot] when compared to the hover and 80 [knot] cases.

6.3.5. Gust From Left Condition

Comparison of maximum and minimum axial force, shear forces, torsional moment, and bending moments obtained by using ROFLOT approach and transient solution for gust from left condition in hover, 80 [knot], and 160 [knot] are given in Figure 94 to Figure 99.

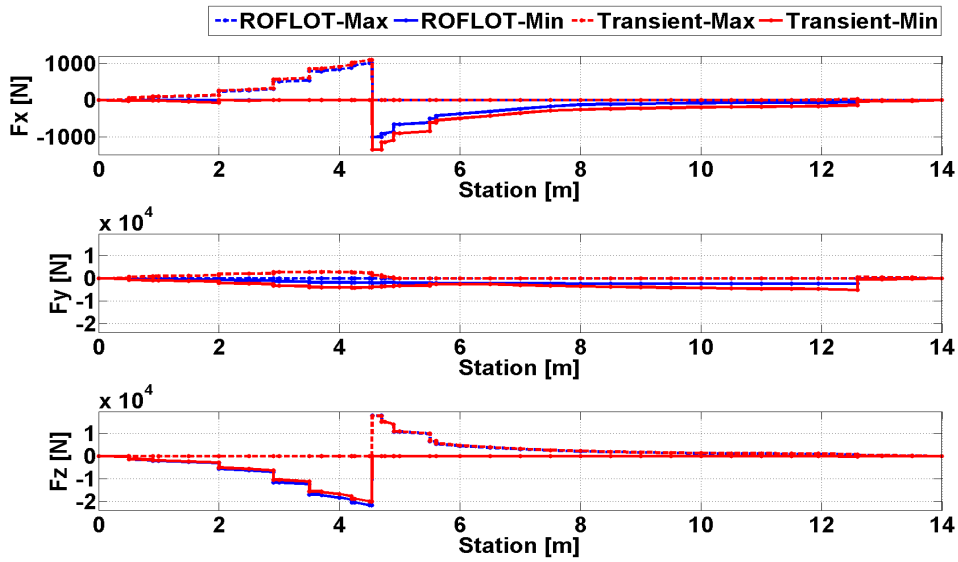

Figure 94. Comparison of Trim and Transient Solution Axial and Shear Forces for Sea Level, Hover, Gust From Left Condition

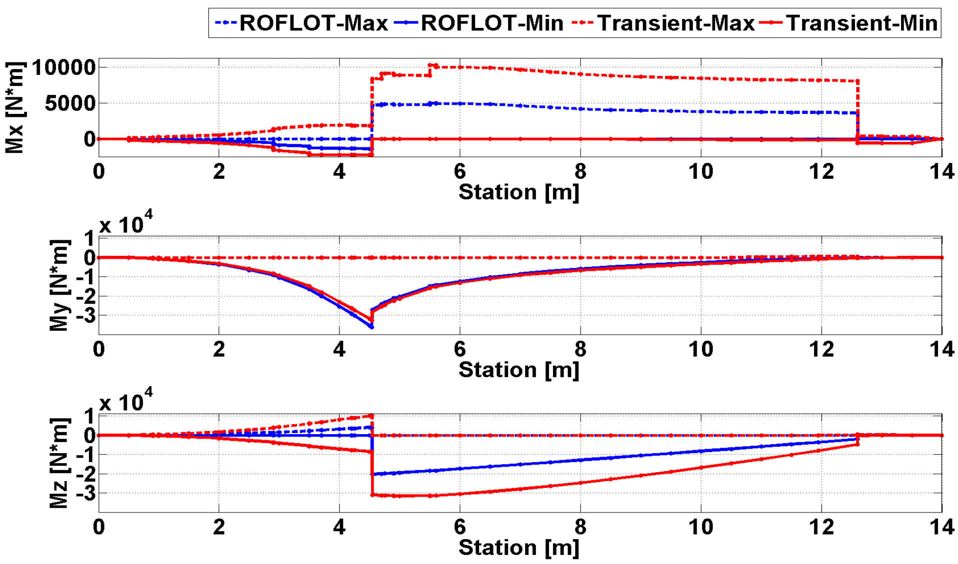

Figure 95. Comparison of Trim and Transient Solution Torsional and Bending Moments for Sea Level, Hover, Gust From Left Condition

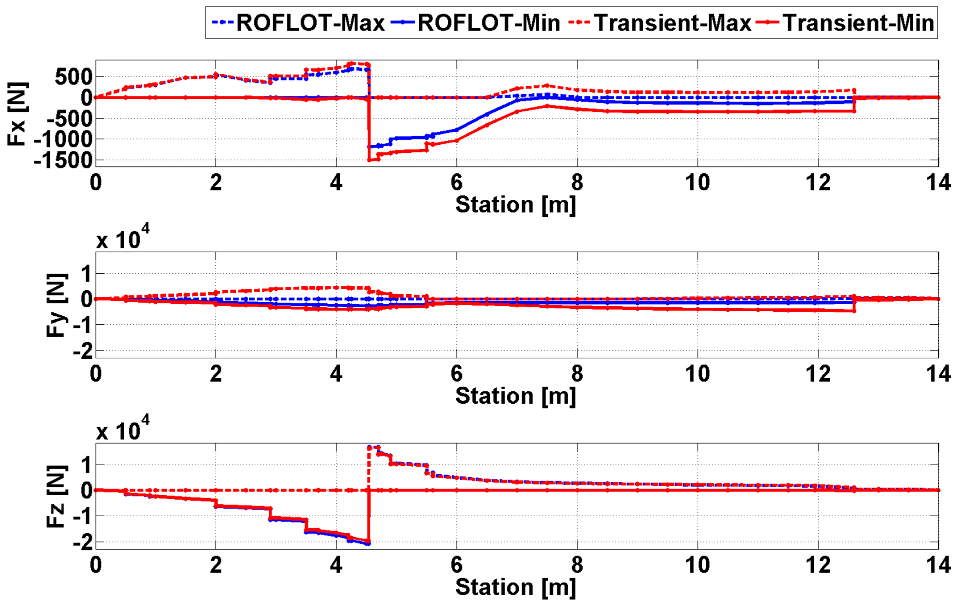

Figure 96. Comparison of Trim and Transient Solution Axial and Shear Forces for Sea Level, 80 [knot] Forward Flight, Gust From Left Condition

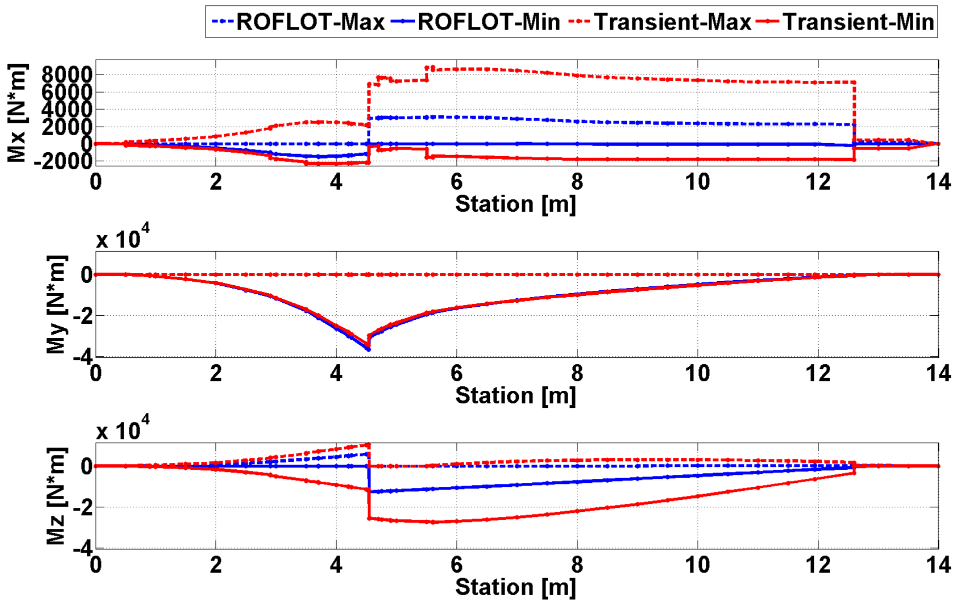

Figure 97. Comparison of Trim and Transient Solution Torsional and Bending Moments for Sea Level, 80 [knot] Forward Flight, Gust From Left Condition

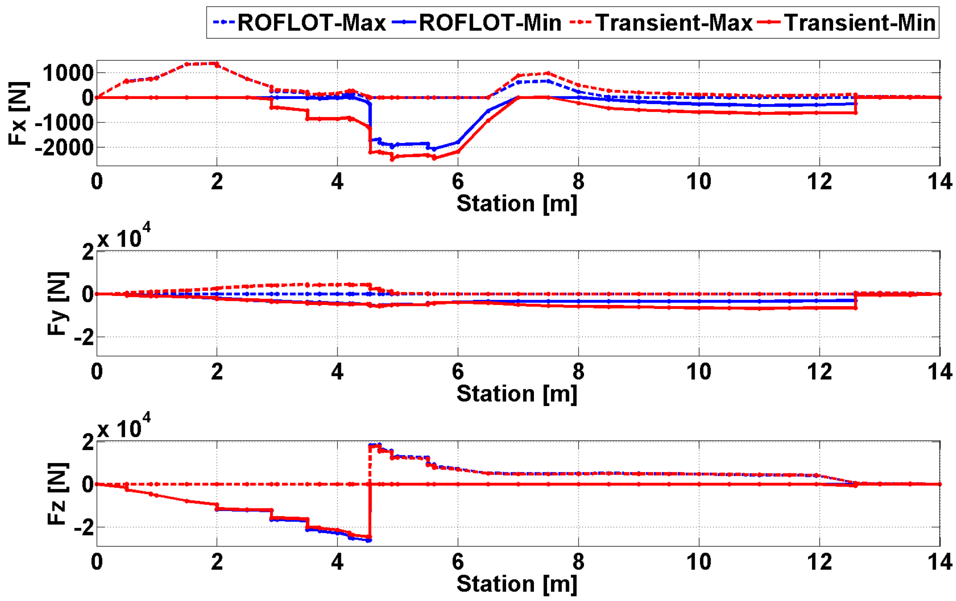

Figure 98. Comparison of Trim and Transient Solution Axial and Shear Forces for Sea Level, 160 [knot] Forward Flight, Gust From Left Condition

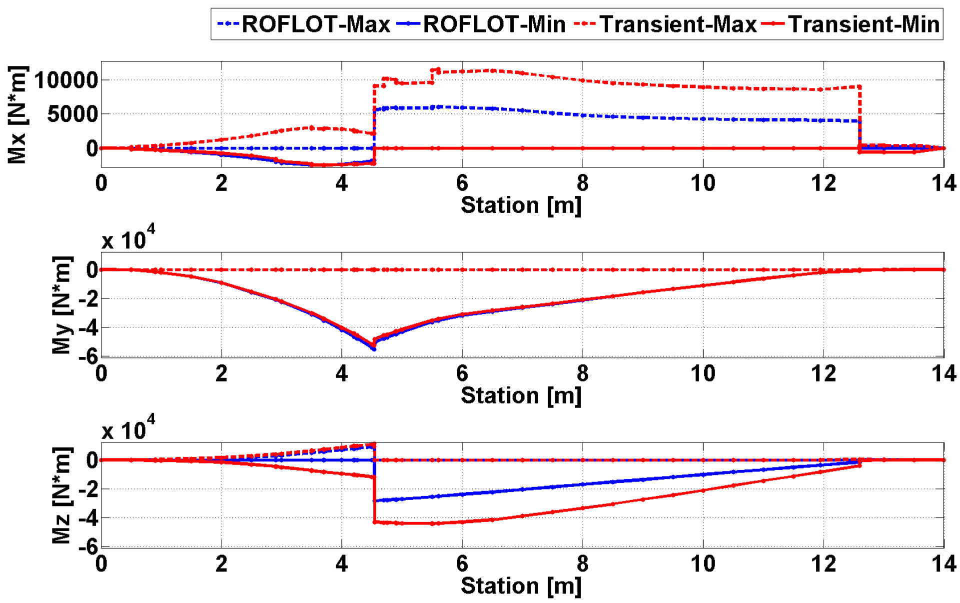

Figure 99. Comparison of Trim and Transient Solution Torsional and Bending Moments for Sea Level, 160 [knot] Forward Flight, Gust From Left Condition

It can be seen in Figure 94 to Figure 99 that F_z and M_y are estimated close to the transient solution results. M_x and M_z are underestimated and F_y is small when compared to F_z. F_x increases as the flight speed increases and ROFLOT approach underestimates this load although not as much as M_x and M_z.

6.3.6. Gust From Right Condition

Comparison of maximum and minimum axial force, shear forces, torsional moment, and bending moments obtained by using ROFLOT approach and transient solution for gust from right condition in hover, 80 [knot], and 160 [knot] are given in Figure 100 to Figure 105.

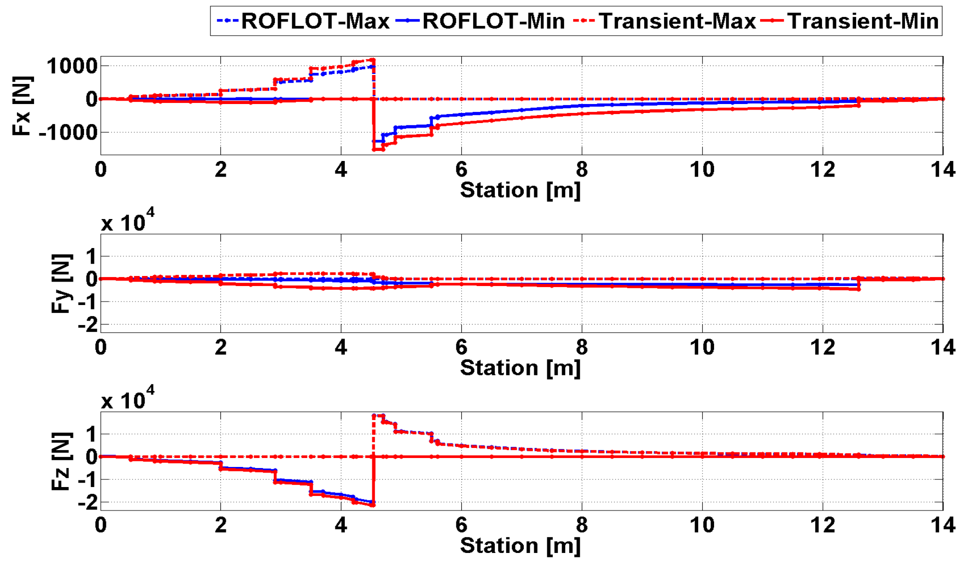

Figure 100. Comparison of Trim and Transient Solution Axial and Shear Forces for Sea Level, Hover, Gust From Right Condition

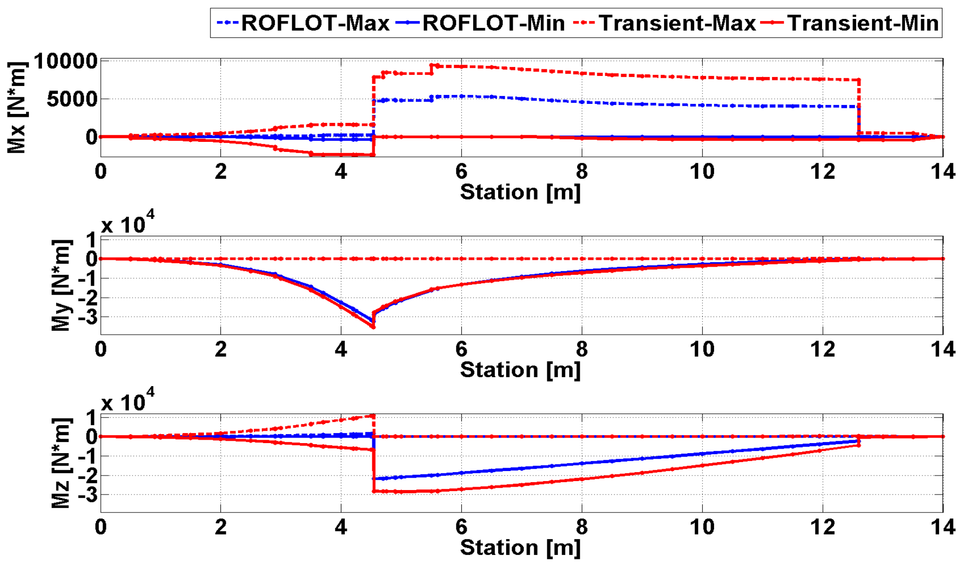

Figure 101. Comparison of Trim and Transient Solution Torsional and Bending Moments for Sea Level, Hover, Gust From Right Condition

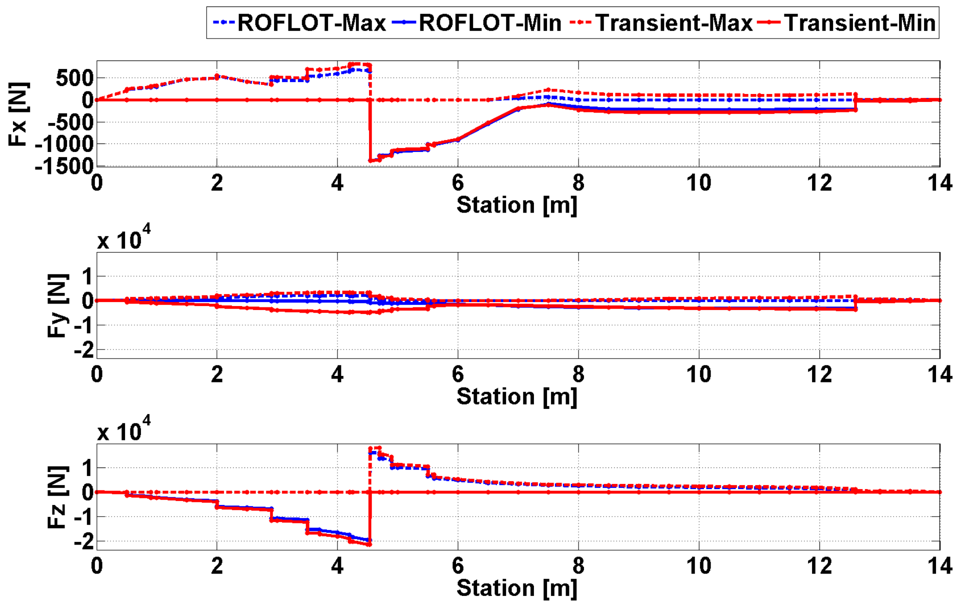

Figure 102. Comparison of Trim and Transient Solution Axial and Shear Forces for Sea Level, 80 [knot] Forward Flight, Gust From Right Condition

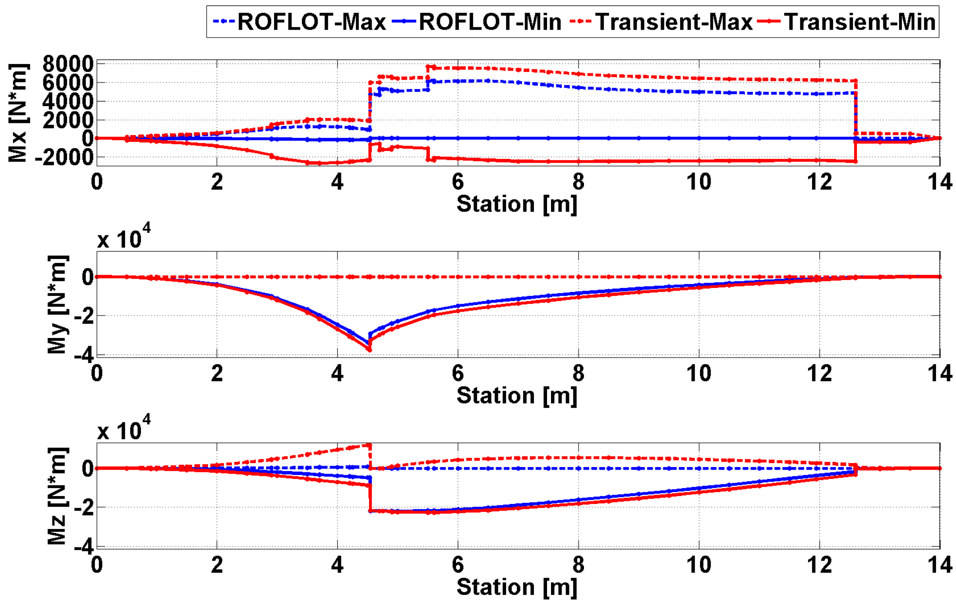

Figure 103. Comparison of Trim and Transient Solution Torsional and Bending Moments for Sea Level, 80 [knot] Forward Flight, Gust From Right Condition

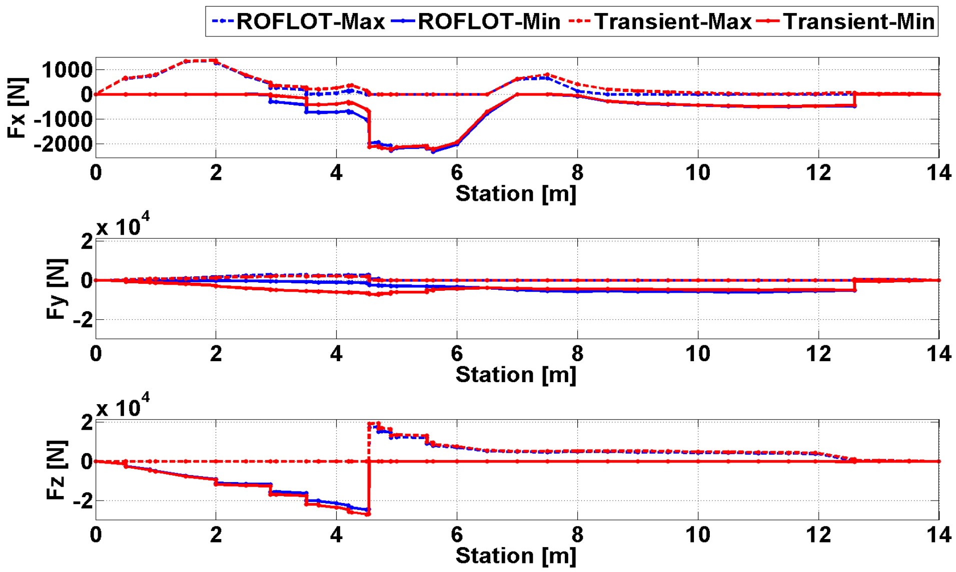

Figure 104. Comparison of Trim and Transient Solution Axial and Shear Forces for Sea Level, 160 [knot] Forward Flight, Gust From Right Condition

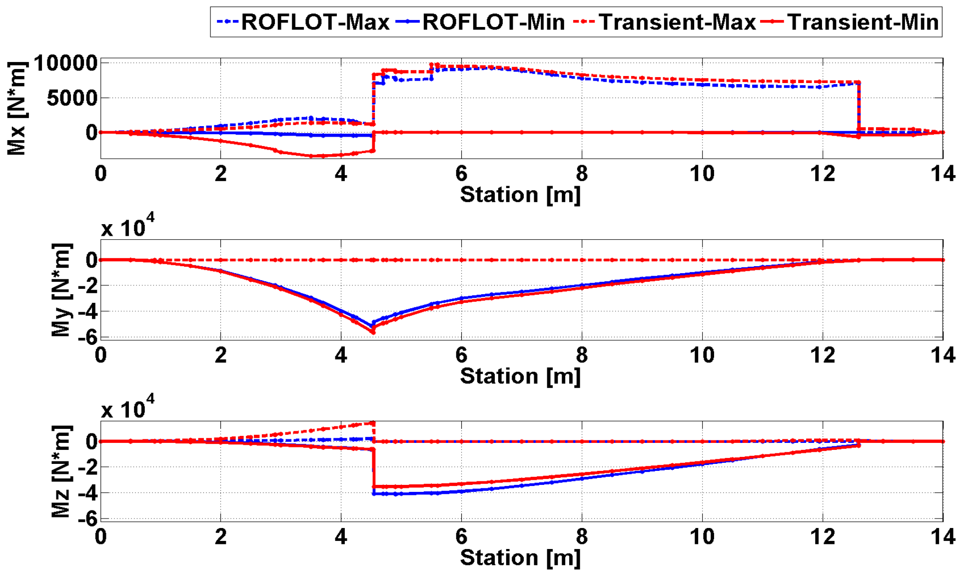

Figure 105. Comparison of Trim and Transient Solution Torsional and Bending Moments for Sea Level, 160 [knot] Forward Flight, Gust From Right Condition

It can be seen in Figure 100 to Figure 105 that F_x, F_y, and F_z are generally in good agreement although slightly underestimated. The agreement for F_x is better for 80 [knot] and 160 [knot] cases when compared to the hover case. Furthermore, the loads are generally the highest for the 160 [knot] case and M_x, M_y, and M_z are estimated well for this case although M_z is slightly overestimated.

6.3.7. All Gust Conditions

Comparison of axial force, shear forces, torsional moment, and bending moments showing the maximum and minimum loads for all the gust conditions obtained by using ROFLOT approach and transient solution are given in Figure 106 and Figure 107.

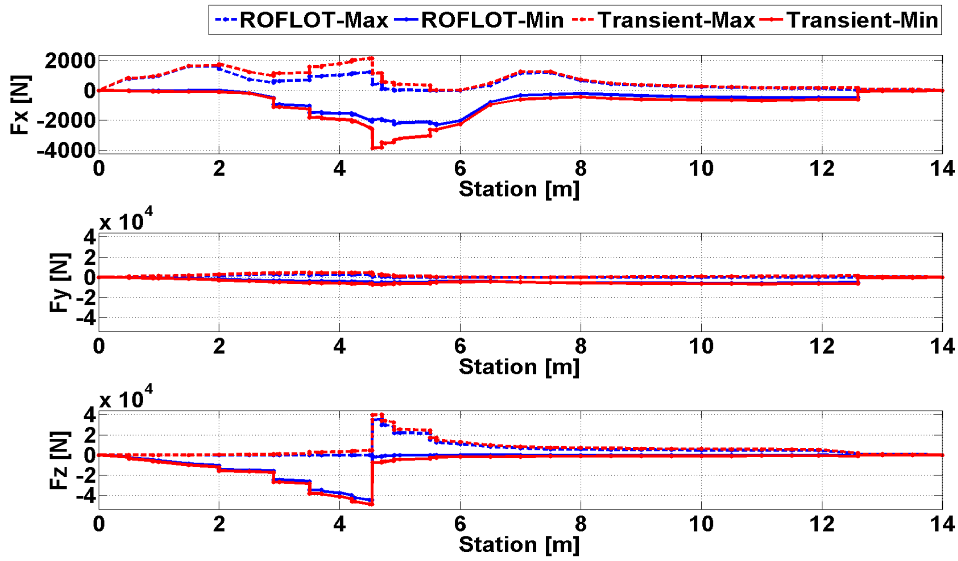

Figure 106. Comparison of Trim and Transient Solution Overall Maximum and Minimum Axial and Shear Forces of the Gust Conditions

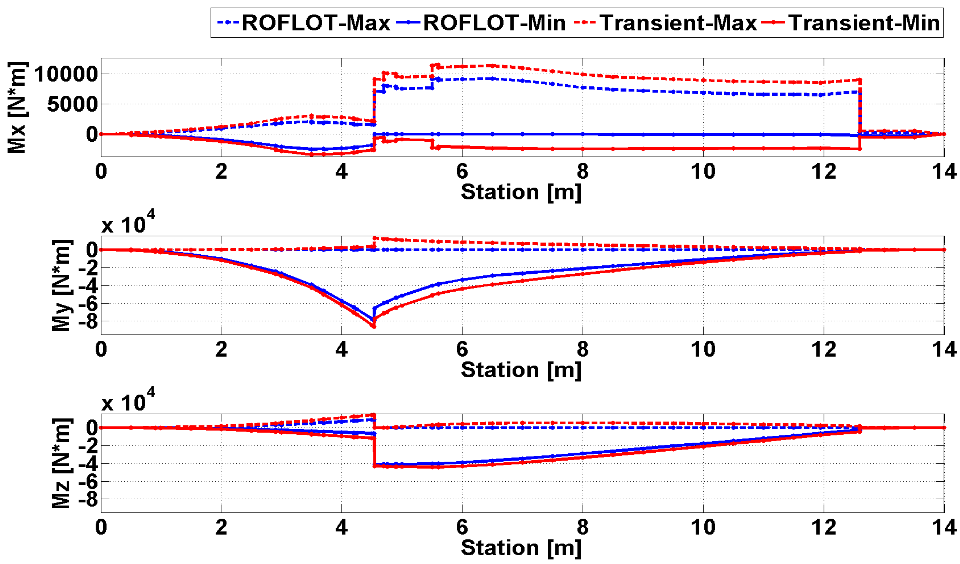

Figure 107. Comparison of Trim and Transient Solution Overall Maximum and Minimum Torsional and Bending Moments of the Gust Conditions

It can be seen in Figure 106 and Figure 107 that ROFLOT approach slightly underestimates the fuselage gust loads when compared to the transient solution. The results may still be satisfactorily close but if higher accuracy is required, the critical conditions can be chosen based on the results of ROFLOT approach and then transient analysis can be employed for these conditions only.

6.5. All Maneuvers and Gust Conditions

Comparison of axial force, shear forces, torsional moment, and bending moments showing the maximum and minimum loads for all the maneuvers and gust conditions obtained by using ROFLOT approach and transient solution are given in Figure 108 and Figure 109 when pull-up and push-over trim methods are employed and in Figure 110 and Figure 111 when high-g and low-g forward flight trim methods are employed.

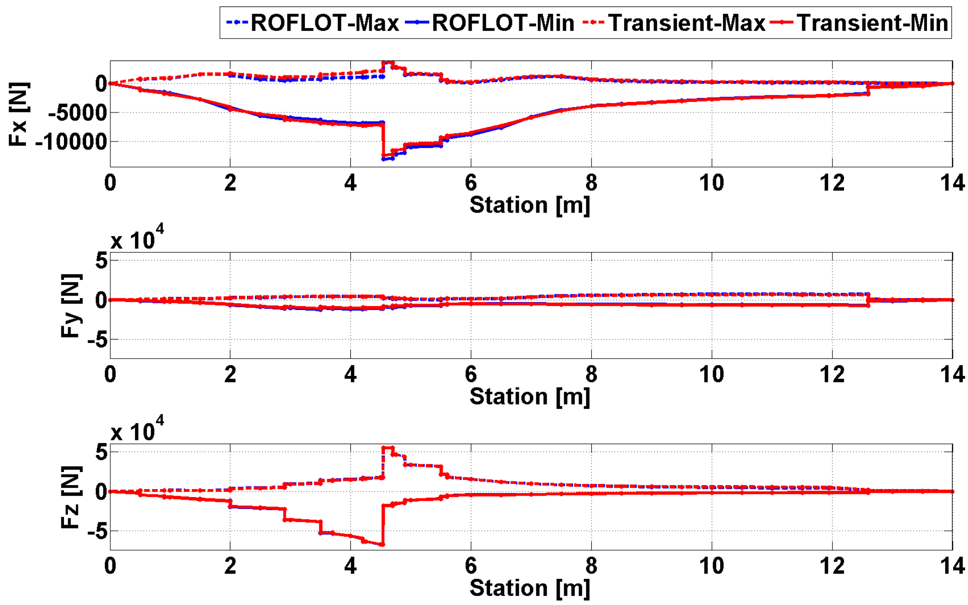

Figure 108. Comparison of Trim and Transient Solution Overall Maximum and Minimum Axial and Shear Forces of All the Maneuvers and Gust Conditions when Pull-up and Push-over Trim Methods are Employed

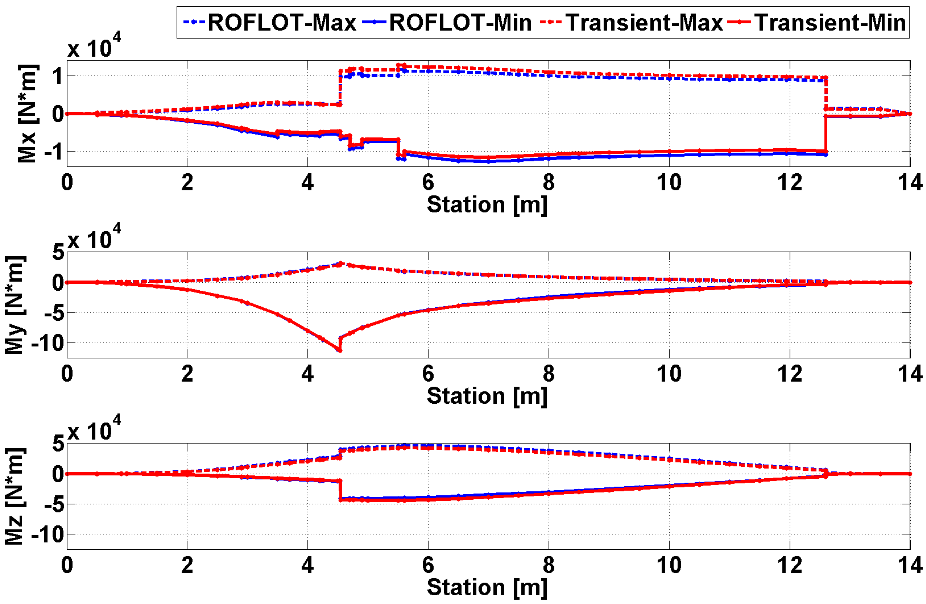

Figure 109. Comparison of Trim and Transient Solution Overall Maximum and Minimum Torsional and Bending Moments of All the Maneuvers and Gust Conditions when Pull-up and Push-over Trim Methods are Employed

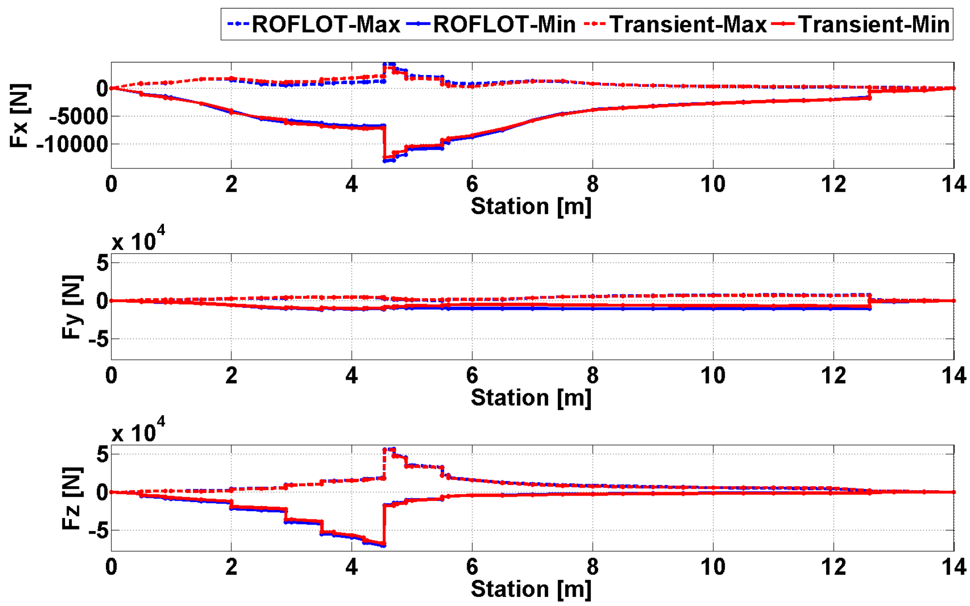

Figure 110. Comparison of Trim and Transient Solution Overall Maximum and Minimum Axial and Shear Forces of All the Maneuvers and Gust Conditions when High-g and Low-g Forward Flight Trim Methods are Employed

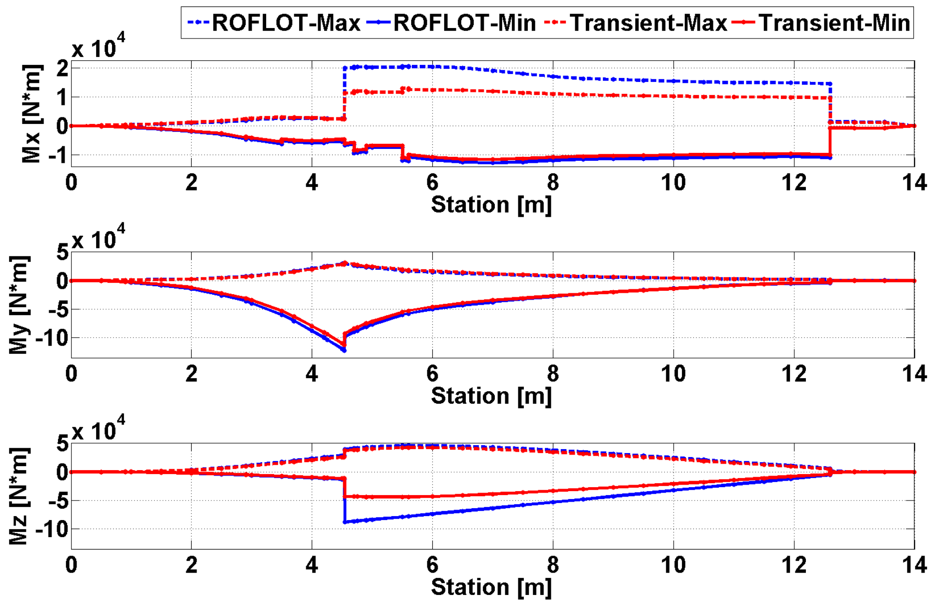

Figure 111. Comparison of Trim and Transient Solution Overall Maximum and Minimum Torsional and Bending Moments of All the Maneuvers and Gust Conditions when High-g and Low-g Forward Flight Trim Methods are Employed

It can be seen in Figure 108 and Figure 109 that the loads calculated by using ROFLOT approach and transient analysis are very close for the maximum and minimum loads of all the maneuvers and gust conditions.

Figure 110 and Figure 111 show that when high-g forward flight trim method is employed, M_x and M_z are overestimated but F_x, F_y, F_z, and M_y are in good agreement.

CHAPTER 7

CONCLUSIONS

7.1. General Conclusions

Rotorcraft fuselage loads encountered during pull-up, push-over, and yaw maneuvers and gust conditions, analysis of which are required by civil and military standards, have been calculated in this thesis. An approach, named as ROFLOT, has been developed to calculate the loads in an efficient manner. In this method, the transient analysis employed for the flight dynamics analysis of pull-up, push-over, and yaw maneuvers and gust conditions have been replaced by trim point(s). The fuselage sectional loads have been obtained by using both transient solutions and ROFLOT approach and comparisons have been performed.

ROFLOT approach includes two different methods for the pull-up maneuver, pull-up trim and high-g forward flight trim methods. Pull-up trim method can estimate the maximum and minimum loads encountered in a pull-up transient analysis very well except from F_x which is underestimated for the sections towards the nose of the rotorcraft. High-g forward flight trim method can estimate F_z and M_y satisfactorily close to the transient analysis but it results in higher M_x and M_z mainly because of the difference in the main rotor torque. Furthermore, F_x is underestimated for the section towards the nose and overestimated for the sections towards the tail. The fact that F_z and M_y are close to the transient analysis shows that the aerodynamic loads are not significant when compared to the inertial loads since the aerodynamic loads for the high-g forward flight trim are different than those of the pull-up transient analysis. Moreover, it can be stated that the effect of inertial loading on F_z and M_y (centrifugal force) is not significant. Employing high-g forward flight trim method is faster than employing pull-up trim method but the latter give more accurate results. Finally, regardless of the methodology employed, F_z and M_y are higher than F_y and M_z for a pull-up maneuver and F_x is low when compared to the yaw maneuver.

Similar to the pull-up maneuver, for the push-over maneuver, ROFLOT approach includes push-over trim and low-g forward flight trim methods. The loads obtained by using the push-over trim method are very close to the transient analysis loads. Furthermore, low-g forward flight trim method also results in satisfactorily close results for the 80 [knot] case when compared to the transient analysis. The same agreement cannot be observed for the 120 [knot] case because of the difference in the aerodynamic loading. However, the difference in the loads for the 120 [knot] case is not observed when the overall maximum and minimum loads are considered. Similar to the pull-up maneuver, low-g forward flight trim method is faster than push-over trim method but the latter give more accurate results. Finally, regardless of the methodology employed, push-over maneuver results in loads in opposite direction when compared with the pull-up maneuver.

The fuselage loads encountered in a yaw maneuver are estimated well by using ROFLOT approach. Because of the high tail rotor thrust, high M_z occurs on the fuselage. Furthermore, yaw maneuver results in significant amount of F_x which is due to combination of high yaw rate and high sideslip angle. These loads can be estimated by combination of four trim points. These trim points are high tail rotor thrust trim, maximum yaw velocity with sideslip angle trim, maximum transient sideslip angle with yaw velocity trim, and return trim.

Each gust condition is represented by a single trim point. This way, the maximum and minimum fuselage loads encountered during gust transient analysis can be estimated. When the maximum and minimum loads of all the gust conditions are considered, it can be seen that ROFLOT approach slightly underestimates the loads. The results may still be satisfactorily close but if higher accuracy is required, the critical conditions can be chosen based on the results of ROFLOT approach and then transient analysis can be employed for these conditions only.

Employing ROFLOT approach instead of transient analysis can reduce the computation time required for the loads analysis of the rotorcraft fuselage by around

85%. In addition, the engineering effort is also reduced. Finally, the need for a stability augmentation system which is often required for the transient analysis of the maneuvers because of high coupling between roll, pitch, and yaw motions of a rotorcraft is eliminated with ROFLOT approach.

7.2. Recommendations for Future Studies

In this thesis, pull-up, push-over, and yaw maneuvers and gust conditions have been analyzed for the limit fuselage loads. The approach developed here can be further expanded by analyzing the loads due to different maneuvers on different parts of the rotorcraft such as;

- Limit loads on horizontal tail, vertical fin, and main rotor and tail rotor blades.
- Fatigue loads due to operational maneuvers on fuselage, horizontal tail, vertical fin, and main rotor and tail rotor blades.

REFERENCES

[1] "Certification Specifications for Small Rotorcraft (CS-27), Amendment 3", European Aviation Safety Agency (EASA), December 11, 2012.

[2] "Certification Specifications for Large Rotorcraft (CS-29), Amendment 3", European Aviation Safety Agency (EASA), December 11, 2012.

[3] "Military Specification, Structural Design Requirements, Helicopters", August 1, 1950.

[4] "Engineering Design Handbook. Helicopter Engineering. Part One. Preliminary Design", Alexandria, Virginia, August 30, 1974.

[5] Leishman, J. G., "Principles of Helicopter Aerodynamics", Cambridge University Press, New York, NY, 2006.

[6] Wright, J. R., Cooper, J. E., "Introduction to Aircraft Aeroelasticity and Loads", John Wiley & Sons Ltd., The Atrium, Southern Gate, Chichester, West Sussex, England, 2007.

[7] "Certification of Transport Category Rotorcraft AC 29-2C", U.S. Department of Transportation, Federal Aviation Administration, July 25, 2014

[8] Hoblit, F. M., "Gust Loads on Aircraft: Concepts and Applications", American Institute of Aeronautics and Astronautics, Inc., Washington, D.C.

[9] Pratt, K. G., "A Revised Formula for the Calculation of Gust Loads", NACA, Washington, June, 1953.

[10] Johnson, W., "Helicopter Theory", New York, NY, U.S., 1994.

[11] Arcidiacano, P. J., Bergquist, R. R., Alexander, W. T., "Helicopter Gust Response Characteristics Including Unsteady Aerodynamic Stall Effects",

AHS/NASA-Ames Specialists' Meeting on Rotorcraft Dynamics, February 13-15, 1974.

[12] Niu, M. C. Y., "Airframe Structural Design Practical Design Information and Data on Aircraft Structures", Conmilit Press Ltd., Los Angeles, California, January, 1995.

[13] Johnson, W., "A History of Rotorcraft Comprehensive Analysis", Ames Research Center, Moffett Field, California.

[14] Austin, E. E., Vann, W. D., "General Description of the Rotorcraft Flight Simulation Computer Program (C-81), U.S. Army Air Mobility Research and Development Laboratory, Fort Eustis, Virginia, June 1973.

[15] Ormiston, R. A., Rutkowski, M. J., Ruzicka, G. C., Saberi, H., Jung, Y., "Comprehensive Aeromechanics Analysis of Complex Rotocraft Using 2GCHAS", American Helicopter Society Aeromechanics Specialists Conference, San Francisco, California, U.S., January 19-21, 1994.

[16] Bir, G. S., "Structural Dynamics Verification of Rotorcraft Comprehensive Analysis System (RCAS)", National Renewable Energy Laboratory, Golden, Colorado.

[17] Johnson, W., "A Comprehensive Analytical Model of Rotorcraft Aerodynamics and Dynamics, Part I: Analysis Development", Ames Research Center, Moffett Field, California, June, 1980.

[18] Johnson, W., "A Comprehensive Analytical Model of Rotorcraft Aerodynamics and Dynamics, Part II: User's Manual", Ames Research Center, Moffett Field, California, July, 1980.

[19] Johnson, W., "A Comprehensive Analytical Model of Rotorcraft Aerodynamics and Dynamics, Part III: Program Manual", Ames Research Center, Moffett Field, California, June, 1980.

[20] Johnson, W., "CAMRAD/JA: A Comprehensive Analytical Model of Rotorcraft Aerodynamics and Dynamics, Johnson Aeronautics Version, Volume I: Theory Manual", Johnson Aeronautics, Palo Alto, California, 1988.

[21] Johnson, W., "CAMRAD/JA: A Comprehensive Analytical Model of Rotorcraft Aerodynamics and Dynamics, Johnson Aeronautics Version, Volume II: User's Manual", Johnson Aeronautics, Palo Alto, California, 1988.

[22] Johnson, W., "Technology Drivers in the Development of CAMRAD II", American Helicopter Society Aeromechanics Specialists Conference, San Francisco, California, U.S., January 19-21, 1994.

[23] Johnson, W., "Rotorcraft Aeromechanics Applications of a Comprehensive Analysis", Heli Japan, Gifu, Japan, April 21-23, 1998.

[24] Howlett, J. J., "UH-60A Black Hawk Engineering Simulation Program: Volume I – Mathematical Model", United Technologies, Sikorsky Aircraft, Stratford, Connecticut, December, 1981.

[25] Howlett, J. J., "UH-60A Black Hawk Engineering Simulation Program: Volume II – Background Report", United Technologies, Sikorsky Aircraft, Stratford, Connecticut, December, 1981.

[26] Saberi, H. A., Jung, Y. C., Anastassiades, T., "Finite Element and Modal Method in Multibody Dynamic Code", Advanced Helicopter Society 2nd International Aeromechanics Specialists' Conference, Bridgeport, Connecticut, October, 1995.

[27] Val, R. D., "A Real-Time Blade Element Helicopter Simulation for Handling Qualities Analysis", Fifteenth European Rotorcraft Forum, Amsterdam, September 12-15, 1989.

[28] Chengjian, H., Zhao, J., Goericke, J., "Multi-Body and Unsteady Rotorcraft/Slung Load Modeling and Simulation", Advanced Rotorcraft Technology, Inc., Mountain View, California.

[29] Internal Communications - TAI

[30] Abbott, I. H., Von Doenhoff, A. E., “Theory of Wing Sections Including a Summary of Airfoil Data”, Dover Publications, Inc., Mineola, N.Y.

[31] Ardakani, H. A., Bridges, T. J., “Review of the 3-2-1 Euler Angles: a yaw-pitch-roll sequence”, Department of Mathematics, University of Surrey, Guildford, UK, April 15, 2010.

[32] Beer, F. P., Johnston, E. R., Clausen, W. E., “Vector Mechanics for Engineers, Dynamics”, McGraw Hill, 2007.

[33] Air Force Test Pilot School Edwards AFBCA, “Flying Qualities Textbook”, Vol. 2, Part I, Chap. 4, USAF Test Pilot School, Edwards AFB, CA, April, 1986.

[34] Bird, J., “Engineering Mathematics”, Elsevier, Oxford OX2 8DP, UK and Burlington, MA, U.S., 2007.

[35] Gul, S., Bilen, M. E., Şahin, M., Gürak, D., Yaman, Y., “A Convergence Study for a Longitudinal Maneuver by Using Various Tools”, American Helicopter Society 72nd Annual Forum, West Palm Beach, Florida, U.S., May 17-19, 2016.

Appendix A: Effect of Number of Monitor Stations on the Sectional Loads

In order to investigate the effect of the number of monitor stations on the sectional axial force, shear force, torsional moment, and bending moments, the number of monitor stations have been doubled and the sectional loads have been calculated once more for the 3.5 [g] pull-up maneuver at 120 [knot] in order to perform a sensitivity analysis. The comparison of the fuselage sectional loads can be seen in Figure 112 and Figure 113.

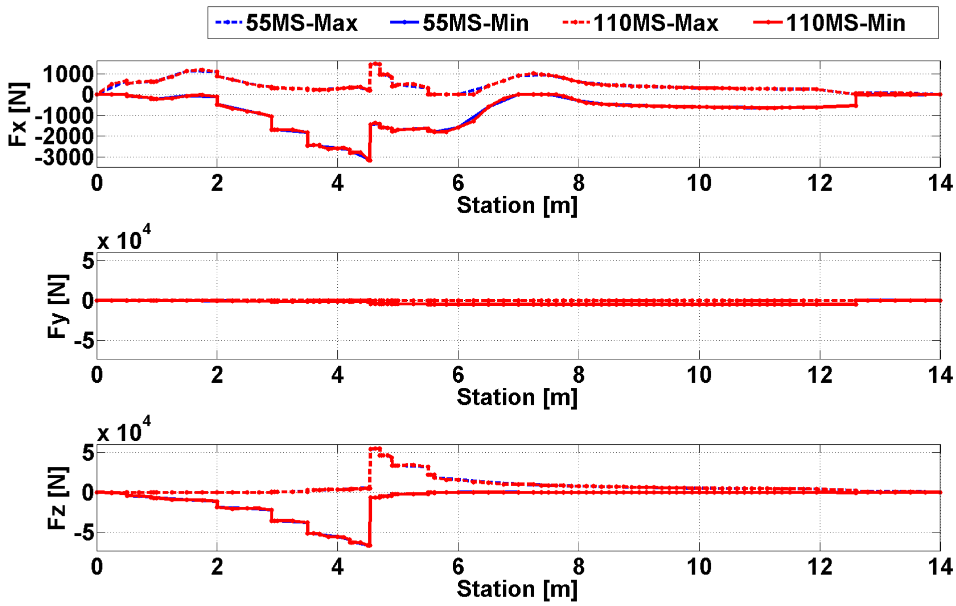

Figure 112. Comparison of Axial and Shear Forces for Two Different Number of Monitor Stations for Sea Level, ISA -55 C^0, 120 [knot], 3.5 [g] Pull-up Maneuver

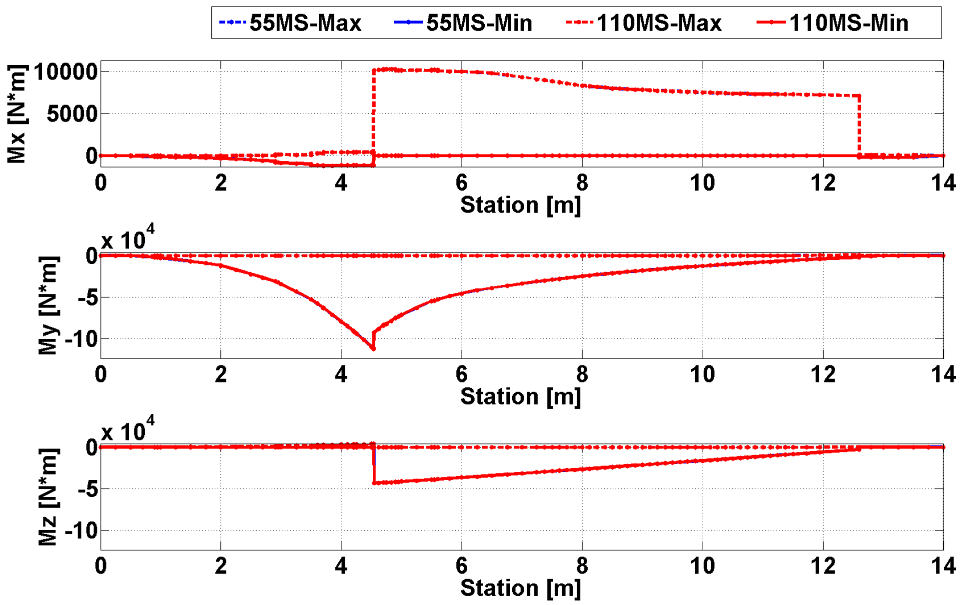

Figure 113. Comparison of Torsional and Bending Moments for Two Different Number of Monitor Stations for Sea Level, ISA -55 C^0, 120 [knot], 3.5 [g] Pull-up Maneuver